VIBRATION BASED DAMAGE IDENTIFICATION FOR PLATE-LIKE STRUCTURES

By

Hussam Saleem

A thesis submitted in partial fulfillment of
the requirements for the degree of

Master of Science in Civil Engineering

WASHINGTON STATE UNIVERSITY
Department of Civil and Environmental Engineering

December 2011

To the Faculty of Washington State University:

The members of the Committee appointed to examine the thesis of HUSSAM SALEEM find it satisfactory and recommend that it be accepted.

Pizhong Qiao, Ph.D. (Chair)

David McLean, Ph.D.

William Franklin Cofer, Ph.D.

Wei Fan, Ph.D.

ACKNOWLEDGMENT

The completion of this thesis would not have been possible without the help and guidance of my advisor, professors, and fellow graduate students with whom I've worked with over the past year in the smart structures laboratory.

I would like to thank my advisor professor Pizhong Qiao for giving me the opportunity to conduct this study by providing me with all the required support and guidance to accomplish my goals. Also, I want to thank my committee members Professor David McLean and professor William Cofer for their help in guiding me through this trip.

A special thanks goes to Dr. Wei Fan, who provided me with all the training required for this study; in both theoretical and experimental aspects, he helped me every step on the way.

I also want to recognize the support of my family and friends throughout the challenging, but rewarding process of this achievement.

VIBRATION BASED DAMAGE IDENTIFICATION FOR PLATE-LIKE STRUCTURES

ABSTRACT

By Hussam Saleem, MS.
Washington State University
December 2011

Chair: Pizhong Qiao

A structural health monitoring system that is able to detect and identify any damage in real time is essential to maintain the structural integrity and safety and to maximize the life span of the structure as much as possible. The objective of this study is to develop and improve the techniques used in structural health monitoring based on the dynamic properties of a plate structure. An E-glass/polyester plate was extensively tested in the healthy state as well as three damage cases. Polyvinylidene fluoride (PVDF) sensors with PZT actuator (PZT-PVDF) as a main system was used for acquiring the modal parameters experimentally. The Hammer-Accelerometer system was also considered. Moreover, the finite element (FE) was used to model the plate and implement the modal analysis. The curvature in the longitudinal direction (κ_x), in the transverse direction (κ_y), and the twist curvature (κ_{xy}) were measured using the PZT-PVDF system. Displacement was measured using the Hammer-Accelerometer system. The curvature measurements exhibited more sensitivity to damage than the displacement. On the other hand, using the PVDF-PZT system to measure the curvature is more susceptible to noise than the Hammer-Accelerometer system, which means that there is a trade-off between the sensitivity to damage and sensitivity to noise for the two systems. Ultimately, the results showed the superiority of the PVDF-PZT system. Three damage detection algorithms were tested

including the gapped smoothing method (GSM), the generalized fractal dimension (GFD) method and strain energy method (SEM). Five modes of vibration were selected for analysis; modes one through five in the FE, and modes three through seven in the experiment. Based on the curvature mode shapes, GSM and GFD performed better than SEM with GSM being superior above all in terms of damage detection, localization and sensor spacing effect. The use of the curvature in separate directions was investigated; the results concluded that using the curvature in the y-direction solely succeeded in detecting the first and second damage cases, and using the twist curvature detected the third damage case. Based on the displacement mode shapes, GSM performed best while GFD performed poorly in detecting the damage.

Table of Contents

List of figures

List of Tables

Chapter 1

INTRODUCTION

1.1 Background

Structural Systems, such as buildings, bridges, planes, trains, or any other, are susceptible to sudden damage, deterioration and aging. Therefore, a health monitoring system that is able to detect and identify any damage in real time in its earliest stage is essential to maintain the structural stability, integrity and to maximize the life span of the structure as much as possible.

Structural Health Monitoring (SHM) is the process of implementing damage identification for engineering structures. It involves the observation of a system over time using periodically sampled response measurements from an array of sensors. “This process involves the observation of a structure or mechanical system over time using periodically spaced measurements, the extraction of damage-sensitive features from these measurements and the statistical analysis of these features to determine the current state of system health.” [1]. For many years people have been performing vibration tests on large civil engineering structures. The dynamic characteristics of the structure contain useful information about its state.

There are four levels of damage identification, as follows [2] :

Level 1: Determination of the existence of damage;

Level 2: Determination of the geometric location of the damage;

Level 3: Quantification of the severity of the damage;

Level 4: Prediction of the remaining service life of the structure.

The term “damage detection method” is often used when the damage identification method only targets problems in levels 1 and 2.

Many damage detection methods have been developed over the years [3], and the local methods such as ultrasonic and X-ray methods are the most popular methods at present. All of these techniques have a drawback in needing the vicinity of the damage to be known a priori and that the portion of the structure being inspected is readily accessible by a labor or machine, which makes automation process almost impossible to perform, not mentioning that these methods are very time-consuming and costly. However the vibration-based damage identification methods have an advantage that lies in their global behavior, in which the damage can be identified in a system without regard to size or accessibility, in addition a system of automated real time damage identification becomes possible.

Vibration-based damage identification techniques are based on the idea that damage modifies both the physical properties of a structure (mass, stiffness and damping) as well as its dynamic characteristics (natural frequencies, damping ratios and mode shapes). Therefore, by examining the dynamic properties of a structure from structural vibration, any damage, including its location and severity, can be identified.

1.2 Objective

The general objective of this study is to develop and improve the techniques used in structural health monitoring based on the dynamic properties of a plate structure. Then, use different damage detection algorithms to process the data acquired from testing as well as from numerical simulation.

The following tasks are to be studied thoroughly:

1. Measure the curvature of composite plates using a PZT patch as an actuator and a mesh of PVDF films as sensors for both the healthy as well as the damaged structure.
2. Measure the displacement of composite plates using an impact hammer as an actuator and an

accelerometer as a sensor on each point within the plate for both the healthy as well as the damaged structure.

3. Create a finite element model of the plate, perform numerical analysis and obtain the curvatures as well as the displacements to the points of interest.
4. Input the data acquired into the algorithms and attempt to detect the damage.
5. Investigate and compare the output of each damage detection algorithm with different damage cases.
6. Compare the effectiveness of measuring the curvature mode shapes and displacement mode shapes.
7. Investigate the sensitivity of the damage detection algorithms to noise.
8. Development of an optimized pattern of sensors for maximum efficiency (sensor spacing).

1.3 Literature review

Significant work has been done in localizing damage with the vibration-based techniques [4]. Many of these techniques use modal parameters such as natural frequencies, damping factors, and mode shapes. The modal properties (i.e., natural frequencies, modal damping, modal shapes, etc.) have their physical meanings and are thus easier to be interpreted in damage detection than those abstract mathematical features directly extracted from the time or frequency domain. The vibration-based detection methods for 1-D beam-type structures have been extensively investigated by many researchers. Some of the methods have been generalized to a 2-D version that can be applied to plate-like structures.

Damage detection methods can be classified into four categories based on the data they require to detect the damage [2]:

- Natural frequency-based methods;

- Mode shape-based methods;
- Curvature/strain mode shape-based methods;
- Other methods based on modal parameters.

Natural frequency information has been used for the detection of damage [5] as well as for characterization of debonding [6], delaminations [7], and determination of elastic constants [8]. Natural frequency-based methods use the natural frequency change of structures as the basic feature for damage detection. The choice of the natural frequency change is attractive because the natural frequencies can be conveniently measured from just a few accessible points on the structure and are usually less contaminated by experimental noise. But it has several limitations such as complexity in structural modeling and damage and non-uniqueness of the solutions. In 1997, Salawu [9] presented an extensive review of publications before 1997 dealing with the detection of structural damage through frequency changes. It was concluded that the natural frequency changes alone may not be sufficient for a unique identification of the location of structural damage because cracks associated with similar crack lengths but at two different locations may cause the same amount of frequency change.

Compared to using natural frequencies, the advantages of using the mode shapes and their derivatives as a basic feature for damage detection are obvious. First, the mode shapes contain local information, which makes them more sensitive to local damages and enables them to be used directly in multiple damage detection. Second, the mode shapes are less sensitive to environmental effects, such as temperature, than natural frequencies [10]. Many damage identification methods have been developed based on direct or indirect use of measured mode shapes. Most of these methods take the mode shape data as a spatial-domain signal and adopt signal processing technique to locate damage by detecting the local discontinuity of mode shapes or their derivatives caused by damage. These methods can be roughly categorized into two types here: displacement mode shape-based methods and curvature mode shape-based methods.

It has been shown by many researchers that the displacement mode shape itself is not very sensitive to small damage, even with high density mode shape measurement [11-13]. As an effort to enhance the sensitivity of mode shape data to the damage, the curvature mode shape is investigated as a promising feature for damage identification. The curvature mode shape can be either obtained by direct measurement of strain mode shape or derived from the displacement mode shape. When the displacement mode shapes are acquired from modal testing, the central difference method or the Chebyshev polynomial approximation can be applied to the measured displacement mode shape to derive the curvature mode shape as follows [14, 15]:

1) Curvatures based on central difference method

The curvatures are calculated by a Laplacian operator in each normal direction (i.e., *x*, *y*) as well as the (*xy*) direction as

$$u_{xx}(x_i, y_j) = \frac{u(x_{i+1}, y_j) - 2u(x_i, y_j) + u(x_{i-1}, y_j)}{h_x^2} \tag{1.1}$$

$$u_{yy}(x_i, y_j) = \frac{u(x_i, y_{j+1}) - 2u(x_i, y_j) + u(x_i, y_{j-1})}{h_y^2} \tag{1.2}$$

$$u_{xy}(x_i, y_j) = \frac{u(x_{i+1}, y_{j+1}) - u(x_{i+1}, y_{j-1}) - u(x_{i-1}, y_{j+1}) + u(x_{i-1}, y_{j-1})}{h_x h_y} \tag{1.3}$$

where $u(x, y)$ is the displacement modeshape, $u_{xx}(x_i, y_j)$, $u_{yy}(x_i, y_j)$, $u_{xy}(x_i, y_j)$ are the curvetures in the $x, y,$ and xy directions, respectively, h_x, h_y is the step size in the x and y directions, respectively.

2) Curvatures based on Chebyshev polynomial approximation-

The following Chebyshev polynomial is used to avoid the error in calculating the curvature from differentiation (as used in the finite difference method),

$$u(x, y) = \sum_{i=1}^{N} \sum_{j=1}^{M} C_{ij} T_i(x) T_j(y) \tag{1.4}$$

where $T_i(x)T_j(\mathrm{y})$ are the first kind Chebyshev polynomials, and N, M are their orders. To map the standard Chebyshev polynomials from the plane domain of $\{\xi, \mu\} = [-1,1]$ x $[-1,1]$ to the plate domain of $\{x, y\} = [0, L_x]\ x\ [0, L_y]$, two linear transfer functions are defined

$$\xi = 2x/Lx - 1;\ \mu = 2y/Ly - 1$$

where Lx and Ly are the dimensions of the plate in the x and y directions, respectively. The Chebyshev polynomials of variables x and y are then written as

$$T_1(x) = \frac{1}{\sqrt{\pi}}\ , T_2(x) = \sqrt{\frac{2}{\pi}}.\left(\frac{2x}{L} - 1\right) \tag{1.5}$$

$$T_{i+1}(x) = 2\left(\frac{2x}{L} - 1\right) T_i(x) - T_{i-1}(x),\ \ i = 2,3, \ldots \ldots, N-1. \tag{1.6}$$

$$T_1(y) = \frac{1}{\sqrt{\pi}}\ , T_2(y) = \sqrt{\frac{2}{\pi}}.\left(\frac{2y}{L} - 1\right) \tag{1.7}$$

$$T_{i+1}(y) = 2\left(\frac{2y}{L} - 1\right) T_i(y) - T_{i-1}(y),\ \ i = 2,3, \ldots \ldots, N-1. \tag{1.8}$$

Assuming $P = N\ x\ M$ points on a rectangular grid and the Chebyshev polynomial approximation can be written in a matrix form

$$\langle u(x_i, y_j) \rangle_{p\times 1} = [T(x_i)T(y_j)]_{p\times p} \langle C_{ij} \rangle_{p\times 1}. \tag{1.9}$$

The coefficient vector $\langle C_{ij} \rangle$ can then be solved as

$$\langle C_{ij} \rangle_{p\times 1} = [T(x_i)T(y_j)]_{p\times p}^{-1} \langle u(x_i, y_j) \rangle_{p\times 1} \tag{1.10}$$

Then, by using the orthogonality property of Chebyshev polynomial, the curvature can be estimated by the second derivatives of the Chebyshev polynomials as

$$u_{xx}(x, y) = \sum_{i=1}^{N} \sum_{j=1}^{M} C_{ij} \frac{\partial T_i^2(x)}{\partial x^2} T_j(y)$$

$$u_{yy}(x, y) = \sum_{i=1}^{N} \sum_{j=1}^{M} C_{ij} \frac{\partial T_i^2(y)}{\partial y^2} T_i(x) \tag{1.11}$$

$$u_{xy}(x,y) = \sum_{i=1}^{N}\sum_{j=1}^{M} C_{ij}\frac{\partial T_i(x)}{\partial x}\frac{\partial T_j(y)}{\partial y}$$

The curvature mode shapes are also closely involved in the modal strain energy-based method [16-20].

Although above-mentioned methods directly use a single type of basic modal characteristics (modal frequencies or mode shapes) to identify damage, further research shows that the basic modal characteristics may not be the most effective and sensitive modal features for damage identification. In order to find an effective and sensitive dynamic feature for damage identification, extensive research effort has also been put into damage identification methods utilizing a combination of the basic modal characteristics or modal parameters derived from these characteristics, such as the modal strain energy [16-21], modal flexibility [22, 23] and uniform load surface [24-26].

In the past three decades, extensive research efforts have been invested into the field of structural damage identification. Most research efforts on damage identification methods still focus on damage localization (the second damage identification stage), since it sets the foundation of further identifying damage type and severity (the third and fourth stages). Some researchers also explored a unified approach to identify damage location as well as quantification.

1.4 Damage detection algorithms for plate structures

Even though numerous theories and algorithms have been developed, up to the present time, most methods are developed in the context of 1-Dimensional beam-type structures. Only limited researches on damage identification of 2-D plate-type structures can be found in the literature. For the existing 2-D damage identification algorithms, most of them are generalized from their 1-D version algorithms. A few 2-D damage detection algorithms are introduced in detail in this section. In this research, the applicability of these selected vibration-based identification techniques are investigated and compared in terms of damage sensitivity, the ability to localize and size the damage, noise immunity, and sensors density. The expected outcome is to have an optimized system of damage detection that can serve for a specific application.

1.4.1 Two-dimensional gapped smoothing method (GSM)

Ratcliffe [27] developed the gapped smoothing method for the one-dimensional beam, which uses only data obtained from the damaged structure to locate the damage. Later, the broadband data were engaged by using the frequency-dependent operating curvature shapes obtained from the FRF (Frequency Response Function) data. As a result, sensitivity is significantly increased for the identification of structural variability [28]. Yoon et al. [29] later developed the global smoothing method which used the mode shape data and mathematical mode shape functions of the beams to calculate the structural irregularity index. This approach showed an improvement over the gapped smoothening method by eliminating the edge effects.

Yoon et al. (2005) [30] then extended this method [29] to 2-D to be used for the plate-like structures.

In the 1-D method, the mode shapes are extracted from the damaged structure, and then converted to curvatures. A gapped cubic polynomial is then fit to the curvature mode shape.

Following the work of Yoon et al. [30], the gapped polynomial at the ith grid, C_i is represented by.

$$C_i = a_0 + a_1 x_i + a_2 x_i^2 + a_3 x_i^3 \tag{1.12}$$

where x_i is distance between the ith grid point and the beam end. The coefficients $a_0, a_1, a_2,$ and a_3 are determined explicitly using the neighboring curvatures from the damaged structure.

Finally, the Structural Irregularity Index is calculated by the squared difference polynomial function and the curvatures as follows.

$$\delta_i = \left(\emptyset''_{i,d} - C_i\right)^2 \tag{1.13}$$

where $\emptyset''_{\mathrm{i,d}}$ is the curvature at the ith grid point from the damaged structure, which can be calculated using a four-point backward/forward looking finite difference approximation that maintains a Bachmann-Landau order of magnitude of $O(h^2)$ as:

$$\emptyset''_i = (\emptyset_{i+1} + \emptyset_{i-1} - 2\emptyset_i)/h^2 \tag{1.14}$$

where $\emptyset''_{\mathrm{i}}$ is the mode shape obtained at the ith grid point and h is the uniform separation of the test grid.

For the two-dimensional gapped smoothing method (2-D GSM), instead of using a gapped line smoothening algorithm, a gapped surface smoothening algorithm is employed. First, the curvature mode shape $\nabla^2\psi_{i,j}$ is calculated from the displacement mode shape ψ_{ij} by the central difference approximation at grid point i, j as follows:

$$\nabla^2\psi_{i,j} = (\psi_{i+1,j} + \psi_{i-1,j} - 2\psi_{i,j})/h_x^2 + (\psi_{i+1,j} + \psi_{i-1,j} - 2\psi_{i,j})/h_y^2 \tag{1.15}$$

In this equation, i and j are the location indicators for the $x -$ and $y -$ directions, respectively, and hx and hy are the horizontal and vertical grid increments, respectively, for the grid points on the edges for which the forward or backward difference approximations are applied.

Next, the smoothed surface is obtained based on the curvature values at its neighboring grid points, by doing a curve fitting. Finally, the structural irregularity index is calculated as:

$$\delta_{i,j} = \left|\nabla^2\psi_{i,j} - C_{i,j}\right| \tag{1.16}$$

where $C_{i,j}$ is the smoothed curvature at point (i, j).

1.4.2 The Strain Energy Method (SEM)

Stubbs et al. [31] presented a method based on the decrease in modal strain energy between the healthy and damaged states as defined by the curvature of the measured mode shapes. The method can only be used for structures that can be simulated with beam-like elements, and it has the same behavior as an assemblage of beams.

Cornwell et al. [32] extended the one dimensional strain energy method to two dimensional plate-like structures. The method requires that the mode shapes before and after damage be known. They subdivided the plate into $Nx\,, Ny$ subdivisions in the x and y directions, respectively, as shown in Fig. 1, so that the damage can be specified in each of them. Then, the fractional strain energy remains relatively constant in undamaged sub-regions. In this case, by assuming that the Young's modulus and the Poisson's ratio are essentially constant over the whole plate for both the undamaged and damaged modes, Young et al. [33] introduced the strain energy for a given mode shape $\psi_i(x, y)$ in an isotropic plate as:

$$U = \frac{D_{jk}}{2}\int_0^b \int_0^a \left(\frac{\partial^2\psi_i}{\partial \mathrm{x}^2}\right)^2 + \left(\frac{\partial^2\psi_i}{\partial \mathrm{y}^2}\right)^2 + 2\nu\left(\frac{\partial^2\psi_i}{\partial \mathrm{x}^2}\right)\left(\frac{\partial^2\psi_i}{\partial \mathrm{y}^2}\right) + 2(1-\nu)\left(\frac{\partial^2\psi_i}{\partial \mathrm{x}\,\partial \mathrm{y}}\right)^2 dxdy \qquad (1.17)$$

where D is the bending stiffness of the plate ($D = Eh^3/12(1-\nu^2)$).

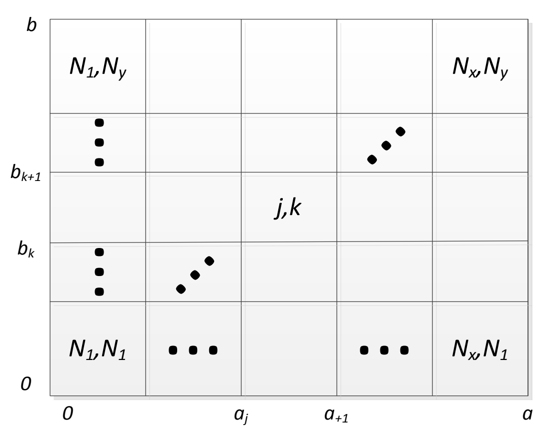

Figure 1.1 A schematic illustrating a plate's Nx X Ny sub-regions [32].

Then the energy associated with sub-region j, k for the ith mode is:

$$U_{ijk} = \frac{D_{jk}}{2}\int_{b_k}^{b_{k+1}}\int_{a_j}^{a_{j+1}}\left(\frac{\partial^2\psi_i}{\partial \mathrm{x}^2}\right)^2 + \left(\frac{\partial^2\psi_i}{\partial \mathrm{y}^2}\right)^2 + 2\nu\left(\frac{\partial^2\psi_i}{\partial \mathrm{x}^2}\right)\left(\frac{\partial^2\psi_i}{\partial \mathrm{y}^2}\right) + 2(1-\nu)\left(\frac{\partial^2\psi_i}{\partial \mathrm{x}\,\partial \mathrm{y}}\right)^2 dxdy \tag{1.18}$$

After summing over all the sub-regions, the total energy is:

$$U_i = \sum_{k=1}^{N_y}\sum_{j=1}^{N_x} U_{ijk} \tag{1.19}$$

The fractional energy at location j, k is defined to be:

$$F_{ijk} = U_{ijk}/U_i \quad \textit{and} \quad \sum_{k=1}^{N_y}\sum_{j=1}^{N_x} F_{ijk} = 1 \tag{1.20}$$

Therefore, the fractional strain energy $\mathrm{f_{ijk}}$ in sub-region (j, k) for the ith mode is given as:

$$f_{ijk} = \frac{\int_{b_k}^{b_{k+1}}\int_{a_j}^{a_{j+1}}\left(\frac{\partial^2\psi_i}{\partial \mathrm{x}^2}\right)^2 + \left(\frac{\partial^2\psi_i}{\partial \mathrm{y}^2}\right)^2 + 2\nu\left(\frac{\partial^2\psi_i}{\partial \mathrm{x}^2}\right)\left(\frac{\partial^2\psi_i}{\partial \mathrm{y}^2}\right) + 2(1-\nu)\left(\frac{\partial^2\psi_i}{\partial \mathrm{x}\,\partial \mathrm{y}}\right)^2 dxdy}{\int_0^b\int_0^a\left(\frac{\partial^2 w}{\partial \mathrm{x}^2}\right)^2 + \left(\frac{\partial^2\psi_i}{\partial \mathrm{y}^2}\right)^2 + 2\nu\left(\frac{\partial^2\psi_i}{\partial \mathrm{x}^2}\right)\left(\frac{\partial^2\psi_i}{\partial \mathrm{y}^2}\right) + 2(1-\nu)\left(\frac{\partial^2\psi_i}{\partial \mathrm{x}\,\partial \mathrm{y}}\right)^2 dxdy} \tag{1.21}$$

By doing the same procedure for the damaged mode shapes indicated with a (*), the damage index β at a sub-region can be obtained from:

$$\beta_{jk} = \sum_{i=1}^{m} f_{ijk}^{*} \,/\, \sum_{i=1}^{m} f_{ijk} \tag{1.22}$$

A normalized damage index can be obtained for the purpose of comparison using:

$$Z_{jk} = \frac{\beta_{jk} - \overline{\beta}}{\sigma_\beta} \tag{1.23}$$

where $\bar{\beta}$ and σ_β represent the mean and standard deviation of the damage indices, respectively. Usually, a damage detection criterion can be set when the normalized damage index Z_{ij} is larger than 2 [50].

It should be noted that the 2-D SEM is a model-based algorithm, requiring a relatively accurate numerical analytical model of the healthy structure, which is not feasible for almost all *in situ* structural tests.

1.4.3 Generalized Fractal Dimension (GFD)

The concept of a fractal and its relevant mathematical model were developed by Mandelbrot in 1968 [34]. If we take an object residing in Euclidean dimension D and reduce its linear size by $1/r$ in each spatial direction, its measure (length, area, or volume) would increase to $N = r^D$ times the original. D is called the fractal dimension (FD) of a fractal curve, and it can be expressed as [35, 36]

$$FD(x) = \frac{\log n}{\log n + \log\left[\frac{d(x_i, M)}{L(x_i, M)}\right]} \tag{1.23}$$

$$L(x_i, M) = \sum_{j=1}^{M} \sqrt{\left(y(x_{i+j}) - y(x_{i+j-1})\right)^2 + \left(x_{i+j} - x_{i+j-1}\right)^2}$$

$$d(x_i, M) = \max_{1 \le i \le M} \sqrt{\left(y(x_{i+j}) - y(x_{i+j-1})\right)^2 + \left(x_{i+j} - x_{i+j-1}\right)^2}$$

where $x = \frac{1}{2}(x_i + x_{i+M})$, $n = \frac{1}{\alpha}$, α is the average distance between successive points, x_i and y_i are the coordinate values of curve. The term M represents the sliding window dimension length. The dimension of a smooth curve is 1, and the more fractions the curve has, the larger the dimension of the curve is. The sharp peak of the FD curve indicates the location of the damage. Therefore, the fractal dimension has the potential to serve as a damage index to reveal the irregularity introduced by local damage in the structure. However, when the higher mode shape is considered, the above FD approach may give some misleading peak information in the location of the maximum and minimum points in a curve. To overcome this shortcoming, a new generalized fractal dimension (GFD) was defined by Wang and Qiao [37] as a modification of the FD method:

$$GFD_s(x) = \frac{\log n}{\log n + \log\left[\frac{d_S(x_i,M)}{L_S(x_i,M)}\right]} \tag{1.23}$$

$$L_s(x_i, M) = \sum_{j=1}^{M} \sqrt{\left(y(x_{i+j}) - y(x_{i+j-1})\right)^2 + S^2\left(x_{i+j} - x_{i+j-1}\right)^2}$$

$$d_s(x_i, M) = \max_{1 \le i \le M} \sqrt{\left(y(x_{i+j}) - y(x_{i+j-1})\right)^2 + S^2\left(x_{i+j} - x_{i+j-1}\right)^2}$$

where s is a scale parameter, as inspired by the wavelet transformation. Compared to the mode shape itself, the irregularity caused by the damage on the deformation mode shape is local and smaller, and it can be filtered as the sharp peak value of FD from the mode shape.

It should be noted that the GFD method is still a 1-D method, and when applying it to a plate like structure, the plate must be divided into slices. Each slice is assumed to behave like a beam. Then, the GFD is applied to each slice. Hadjileontiadis et al. [36] successfully applied the FD method to a thin plate with a crack lying parallel to one side of the plate. They considered a signal consisting of spatial data (i.e. displacement of a 2-D structure) from a 2-D vibration mode. The fundamental mode was only considered for the reasons mentioned earlier. The FD operator was applied to succeeding horizontal, vertical and diagonal 1-D slices of the 2-D vibration mode. The method was able to accurately identify the location and length of the crack. In addition, a noise test was performed, and it confirmed the ability of the method to identify the cracks in the presence of noise.

1.4.4 Uniform Load Surface (ULS)

Researchers have found that the modal flexibility can be sensitive to structural damage more than the currently used parameters such as stiffness, mass, and damping. Raghavendrachar and Aktan [23] applied the modal flexibility for a three span concrete bridge. They compared the results from using the natural frequency and mode shapes versus the modal flexibility. They concluded that the later has shown more sensitivity for local damages. Zhao and Dewolf [38] performed a similar but theoretical study and concluded the superiority through using the modal flexibility. Pandey and Biswas [22] proposed to base on directly observing the changes in the measured modal flexibility of a beam structure. Lu et al. [15] extended that study to include multi damage detection by proposing the modal flexibility curvature for multiple damage localization due to its high sensitivity to closely distributed structural damages. Zhang and Aktan [23] comparatively studied the modal flexibility and its derivative and proposed the uniform load surface (ULS). They suggested that the ULS has much less truncation effect and is less susceptible to experimental errors. This is because the summation of all of the modal coefficients of one mode is a way of averaging the random error in that mode at every measurement point.

Most damage detection methods are formulated in one-dimensional space, Therefore, they can only be applied to the beam-like structure or two-dimensional structures that can be dissembled into beam elements. Wu and Law [24] proposed an approach to compute the ULS curvature based on the Chebyshev polynomial approximation to decrease the errors rising from the differentiation process. They applied their approach to a plate structure and were able to detect the damage successfully.

For a structural system with n degrees-of-freedom (d.o.f.), the flexibility matrix can be expressed by superposition of the mass normalized modes ϕ_r [39]:

$$F = \sum_{r=1}^{n} \frac{\phi_r \phi_r^T}{\omega_r^2} \tag{1.24}$$

where ω_r is the *r*th natural frequency. It can be seen that as the frequency increases, the flexibility decreases substantially, so that the flexibility matrix converges quickly with several lower modes, which make it easier to approximate the matrix with a few lower modes (m) as:

$$F_T = [f_{k,l}] = \sum_{r=1}^{m} \frac{\phi_r \phi_r^T}{\omega_r^2} \tag{1.25}$$

where the modal flexibility, $f_{k,l}$, at the kth point under the unit load at point l, is the summation of the products of two related modal coefficients for each available mode

$$f_{k,l} = \sum_{r=1}^{m} \frac{\phi_r(k)\phi_r^T(l)}{\omega_r^2} \tag{1.26}$$

Then, the ULS is defined as the deflection vector under uniform load as:

$$U_T = \{u(k)\} = F_T.L \tag{1.27}$$

where $L = \{1 \quad 1 \quad \dots \quad \dots \quad 1\}_{1x\,n}^T$ then,

$$U_T = \{u(k)\} = \begin{bmatrix} f_{1,1} & f_{1,2} & \cdots & f_{1,n} \\ f_{21} & f_{2,2} & & f_{2,n} \\ \vdots & & \ddots & \vdots \\ f_{n,1} & f_{n,2} & \cdots & f_{nn} \end{bmatrix} \begin{Bmatrix} 1 \\ 1 \\ \vdots \\ \vdots \\ 1 \end{Bmatrix}$$

$u(k)$ is the modal deflection at point k under uniform unit load all over the structure that can be approximated as (assuming linearity of the system) [23]:

$$u(k) = \sum_1^n f_{k,l} = \sum_{r=1}^{m} \frac{\phi_r(k)\sum_{l=1}^{n}\phi_r^T(l)}{\omega_r^2} \tag{1.28}$$

After getting the ULS of the original mode shape, the curvature of the ULS can be acquired by one of the following three ways

1. Using the central difference method.
2. Using Chebyshev polynomial approximation to the measured displacement.
3. If the original mode shape was a direct measurement of curvature, we can skip the curvature calculation step and go directly to equation (1.29).

Finally, after the curvature has been acquired, the curvature changes between the damaged and undamaged structures will be investigated to detect the damage. Therefore, the damage index can be formulated as follows:

$$d(x_i, y_j) = \left[\propto_{xx} |u_{xx}^D - u_{xx}| + \propto_{yy} |u_{yy}^D - u_{yy}| + \propto_{xy} |u_{xy}^D - u_{xy}|\right]^2 \qquad (1.29)$$

where u_{xx}, u_{yy}, u_{xy} $u_{xx}^D, u_{yy}^D, u_{xy}^D$ are the measured curvature values of the intact structure and the damaged structure. $\propto_{xx}, \propto_{yy}, \propto_{xy}$ are the weights that can be set from 0 to 1 to account for the importance of the curvature in the corresponding direction.

1.4.5 2-D Continuous Wavelet Transform

Wavelets are localized waves, in other words signals with a zero average value that drop to zero after a few oscillations [40]. The first attempt to use the wavelet theory for crack identification was done by Liew and Wang [41], and they have successfully detected a non-propagating edge crack in a beam. Afterwards, more researchers investigated damage detectability using the wavelet theory for beam structures [42-44]. Later the method was extended to include plate-like structures, Chang and Chen [45] applied a 1-D wavelet to a plate structure with damage represented by the reduced stiffness. The wavelet was applied to slices in both the longitudinal and the transverse directions, respectively. Douka et al. [46] applied a 1-D continuous wavelet transform to a plate with an all-over part-through crack parallel to one edge. Both the location and depth of the crack were estimated successfully. Although the latter was successful in detecting and locating the damage, the method still a one dimensional method that can be applied to slices in both direction of a plate structure, thus ignoring the coupling effect between these slices.

However, Loutridis et al. [47] used a 2-D discrete wavelet transform (DWT) and applied it to the vibration mode of a cracked plate, and both the location and extent of the crack were accurately measured. The wavelet coefficients of the detail of the first level decomposition were used to determine the location. Kim et al. [48] used a multi-resolution analysis of two-dimensional Haar wavelet to solve a damage index (DI) equation introduced within the context of elasticity, and this technique requires only a few of the lower mode shapes before and after a small damage event in order to detect, locate, and size damage on a plate. Rucka [49] used the Gaussian wavelet for one-dimensional problems and reverse biorthogonal wavelet for two-dimensional structures to locate damage in a plate. The wavelet was formulated using a 2-D discrete wavelet. The wavelets in both the longitudinal and transverse directions were taken as tensor products of a 1-D scaling function and 1-D wavelets function. Then, the transform were implemented separately in both directions. A modulus and angle of the wavelet transform were defined to combine the information of two transforms and adopted as the indicator of damage.

Two types of wavelet transform should be addressed here: the continuous wavelet transform (CWT), and the discrete wavelet transform (DWT). The first delivers accurate resolution of wavelet coefficients for damage detection; therefore, it is mostly used for feature detection and analysis in signals; whereas the DWT provides a fast algorithm of evaluating wavelet coefficients in discrete resolutions, and it is thus more appropriate for data compression and signal reconstruction [50].

One limitation should be addressed is the need for high resolution mode shape measurement, which is difficult to accomplish with the traditionally used sensors such as an accelerometer or a PVDF without doing a large number of tests to increase the accuracy and decrease the noise effects. On the other hand, the new advanced instruments, such as scanning laser vibrometer (SLV) [51] [52], can provide such high resolution and overcome the limitations.

Fan and Qiao [53] presented a 2-D CWT-based method for damage detection in plates. The 2-D CWT of the mode shapes of a plate is applied and used to identify the location and shape of damage in the plates. The algorithm of the 2-D CWT was based on the formulation by Antoine et al. [50], and it is formulated as follows:

Like in 1-D case the, the 2-D wavelet is an oscillatory, real or complex-valued function $\psi(\vec{x}) \in L^2(\mathbb{R}^2, d^2\vec{x})$ that satisfies the admissibility condition on real plane $\vec{x} \in \mathbb{R}^2$. $L^2(\mathbb{R}^2, d^2\vec{x})$ denotes the Hilbert space of measurable, square integrable 2-D functions. If ψ is regular enough as in most cases, the admissibility condition can be expressed as:

$$\hat{\psi}(0) = 0 \Leftrightarrow \int_{\mathbb{R}^2} \psi(\vec{x})\, d^2\vec{x} = 0 \qquad (1.30)$$

where $\hat{\psi}(\vec{k})$ is the Fourier transform of $(\vec{x})$, and $\vec{k} \in \mathbb{R}^2$ is the spatial frequency.

Function $\psi(\vec{x})$ is called a mother wavelet and usually localized in both the position and frequency domains. The mother wavelet ψ can be transformed in the plane to generate a family of wavelet $\psi_{\vec{b},a,\theta}$. A transformed wavelet $\psi_{\vec{b},a,\theta}$ under translation by a vector $\vec{b}$, dilation by a scaling factor a, and rotation by an angel θ can be derived as

$$\psi_{\vec{b},a,\theta}(\vec{x}) = a^{-1}\psi\left(a^{-1}r_{-\theta}\left(\vec{x}-\vec{b}\right)\right) \qquad (1.31)$$

Given a 2-D signal $s(\vec{x}) \in \mathrm{L}^2(\mathbb{R}^2, d^2\vec{x})$, its 2-D CWT (with respect to the wavelet ψ) $S(\vec{b}, a, \theta) \equiv T_\psi s$ is the scalar product of s with the transformed wavelet $\psi_{\vec{b},a,\theta}$ and considered as a function of $(\vec{b}, a, \theta)$ as:

$$S\left(\vec{b}, a, \theta\right) \equiv \langle \psi_{\vec{b},a,\theta}, s\rangle = a^{-1}\int_{\mathbb{R}^2} \overline{\psi\left(a^{-1}r_{-\theta}\left(\vec{x}-\vec{b}\right)\right)}\, s(\vec{x}) d^2\vec{x} =$$

$$a\int_{\mathbb{R}^2} \overline{\hat{\psi}\left(ar_{-\theta}\left(\vec{k}\right)\right)}\, e^{i\vec{b}.\vec{k}}\hat{s}\left(\vec{k}\right) d^2\vec{k} \qquad (1.32)$$

Because Eq. (1.32) is essentially a convolution of a 2-D signal s with a function $\vec{b}, a, \theta$ of zero mean, the transform $S(\vec{b}, a, \theta)$ is appreciable only in regions of parameter space $(\vec{b}, a, \theta)$ where $\psi_{\vec{b},a,\theta}$ matches the features of signal s. When ψ is well localized in the spatial frequency domain and position domain, the 2-D CWT acts as a local filter in parameter space.

In the 1-D wavelet analysis, due to its intrinsic characteristic of keeping constant relative bandwidth, the wavelet analysis is more advantageous in detecting singularities at high frequency or small scale than, e.g., the windowed Fourier transform. The same argument applies to the 2-D wavelet analysis. When appropriately designed, the 2-D wavelet transform is also an effective singularity scanner for 2-D signals. As in the 1-D case, the vanishing moments of the wavelet play an important role in detection of singularities.

A wavelet ψ usually has vanishing moments $N \geq 1$:

$$\int x^{\alpha} y^{\beta} \psi(\vec{x})\, d^2\vec{x} = 0, \vec{x} = (x, y), \;\; 0 \leq \alpha + \beta \leq N \tag{1.33}$$

This property improves its efficiency at detecting singularities. A wavelet with vanishing moments N will not see the smooth part of the signal but only detects singularities in the (N + 1)th derivatives of the signal.

One typical example of 2-D wavelets is the 2-D Mexican hat wavelet, which is simply the Laplacian of a 2-D Gaussian. Another example is the 2-D Morlet wavelet, which is the product of a plane wave and a Gaussian window. Both the wavelets can find their well-known counterpart in the 1-D wavelet analysis. Their expressions in the position domain are given as follows:

The 2-D Mexican hat wavelet:

$$\psi(\vec{x}) = (2 - |\vec{x}|^2 exp\left(-\frac{1}{2}|\vec{x}|^2\right) \tag{1.34}$$

The 2-D Morlet wavelet:

$$\psi(\vec{x}) = exp\left(i\overrightarrow{k_0}.\vec{x}\right)exp\left(-\frac{1}{2}|\vec{x}|^2\right) + \text{correction term} \tag{1.35}$$

As already discussed before it has been shown that the displacement mode shape is not so sensitive to small damages [54]. Even when using high resolution measurements techniques like the scanning laser vibrometer. Therefore the derivatives of the displacement mode shape were investigated for damage detection [30], and they were proved to be sensitive and superior over the displacement mode shape. However, the differentiation is usually done through numerical methods such as the Laplace operator. But using such methods has the tendency to enhance high frequency noise, hence arouse the need for a filtering process to compensate for such an effect. One of the famous methods is the Gaussian filtering technique, which is basically obtained by convolving the differentiated mode shape $s(x, y)$ with a Gaussian $g(x, y)$ to get the desired signal as:

$$\overline{s} = g(x, y) * \left(\frac{\partial}{\partial x}\right)^m \left(\frac{\partial}{\partial y}\right)^n s(x, y) \tag{1.36}$$

where (*) denotes the convolution operator. The 2-D Gaussian $g(x, y)$ is defined as

$$g(x, y) = exp\left(-\frac{|\vec{x}|^2}{2\sigma^2}\right) = exp\left(-\frac{x^2+y^2}{2\sigma^2}\right), \vec{x} = (x, y) \tag{1.36}$$

Then, using the property of convolution

$$\overline{s} = g(x, y) * \left(\frac{\partial}{\partial x}\right)^m \left(\frac{\partial}{\partial y}\right)^n s(x, y) = \left(\frac{\partial}{\partial x}\right)^m \left(\frac{\partial}{\partial y}\right)^n g(x, y) * s(x, y) \tag{1.37}$$

Then, if we adopt the derivative of 2-D Gaussian as the mother wavelet, and rewrite Eq. (1.32) as a convolution, we can get

$$S(\vec{b}, a, \theta) \equiv \langle\psi_{\vec{b},a,\theta}, s\rangle(\vec{b}) = \left(\left(\frac{\partial}{\partial x}\right)^m \left(\frac{\partial}{\partial y}\right)^n g_{a,\theta} * s\right)(\vec{b}) = \tilde{s}_{a,\theta}(\vec{b}) \tag{1.38}$$

Therefore, the desired differentiated and filtered signal can be obtained by a 2-D wavelet transform of the original mode shape with the derivative of 2-D Gaussian as the wavelet.

In conclusion, the GSM, GFD and SEM are selected for this study. The decision is based on the fact that all these three methods are the damage index-based methods, which means that the damage is represented by a peak on a flat surface, making them comparable to each other. While the ULS and 2D-CWT represents the damage as an irregularity on a surface, and the 2D-CWT method requires high resolution data which may not be available using the current experimental setup.

Chapter 2

EXPERIMENTAL MODAL TESTING

2.1 Introduction

Experimental program was conducted to extract the dynamic parameters required to evaluate the damage detection algorithms and their effectiveness in different damage cases. Experimental Modal Analysis was utilized to achieve the goal. Two types of sensors were used in the process, Accelerometer and Polyvinylidene Fluoride (PVDF) films. The accelerometer behaves as a damped mass on a spring. When the accelerometer experiences acceleration, the mass is displaced to the point that the spring is able to accelerate the mass at the same rate as the casing. The displacement is then measured to give the acceleration. Piezoelectric materials are used to manufacture some of the components of the accelerometer; they are used to convert the mechanical motion to electrical signal that can be read using the data acquisition system. On the other hand, PVDF is a highly non-reactive and pure thermoplastic fluoropolymer that has strong piezoelectricity [55]. The latter detect the motion in either tension or compression; therefore, it measures the strain in surfaces. Impact hammer and Lead Zirconate Titanate (PZT) ceramic patch were used as actuators; the hammer has a load cell attached to its head to measure the input force, and whenever it is used to impart the proper excitation to the system while measuring the input force to be used later in the modal analysis. A surface-bonded PZT patch exerts its excitation as bending moment (according to the size, shape and mounting of the PZT in this test) when charged with electricity. Two systems were created using a combination of the actuators, sensors mentioned, i.e., PZT-PVDF system and Hammer-Accelerometer system. In the PZT-PVDF system, the PZT was used as an actuator and PVDF films as sensors at each point of the plate mesh. The outcome of this system is strain mode shapes. While in the Hammer-Accelerometer system, the hammer is used as an actuator and the accelerometer as a sensor. The outcome results in the displacement mode shapes.

2.2 Modal Analysis of FRP Composite Plates

Composite structures are classified into three categories [56]: particulate composite structures, which consist of particles of various shapes and sizes dispersed randomly and embedded within a matrix; continuous fiber composite structures, which consist of a matrix, embedded and reinforced with long and continuous fibers; and short fiber composites, which contain short discontinuous fibers embedded within a matrix.

The composite laminates in general consist of thin layers, or laminae, which can be orthotropic, transverse isotropic or isotropic in behavior. A number of layers of laminae are stacked together with arbitrary or specified ply-orientation angles. The configuration indicating the ply make-up is referred to as its lay-up [56].

In this study, the test specimen is a pultruded FRP plate manufactured by Creative Pultrusions, Inc., Alum Bank, PA (CP). The plate is made of E-glass/thermoset polyester (1525 series). The latter contain 60% glass by weight. The mechanical properties of the plate were provided by the manufacturer, and they are shown in Table 2.1. The dimensions were measured physically from the plate, and they are 19 in. $\times$ 10 in. $\times$ 0.125 in. in length, width and thickness, respectively. A mesh was created with 180 points spaced at one inch in both directions (see Figure 2.1). The layup of the composite is shown in Figure 2.2.

Table 2.1 Material properties of the E-glass fiber composite plate

ρ	0.065 lb/in^3
E_x	1800000 psi
E_y	1000000 psi
v_{xy}	0.32
G_{xy}	351000 psi
G_{xz}	351000 psi
G_{yz}	324000 psi

where

ρ : density.
E_x : Modulus of elasticity in the x-direction.
E_y : Modulus of elasticity in the y-direction.
G_{xy} : Shear modulus in the xy plane.
v_{xy} : Poisson's ratio.

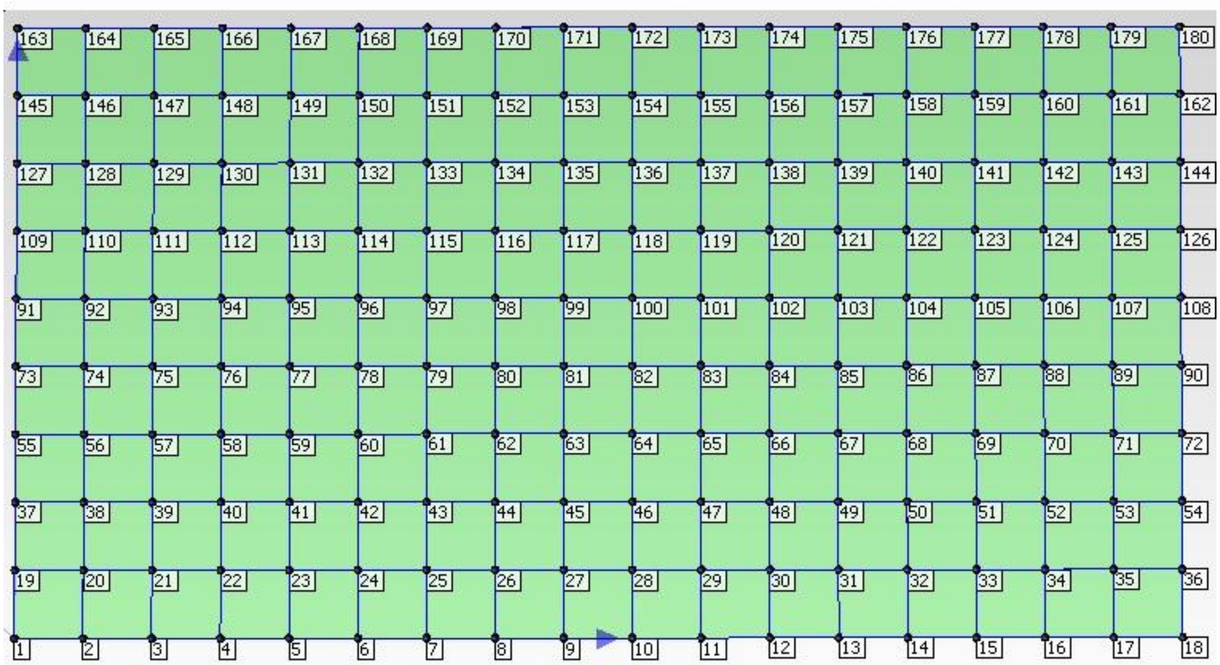

Figure 2.1 FRP plate mesh

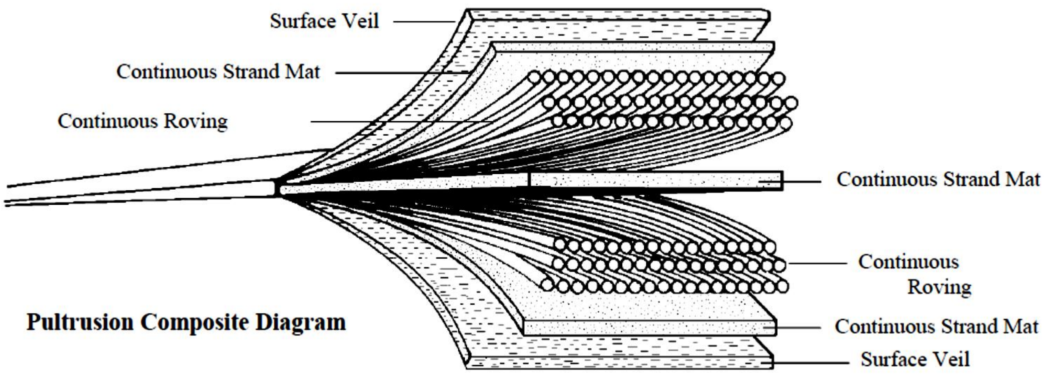

Figure 2.2 Typical Lay-up of pultruded FRP laminated plates [57]

2.2.1 Experimental modal analysis

Modal analysis is the process where a system is described in terms of its dynamic properties including the modal frequencies, damping and mode shapes. It employs these dynamic properties to build a mathematical model for its dynamic behavior, i.e., the modal model of the system [58].

Modal testing is an experimental technique which is used to derive the modal model of a system. In this technique, both the applied force (e.g., from either the impact hammer or the PZT) and the response (e.g., from the accelerometer or the PVDF films) of the structure due to the applied force are measured simultaneously. Then, the measured time data are transformed from the time domain to the frequency domain using a Fast Fourier Transform algorithm by means of computer software (e.g., MATLAB). As a result, the frequency response function (FRF) is obtained, and it represents the ratio of the output response of a structure due to an applied force (output/input) [58]. The type of FRFs produced depends on the kind of sensor(s) used. The curvature FRFs and displacement FRFs are two common types.

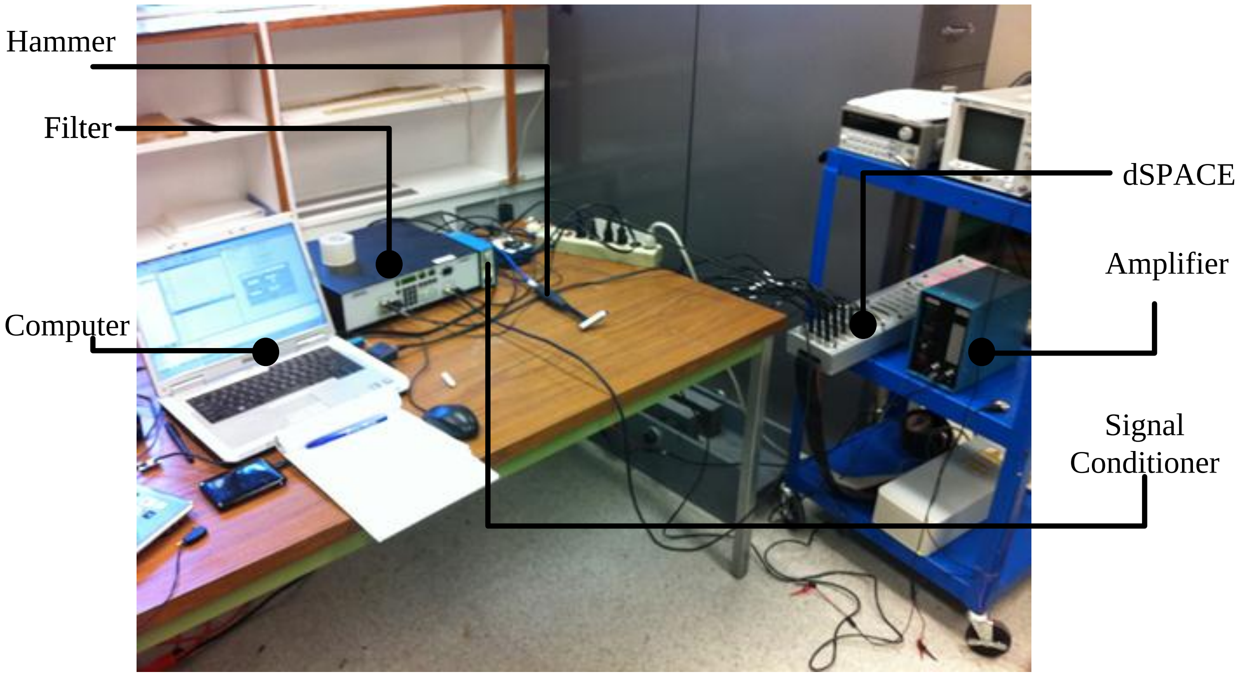

Figure 2.3 Experimental set-up

The FRF measurement can be implemented depending on the system (Figure 2.3) used. In this study, two sensor-actuator systems are considered, and the details are introduced as follows:

2.2.1.1 PZT-PVDF system (see Figure 2.4), in which the structure is excited with a measured force at one location of the structure by the surface-bonded PZT actuator and the vibration responses at all other locations of interest are measured with the PVDF thin film sensors (Roving sensor or Roving Response Test Scenario). The following procedure was followed to implement the test.

a. The experiment instructions are programmed using the data acquisition dSPACE software to define all the parameters related to the acquisition process such as defining which port represent which data.
b. dSPACE is used to generate a sweep sinusoidal signal (Chirp signal) with a frequency that increases from 0 to 500 Hz in the first 10 seconds and then decreases from 500 to 0 Hz in the next 10 seconds (bi-directional signal).
c. The signal is then amplified through a power amplifier and delivered to the PZT actuator.
d. dSPACE is used again to collect the signal data in time domain from all the PVDF films (in the *x*, *y* and *xy* directions as shown in Figure 2.5) attached to the plate. 18 PVDF sensors were used per column, and there were 10 columns in the plate, leading to a total of 180 reading points with nine PVDF sensors reading and collecting the data at each time).
e. Fast Fourier Transform is then used to transform the data from the time domain to the frequency domain. The FRFs are obtained and plotted using MATLAB. The time domain, frequency domain, and FRF plots for one slice of the plate are shown in Figures 2.6, 2.7 and 2.8, respectively.

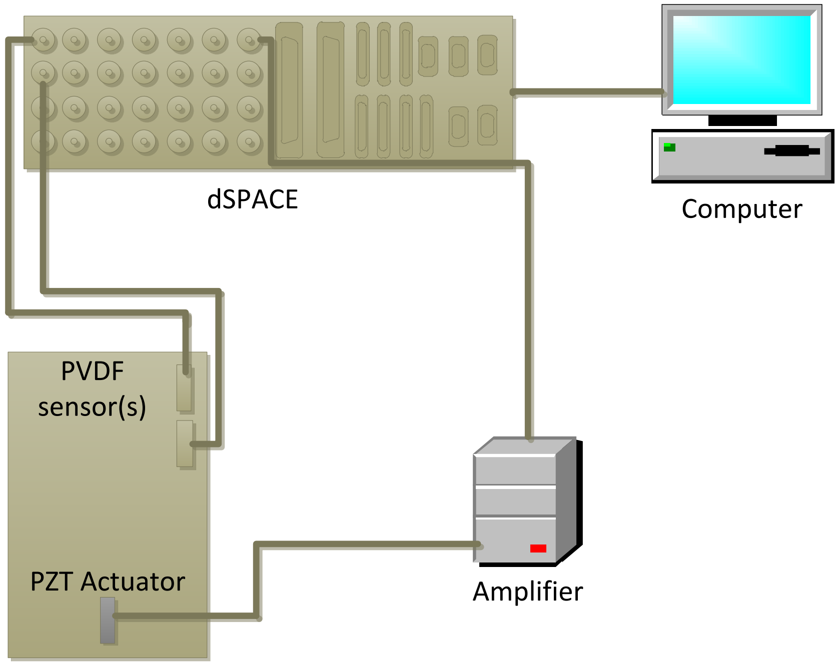

Figure 2.4 PZT-PVDF system components

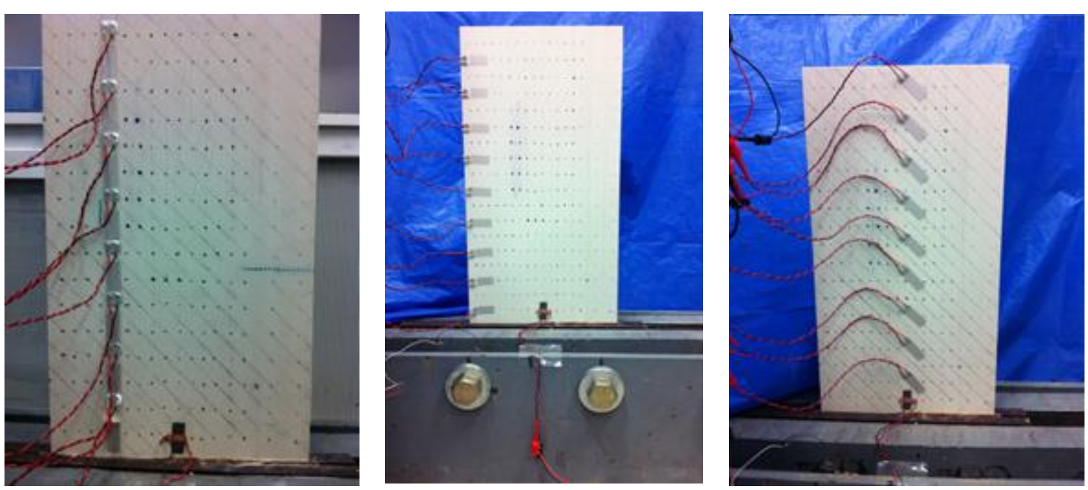

(a) (b) (c)

Figure 2.5 Sensor attachments to the FRP plate in the x, y and xy directions, respectively

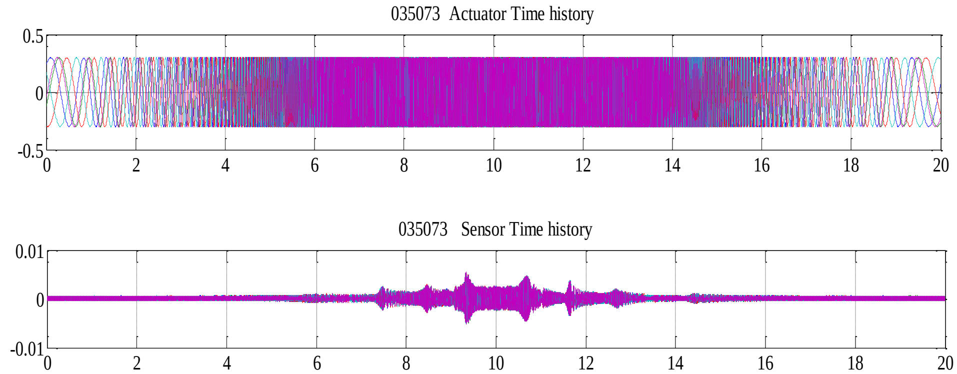

Figure 2.6 Time history plot for the actuator and sensor signals

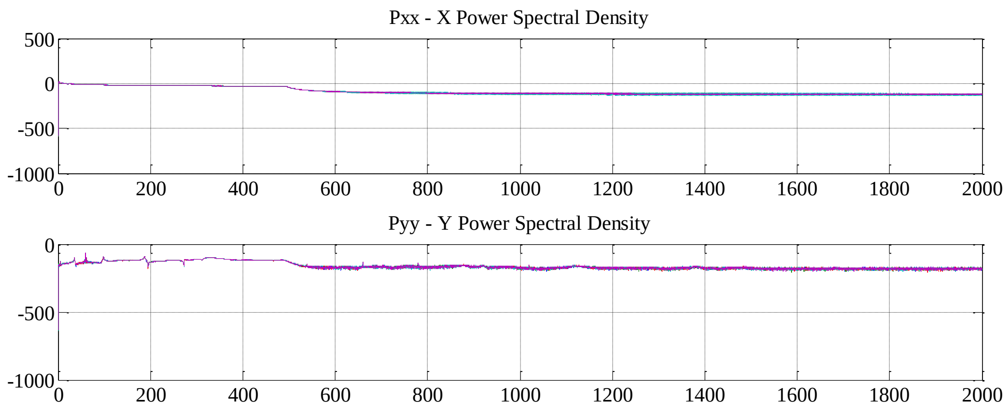

Figure 2.7 Frequency domain power spectral density for the actuator and sensor signals

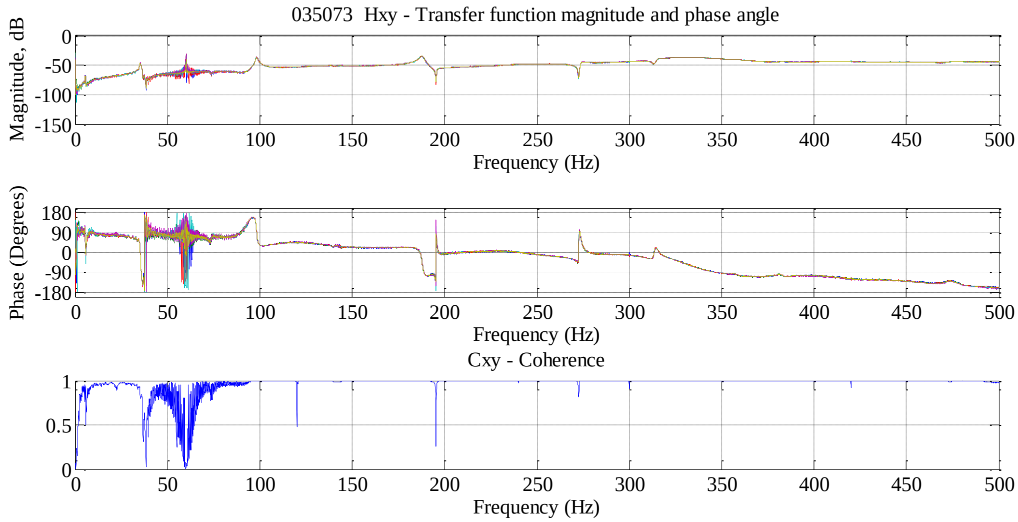

Figure 2.8 Frequency Response Function (FRF)

2.2.1.2 Hammer-Accelerometer system (see Figure 2.9), where an accelerometer sensor is fixed in one location while the plate is excited in all other locations of interest by the impact hammer (Roving Actuator or Roving Impact Test Scenario) as shown in Figure 2.10. This is the most common type of testing. In this test, the accelerometer (sensor) is fixed at a single DOF, and the structure is impacted by the hammer at as many DOFs as desired to define the mode shapes of the structure. Impact testing is a fast, convenient, and low cost way of finding the dynamic modes of machines or structures [59]. The following procedure is used to implement the test with the Hammer-Accelerometer system:

a. The experiment is programmed using the data acquisition dSPACE software.
b. A modally tuned ICP® impact hammer is used to excite the plate at each point within the area of interest.
c. The signal from the hammer and the accelerometer has to pass through a signal conditioner, in which signals are normalized and filtered to levels suitable for analog-to-digital conversion

read by computerized devices. Then, both the actuator and sensor analog signals must be filtered to assure not to include the unwanted higher frequencies (> 500 Hz) into the analysis frequency range.

d. dSPACE is used to collect the signal data in the time domain from the hammer as well as the Accelerometer.

e. Fast Fourier Transform is then used to transform the data to the frequency domain. The FRFs are obtained and plotted using MATLAB.

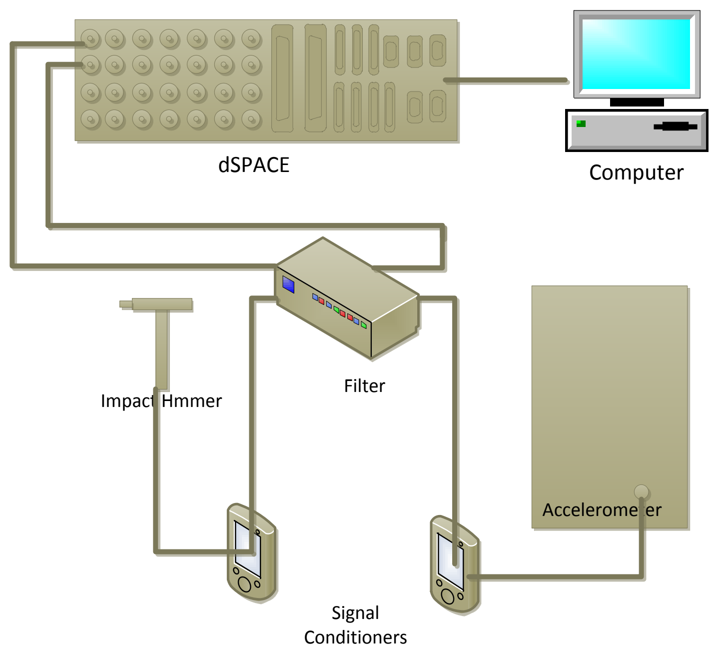

Figure 2.9 Hammer-Accelerometer system components

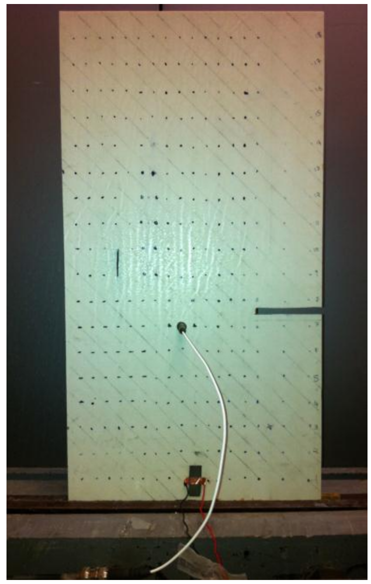

Figure 2.10 Attachment of accelerometer to the FRP plate

After acquiring the FRFs for all the points of interest, the next step is to calculate the modal parameters that include the frequencies, damping ratios and mode shapes for each mode of vibration. The fundamental of modal analysis using the measured FRF data is to curve-fitting the data using a predefined mathematical model of the measured structure.

The methods used to acquire the modal parameters can be classified into two categories: the Single-Degree-Of-Freedom (SDOF) methods, and the Multi-Degree-Of-Freedom (MDOF) methods. The SDOF methods are based on the SDOF assumption, which states that the FRF is dominated by the contribution of a specific mode of vibration neglecting all the others; therefore, they can easily be applied to obtain the modal parameters for each mode, provided that the modes are well separated. On the other hand, the MDOF methods consider the effect of all the modes simultaneously [58]. The MDOF methods are useful in case of the existence of two close modes of vibration. In this test, the software ME'scope was utilized to perform modal analysis, and it offers both kinds of modal analysis for the SDOF and the MDOF methods. In particular, the MDOF-based Polynomial method is used. An example of the curve fitting process using ME'scope is shown in Figure 2.11. The acquired displacement mode shape of a damaged plate generated by ME'scope is shown in Figure 2.12. After getting the modal parameters, the software attempt to save the mode shapes which are exported into MATLAB for algorithm application.

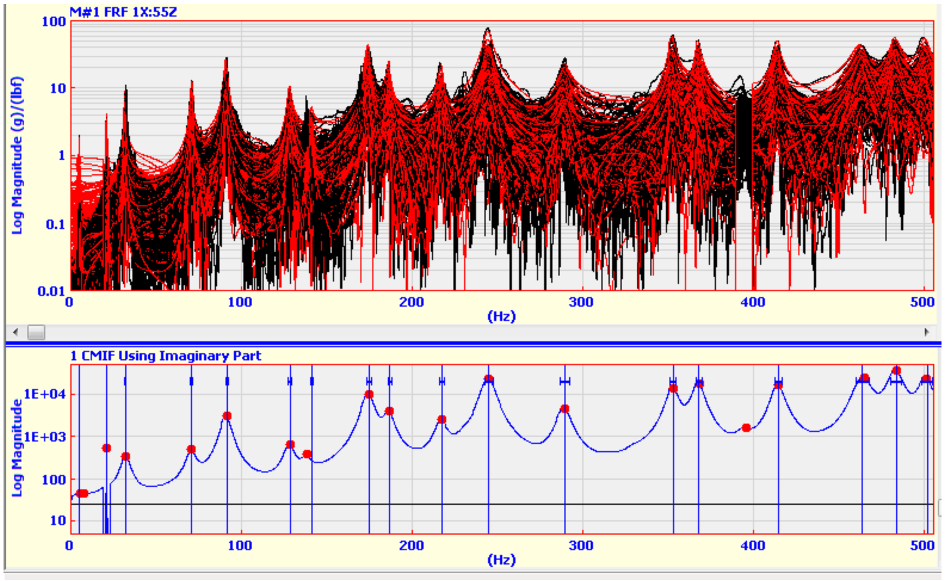

Figure 2.11 Modal parameter extraction using ME'scope

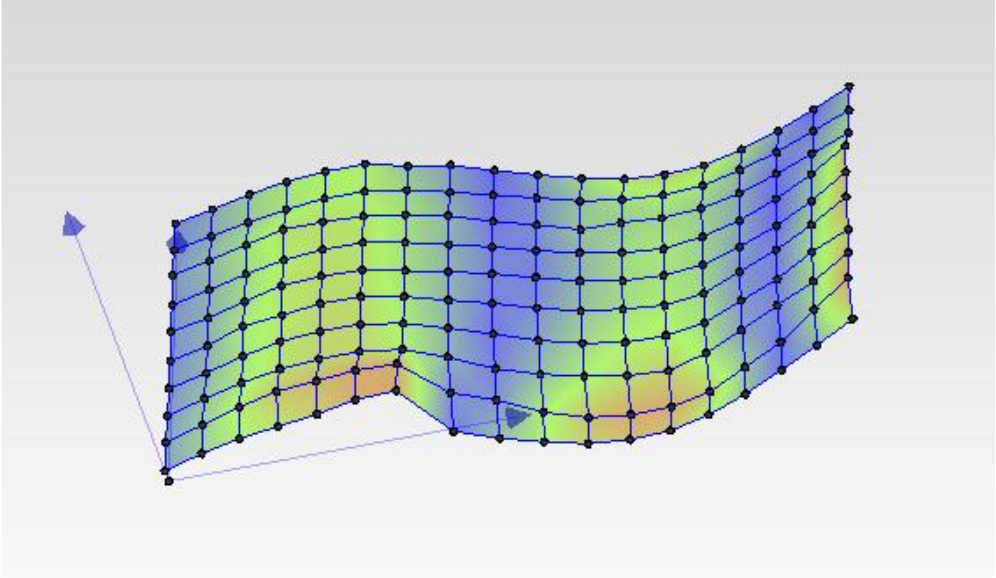

Figure 2.12 Displacement mode shape (3rd mode)

2.3 Experiment of an FRP Composite Plate

The procedure explained above was applied to the specimen. Four cases were considered (see Figure 2.13): one healthy (H) and three damage (D1, D2 and D3) cases. The first damage (D1) is an edge saw-cut, and the second (D2) was created to simulate a manifestation of the first damage. While the third damage case (D3) is a hole in the plate. The cantilever boundary condition was used for all the cases for the comparison purposes. For the healthy plate as well as the first damage case, the PVDF-PZT system was used to extract the curvatures only. While for the second and the third damage cases, both the sensor-actuator systems were used to extract the curvatures. In the Hammer-Accelerometer system, the displacement is measured first and used to compute the curvature.

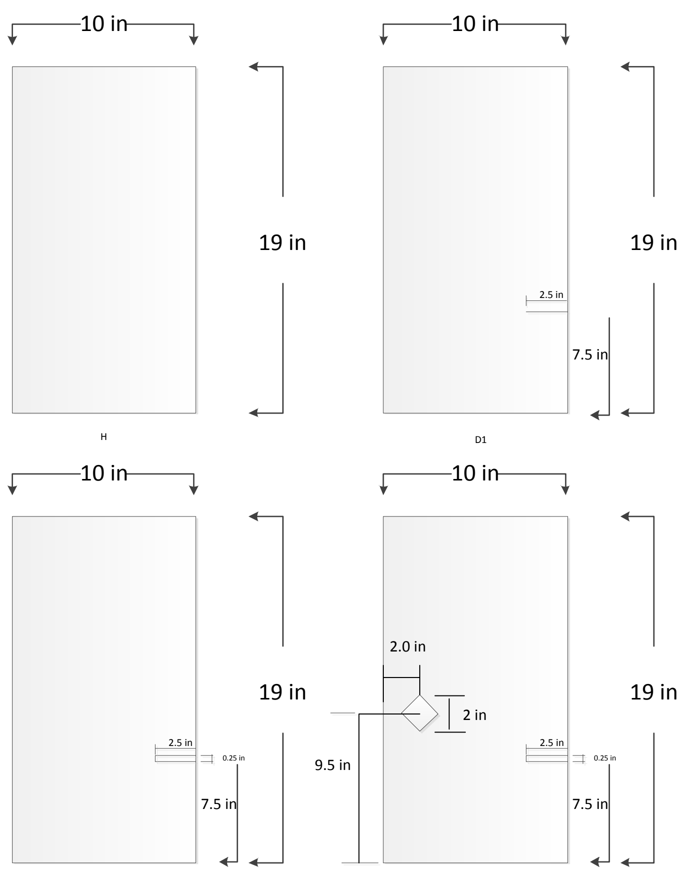

Figure 2.13 Four damage cases: H, D1, D2, and D3

2.3.1 Experimental Results

The results of the experiment conducted on the FRP plate are presented in this section. The frequency of each mode of vibration at different damage scenarios is given in Table 2.2, and it can be seen that there is a slight change in the values as the damage severity changes. As expected, the frequency is inversely proportional to damage severity.

As mentioned before the in the PVDF-PZT system, the strain is being measured. Using strain transformation and rosette gage theory, the longitudinal and transverse strains are directly measured, but the shear strain should be computed using the following equation,

$$\varepsilon_{xy} = 2 * \varepsilon_{45} - (\varepsilon_x + \varepsilon_y)$$

where ε_{45} is the extensional strain measured in 45 degrees.

The mode shapes of five modes of vibration are shown in Tables 2.3 to 2.6. The first two modes were ignored due to the presence of high ambient noise at low frequency (less than 50 Hz). Based on the measurement from the PVDF-PZT system, the curvatures in the *x*, *y* and *xy* direction were obtained. The displacements were obtained from the Hammer-Accelerometer system. Because the curvature is related to the second derivative of the displacement, the considered sensor-actuator systems can validate one another. Moreover, a numerical study was performed to simulate the same four cases of the plate using ABAQUS, and the results confirmed the validity of both the methods.

Table 2.2 Frequency values for the first five modes at different damage cases.

	Frequency for each Damage Case			
Mode No.	H	D1	D2	D3
1	5.54	5.31	5.17	5.10
2	35.9	33.8	32.8	32.0
3	98.9	95.0	92.3	91.0
4	144	132	129	127
5	189	181	177	174

Table 2.3 Mode shapes of the Healthy plate

<table>
<tr><th>EXP (κ_x)</th><th>EXP (κ_y)</th><th>EXP (κ_{xy})</th></tr>
<tr>
<td>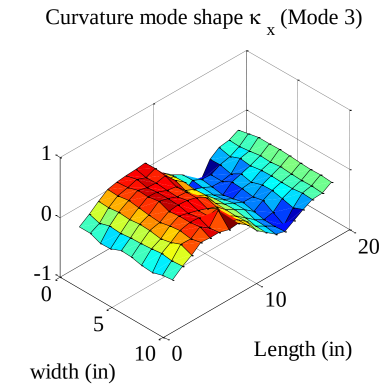
</td>
<td>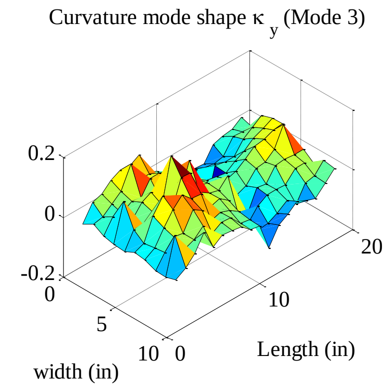
</td>
<td>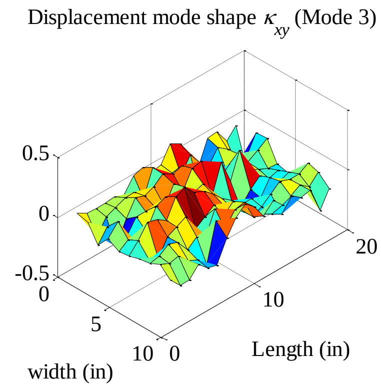
</td>
</tr>
<tr>
<td>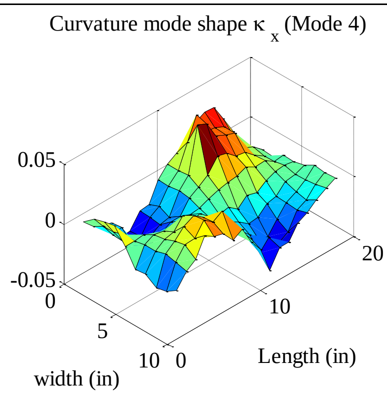
</td>
<td>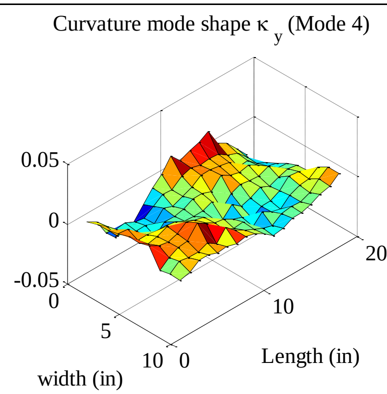
</td>
<td>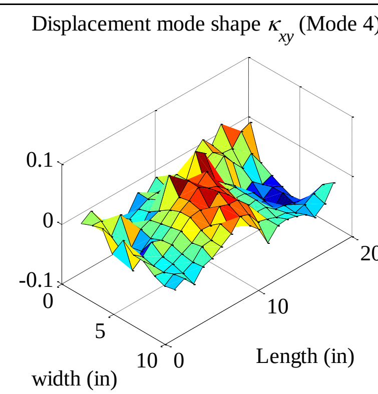
</td>
</tr>
</table>

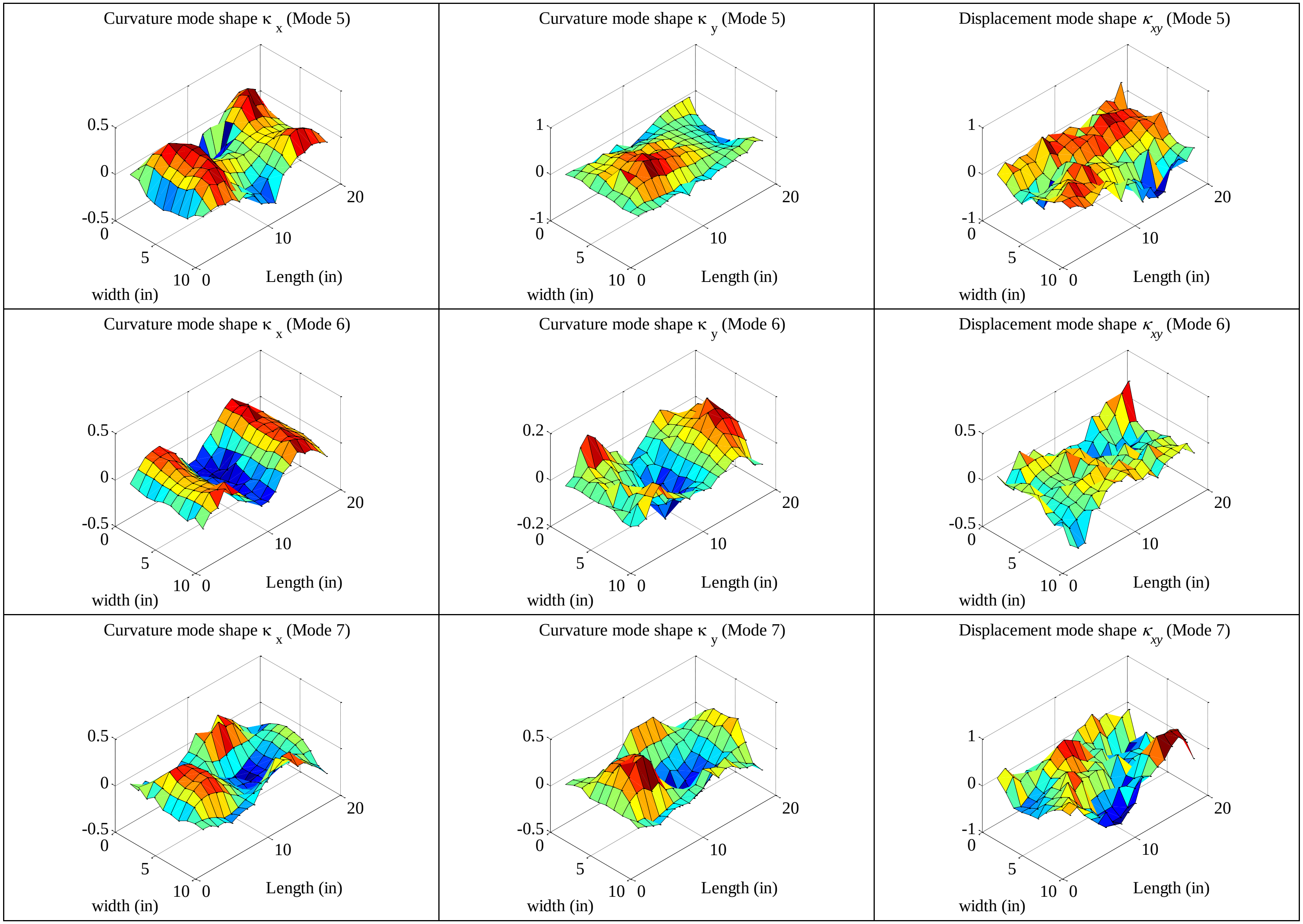

Curvature mode shape κ x (Mode 5)
Curvature mode shape κ y (Mode 5)
Displacement mode shape κxy (Mode 5)
Curvature mode shape κ x (Mode 6)
Curvature mode shape κ y (Mode 6)
Displacement mode shape κxy (Mode 6)
Curvature mode shape κ x (Mode 7)
Curvature mode shape κ y (Mode 7)
Displacement mode shape κxy (Mode 7)
width (in)
Length (in)

Table 2. 4 Mode shapes of the damaged plate (D1)

EXP (κ_x)	EXP (κ_y)	EXP (κ_{xy})
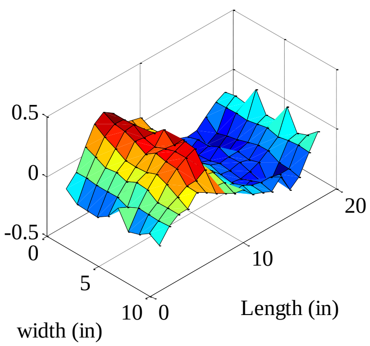	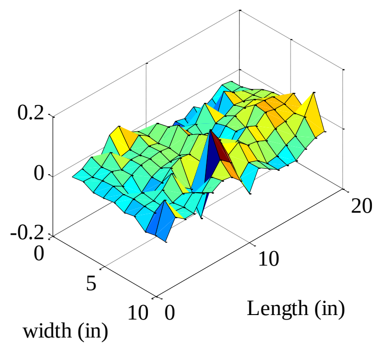	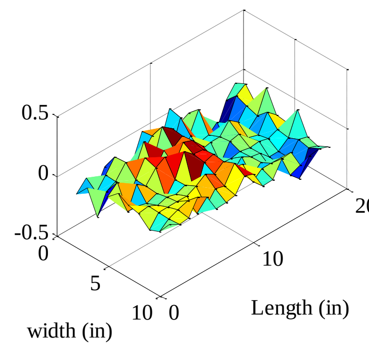
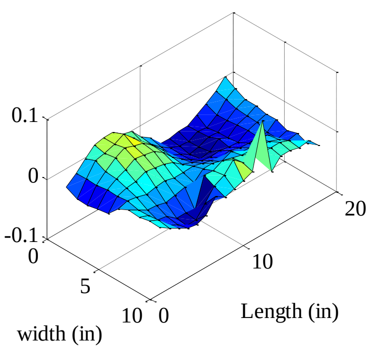	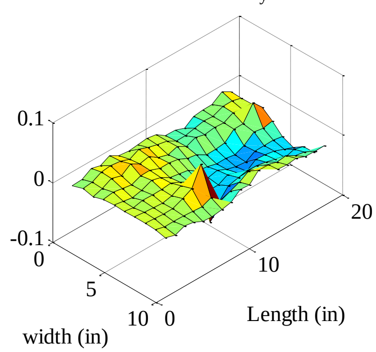	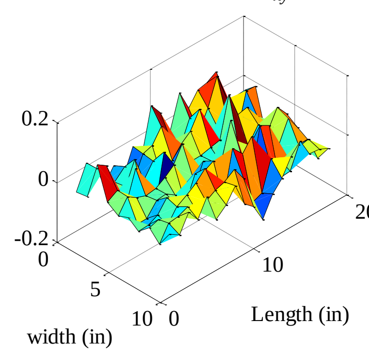

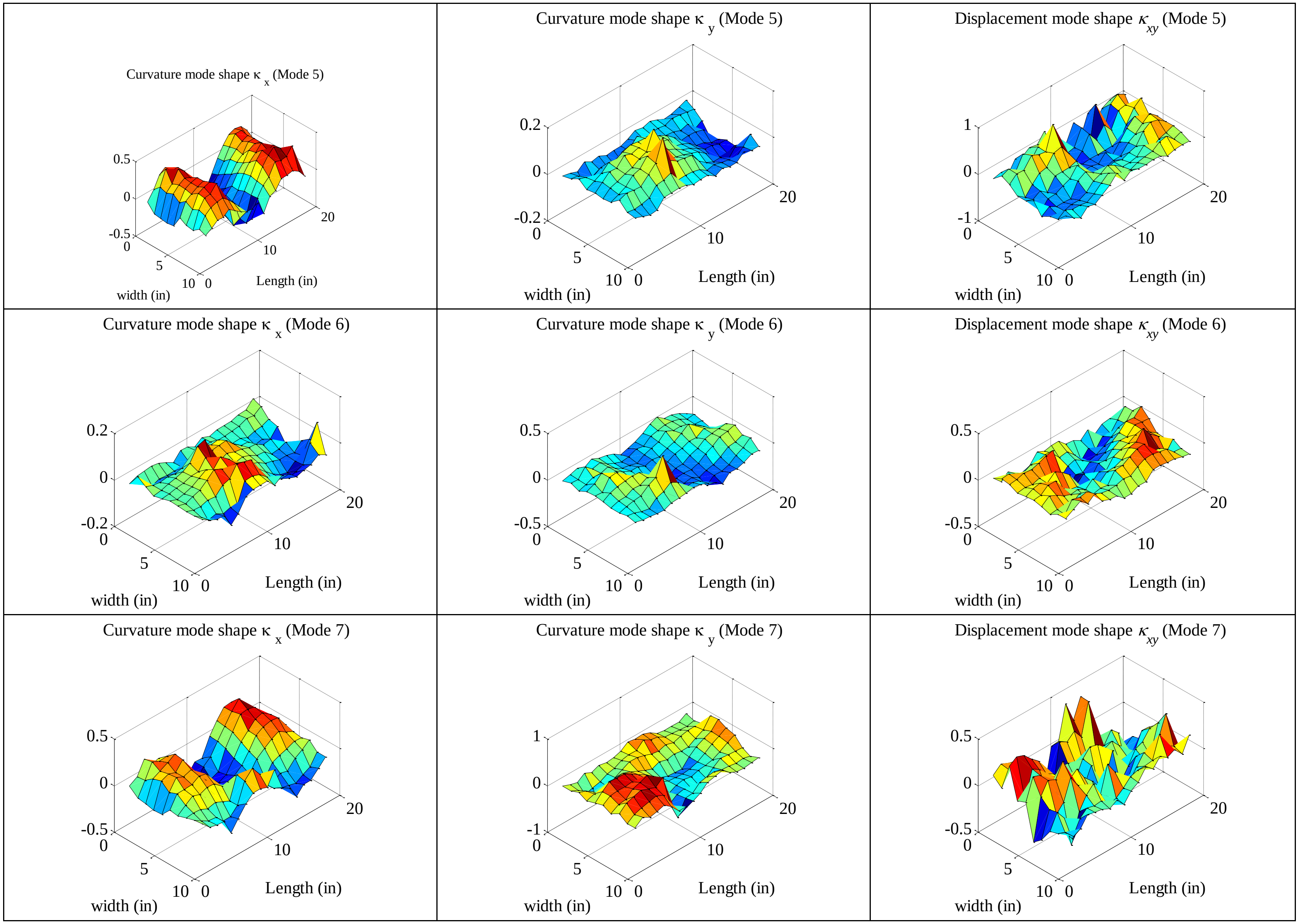
Curvature mode shape κ x (Mode 5)
0.5
0
-0.5
0
5
10
0
10
20
width (in)
Length (in)
Curvature mode shape κ y (Mode 5)
0.2
0
-0.2
0
5
10
0
10
20
width (in)
Length (in)
Displacement mode shape κxy (Mode 5)
1
0
-1
0
5
10
0
10
20
width (in)
Length (in)
Curvature mode shape κ x (Mode 6)
0.2
0
-0.2
0
5
10
0
10
20
width (in)
Length (in)
Curvature mode shape κ y (Mode 6)
0.5
0
-0.5
0
5
10
0
10
20
width (in)
Length (in)
Displacement mode shape κxy (Mode 6)
0.5
0
-0.5
0
5
10
0
10
20
width (in)
Length (in)
Curvature mode shape κ x (Mode 7)
0.5
0
-0.5
0
5
10
0
10
20
width (in)
Length (in)
Curvature mode shape κ y (Mode 7)
1
0
-1
0
5
10
0
10
20
width (in)
Length (in)
Displacement mode shape κxy (Mode 7)
0.5
0
-0.5
0
5
10
0
10
20
width (in)
Length (in)

Table 2.5 Mode shapes of the damaged plate (D2)

EXP(Displacement)	EXP (κ_x)	EXP (κ_y)	EXP (κ_{xy})
Displacement mode shape w (Mode 3) 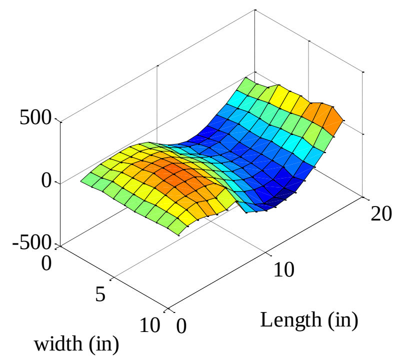	Curvature mode shape κ_x (Mode 3) 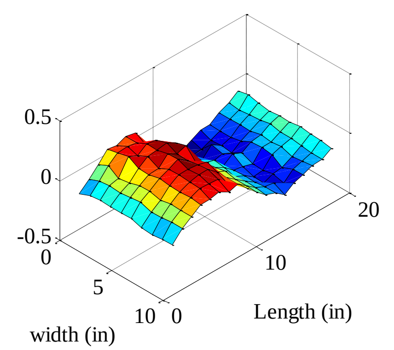	Curvature mode shape κ_y (Mode 3) 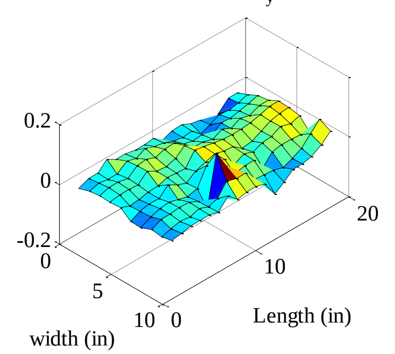	Displacement mode shape κ_{xy} (Mode 3) 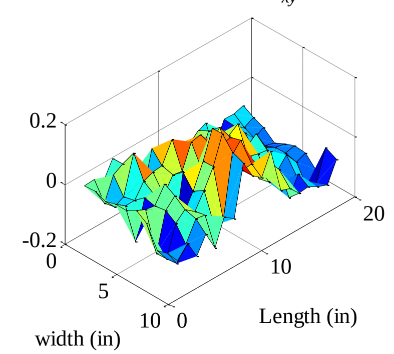
Displacement mode shape w (Mode 4) 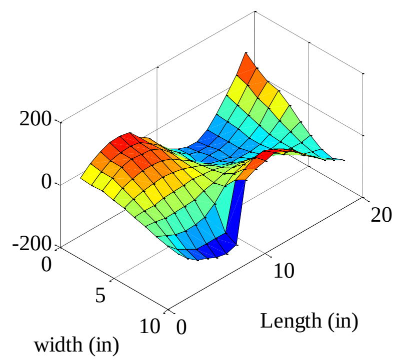	Curvature mode shape κ_x (Mode 4) 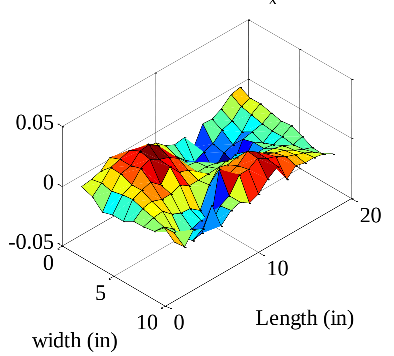	Curvature mode shape κ_y (Mode 4) 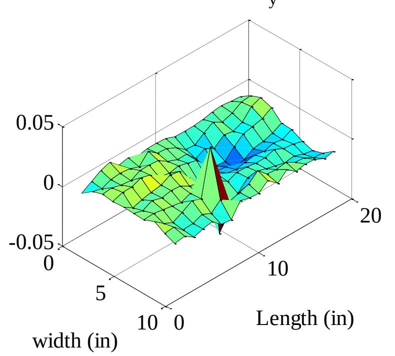	Displacement mode shape κ_{xy} (Mode 4) 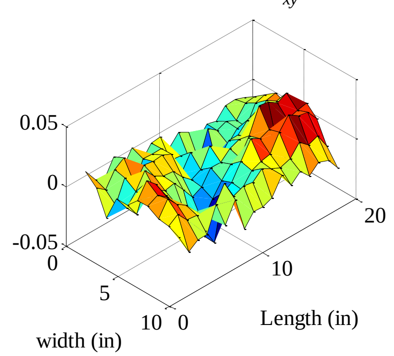

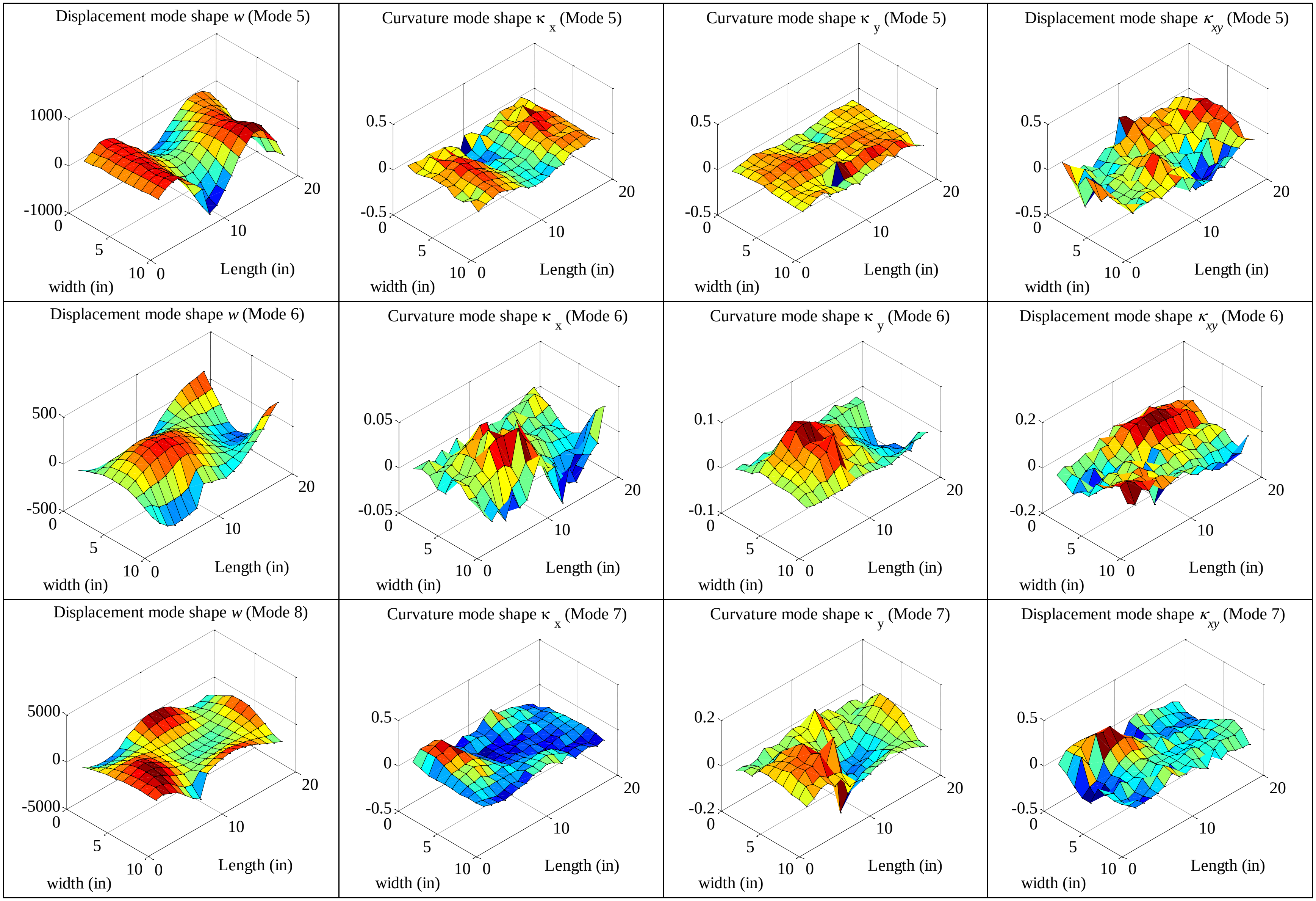

Displacement mode shape w (Mode 5)
Curvature mode shape κ x (Mode 5)
Curvature mode shape κ y (Mode 5)
Displacement mode shape κxy (Mode 5)
Displacement mode shape w (Mode 6)
Curvature mode shape κ x (Mode 6)
Curvature mode shape κ y (Mode 6)
Displacement mode shape κxy (Mode 6)
Displacement mode shape w (Mode 8)
Curvature mode shape κ x (Mode 7)
Curvature mode shape κ y (Mode 7)
Displacement mode shape κxy (Mode 7)
width (in)
Length (in)

Table 2.6 Mode shapes of the damaged plate (D3)

EXP(Displacement)	EXP (κ_x)	EXP (κ_y)	EXP (κ_{xy})
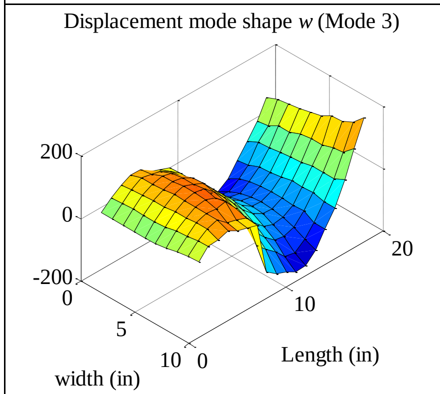	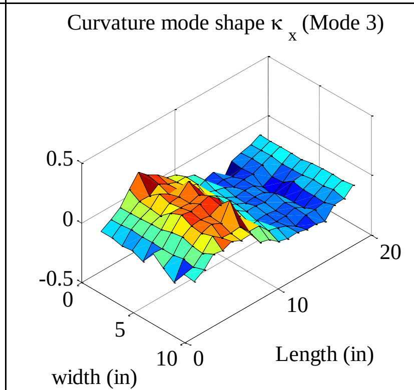	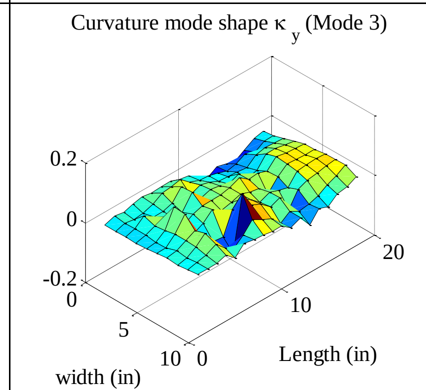	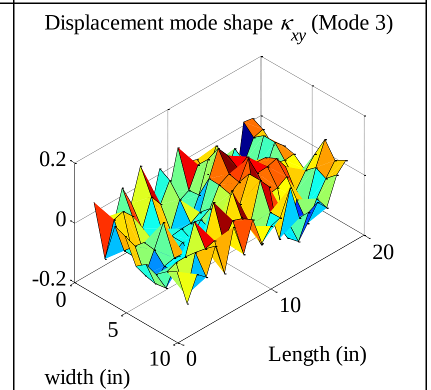
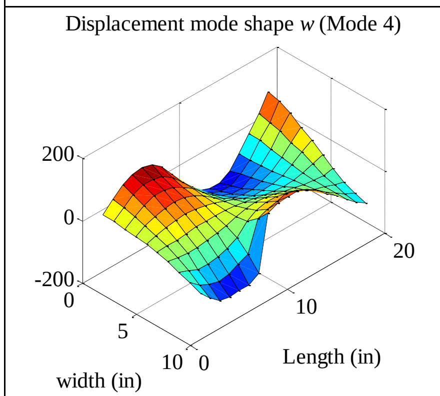	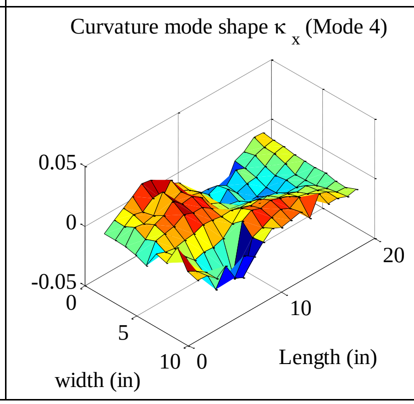	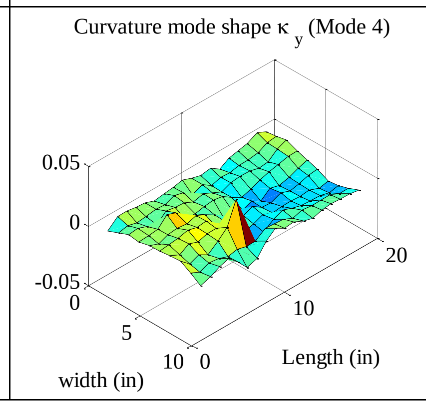	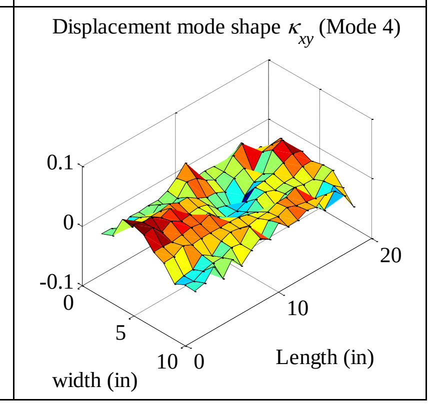

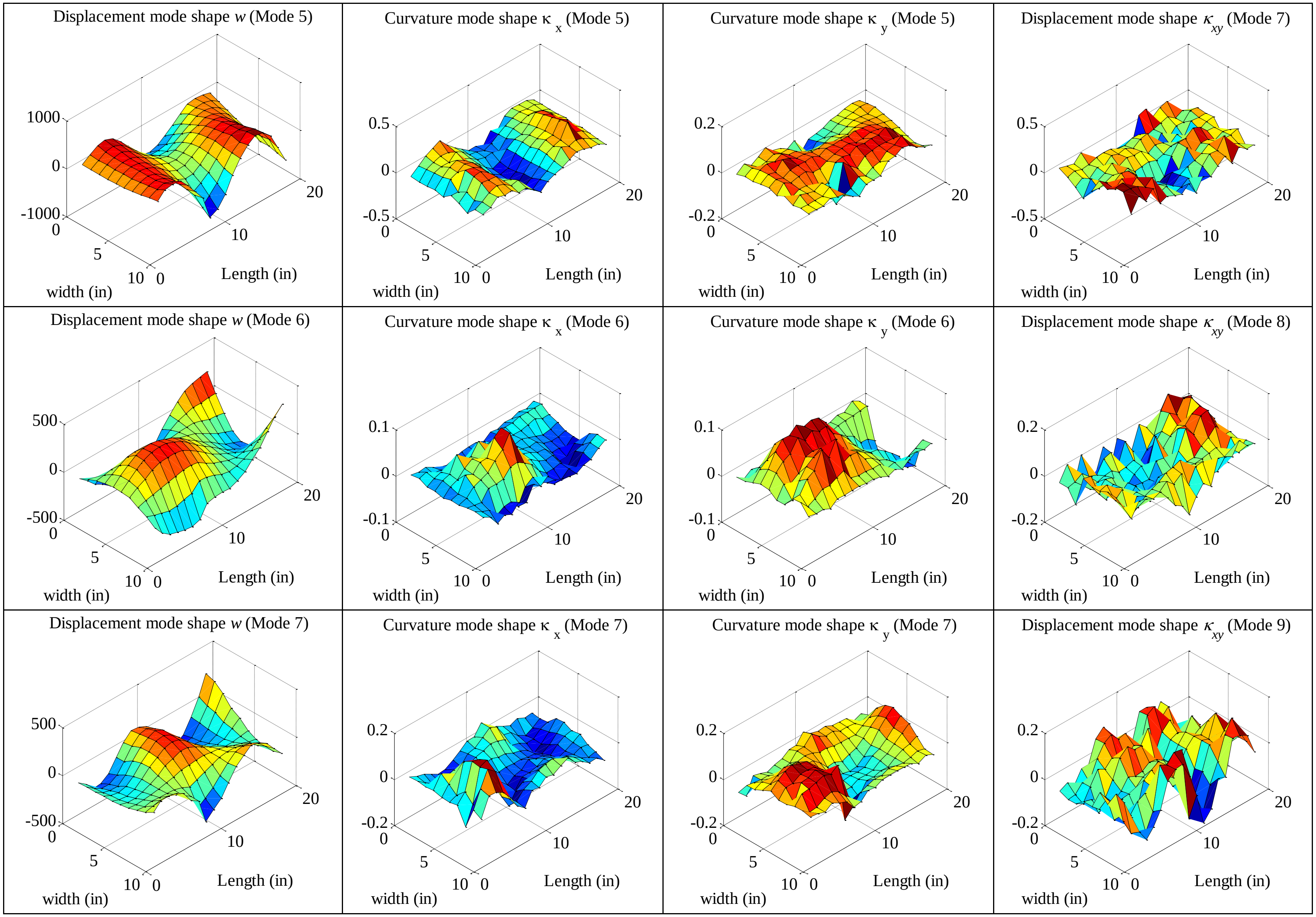
Displacement mode shape w (Mode 5)
Curvature mode shape κ x (Mode 5)
Curvature mode shape κ y (Mode 5)
Displacement mode shape κxy (Mode 7)
Displacement mode shape w (Mode 6)
Curvature mode shape κ x (Mode 6)
Curvature mode shape κ y (Mode 6)
Displacement mode shape κxy (Mode 8)
Displacement mode shape w (Mode 7)
Curvature mode shape κ x (Mode 7)
Curvature mode shape κ y (Mode 7)
Displacement mode shape κxy (Mode 9)
width (in)
Length (in)

Chapter 3

DAMAGE DETECTION OF FRP COMPOSITE PLATE FROM NUMERICAL SIMULATION DATA

3.1 Introduction

Numerical modal analysis is performed using Finite Element Method (FEM) to study the vibration response of a Fiber Reinforced Plastic (FRP) plate. The study aims to compare and verify the results acquired from the experimental testing. The frequencies and mode shapes for each mode of vibration are extracted. The commercial finite element software ABAQUS/CAE 6.10 is used to perform the numerical analysis for the plate.

The plate is modeled with the cantilevered boundary conditions, and it is fixed from one edge and free on all the others. The fine meshing was used with an element size of 0.05 x 0.05 in. generating a total of about 76,581 elements for the plate. Three damage cases were considered: (1) a 2.5×0.05 in. saw-cut (D1), (2) an enlarged 2.5×0.25 in. saw-cut (D2), and (3) an added 1 in. diamond shape hole (D3). All three damage cases were simulated using FEM and experimentally tested as well. The plate model is shown in Figure 3.1 with different cases of damage.

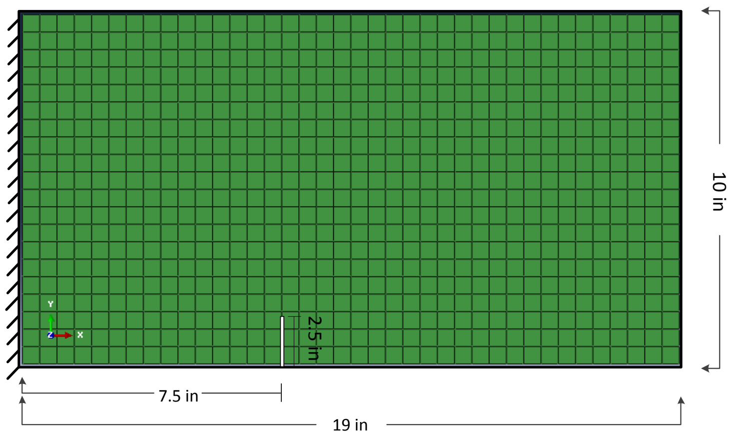

(a)

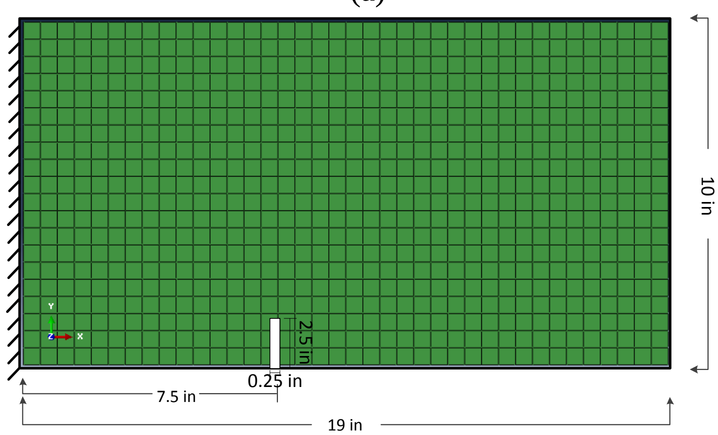

(b)

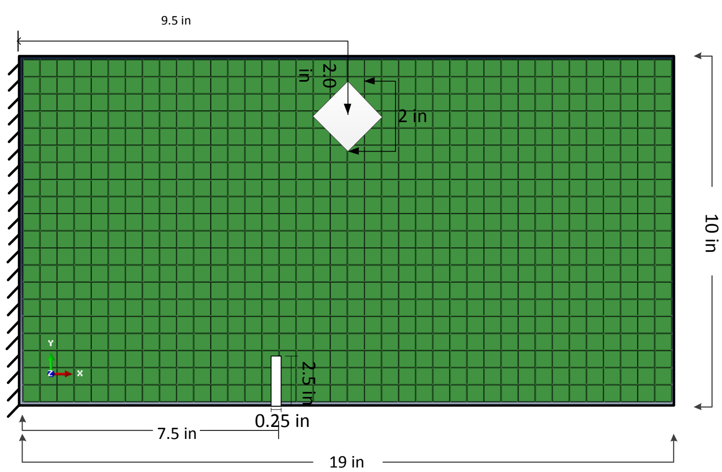

(c)

Figure 3.1 FE model of an E-glass fiber composite with (a) an edge saw cut (Damage1) (b) enlarged 2.5 x 0.25 in. saw-cut and (c) an added hole (Damage3)

ABAQUS offers several methods for performing dynamic analysis, which includes a full range of modal superposition procedures, such as the mode-based steady-state harmonic, response analysis, subspace-based steady-state harmonic response analysis, mode-based transient response analysis, response spectrum analysis, Random response analysis, etc. In this study, the mode-based transient response analysis is used, and this method can analyze the transient linear dynamic problems using the modal superposition, It can be performed only after a frequency extraction procedure since it bases the response of a structure on the modes of the system. Frequency extraction procedure in ABAQUS can be done using three methods: Lanczos, Automatic Multi-level Substructuring (AMS) and Subspace iteration. In this study, the Lanczos solver was used as the eigenvalue extraction method because it has the most general capabilities. The results of the analysis were similar to those acquired from the experimental modal testing. The third mode of vibration acquired from the finite element solution as along with the experimental testing for the third damage scenario is shown in Figure 3.2.

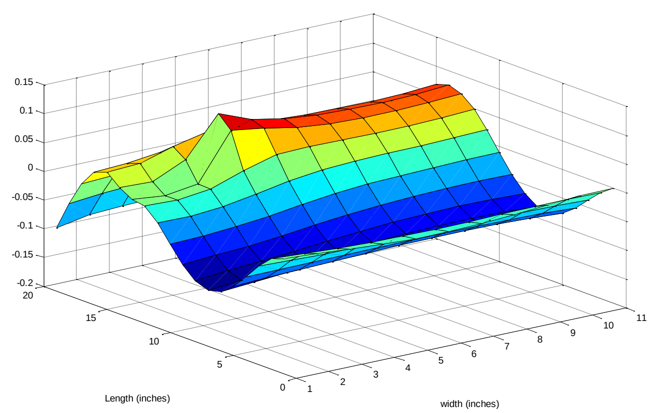

(a)

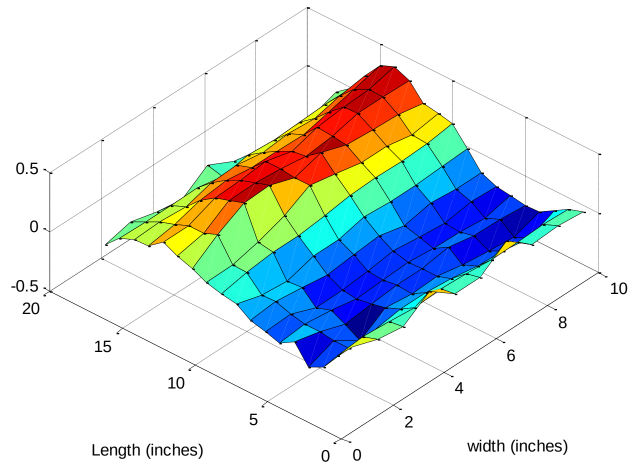

(b)
Figure 3.2 Third mode shape for a plate with damage case 1 (D1) using finite element (a) and experimental (b) results

The results were not taken from all the points in the fine mesh. But the plate was modeled with the fine mesh to get accurate analysis while simulating the real plate. In order to simulate the sensors system, only a few points matching the sensor system in the experimental analyses were selected.

The strain mode shape as well as the curvature mode shape for the third mode of vibration of damage case 2 (D2) is shown in Table 3.1. The purpose is to illustrate that the measured strain is proportional to the curvature, so that using the results from the PVDF-PZT experimental system is valid because the damage detection process only requires the relative or normalized mode shape rather than the values of the curvature.

Table 3.1 Comparison between the strain mode shape and curvature mode shape in the *x*, *y*, and *xy* directions.

<table>
<tr><th>Direction</th><th>Strain</th><th>Curvature</th></tr>
<tr><td>(x-direction)</td><td>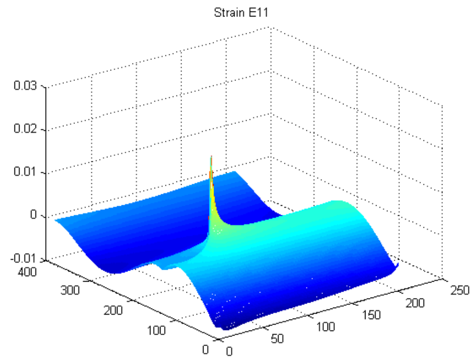</td><td>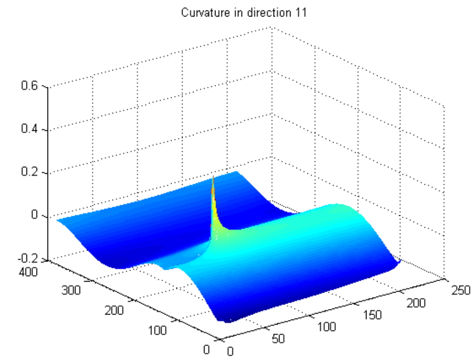</td></tr>
<tr><td>(y-direction)</td><td>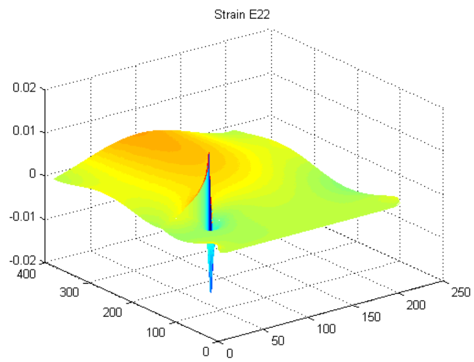</td><td>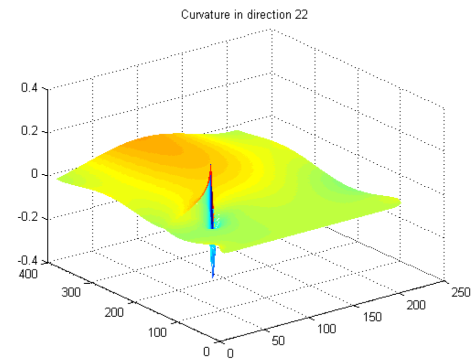</td></tr>
<tr><td>(xy-direction)</td><td>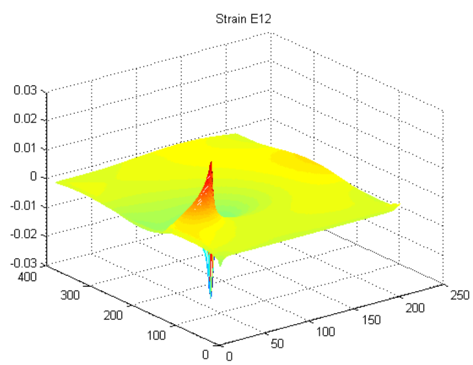</td><td>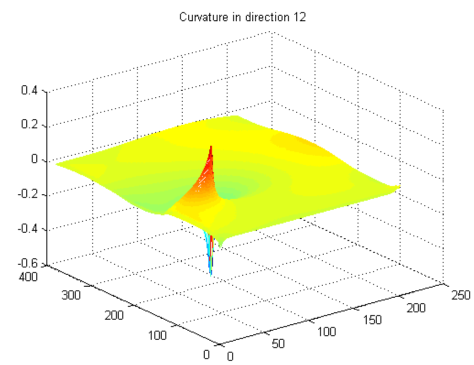</td></tr>
</table>

3.2 Numerical results

The results of the analyses conducted using ABAQUS for all the damage cases are shown in Table 3.2 to 3.4. The displacement as well as the curvature mode shapes are included for modes 1 to 5.

Table 3.2 Mode shapes of the damaged plate case 1 (D1)

FE(Displacement)	FE (κ_x)	FE (κ_y)	FE (κ_{xy})
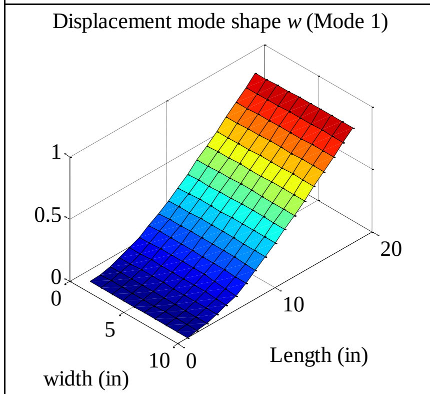	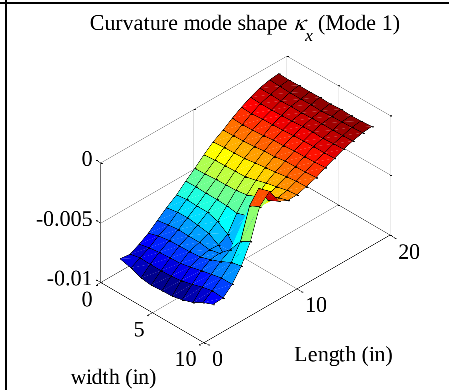	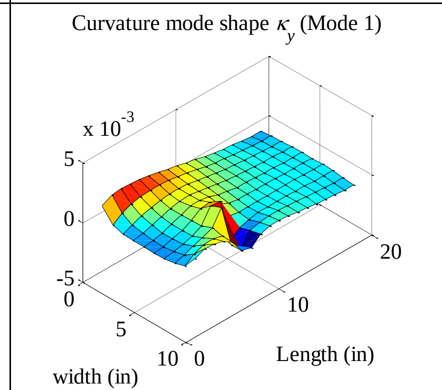	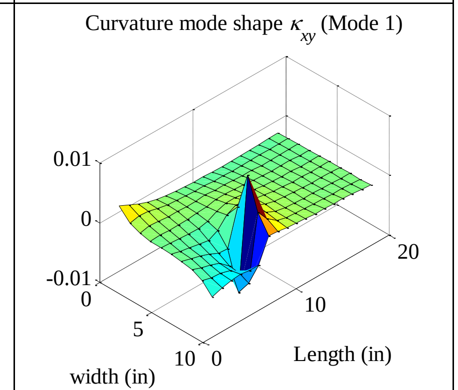
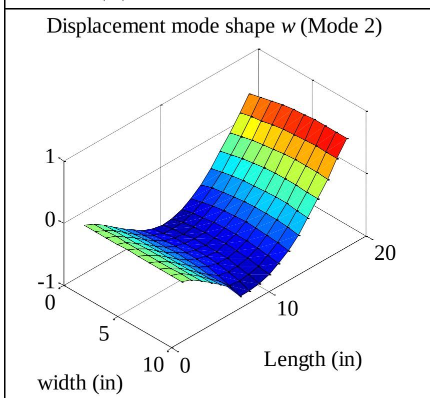	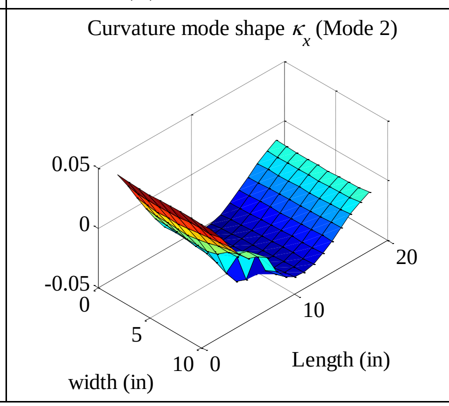	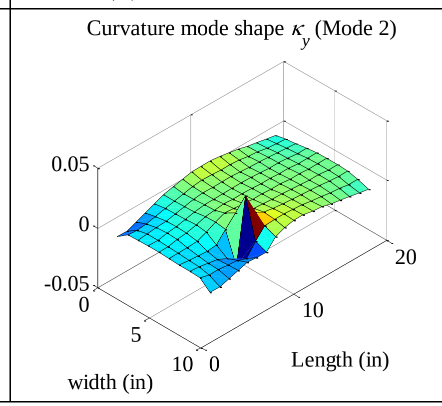	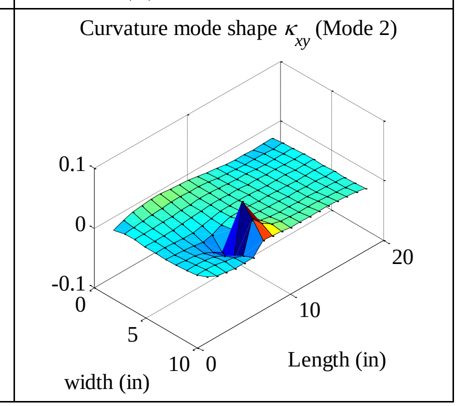

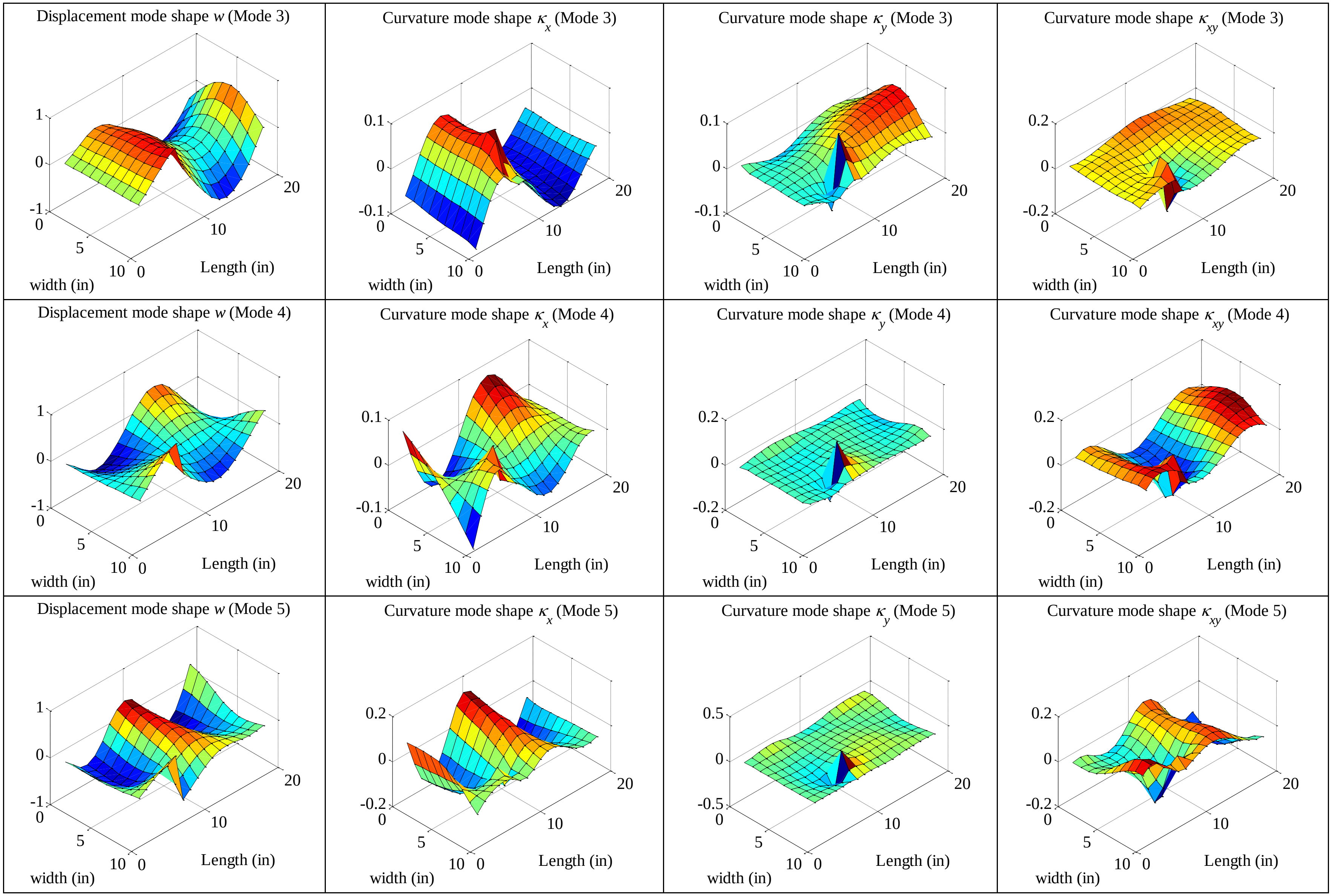
Displacement mode shape w (Mode 3)
Curvature mode shape κ_x (Mode 3)
Curvature mode shape κ_y (Mode 3)
Curvature mode shape κ_{xy} (Mode 3)
Displacement mode shape w (Mode 4)
Curvature mode shape κ_x (Mode 4)
Curvature mode shape κ_y (Mode 4)
Curvature mode shape κ_{xy} (Mode 4)
Displacement mode shape w (Mode 5)
Curvature mode shape κ_x (Mode 5)
Curvature mode shape κ_y (Mode 5)
Curvature mode shape κ_{xy} (Mode 5)
width (in)
Length (in)

Table 3.3 Mode shapes of the damaged plate case 2 (D2)

FE(Displacement)	FE (κ_x)	FE (κ_y)	FE (κ_{xy})
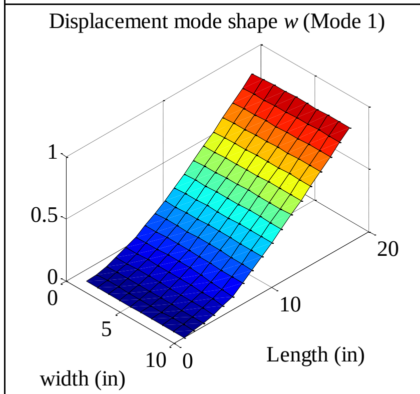	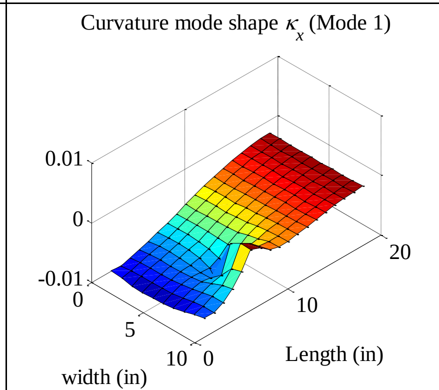	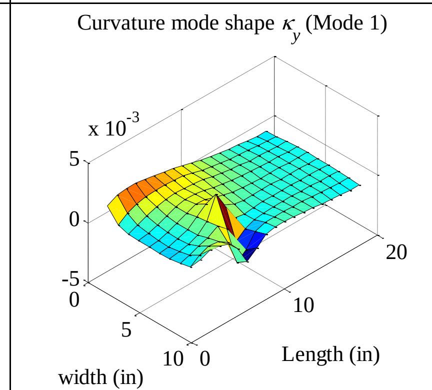	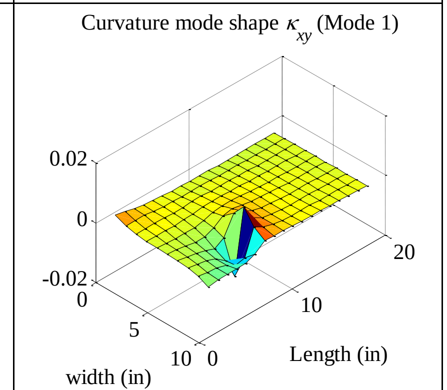
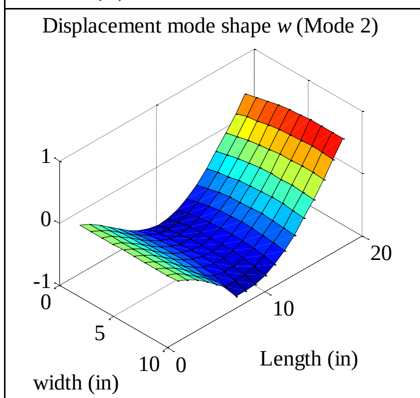	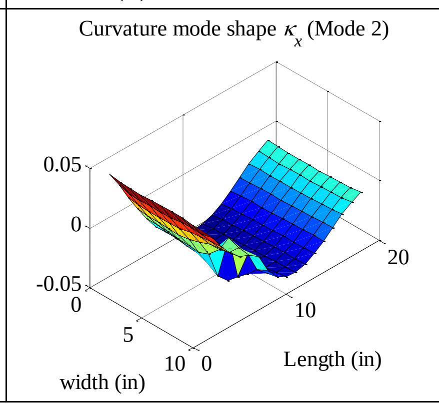	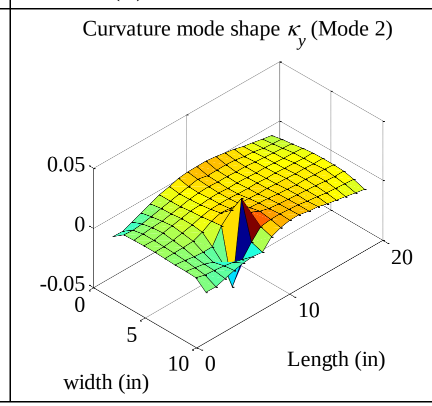	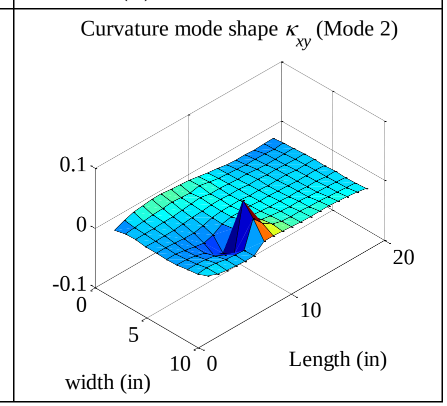

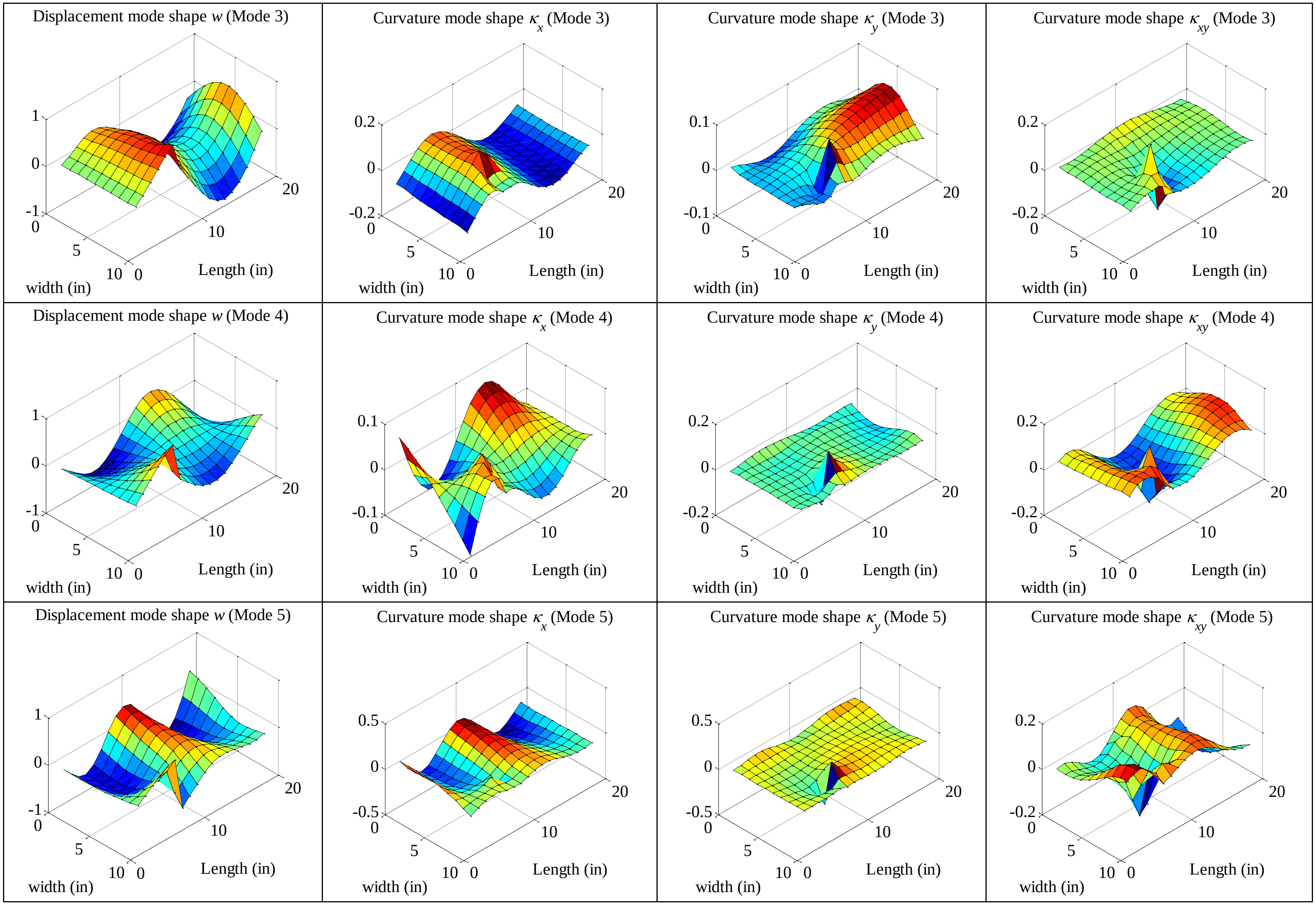

Displacement mode shape w (Mode 3)
Curvature mode shape κx (Mode 3)
Curvature mode shape κy (Mode 3)
Curvature mode shape κxy (Mode 3)
Displacement mode shape w (Mode 4)
Curvature mode shape κx (Mode 4)
Curvature mode shape κy (Mode 4)
Curvature mode shape κxy (Mode 4)
Displacement mode shape w (Mode 5)
Curvature mode shape κx (Mode 5)
Curvature mode shape κy (Mode 5)
Curvature mode shape κxy (Mode 5)
width (in)
Length (in)

Table 3.4 Mode shapes of the damaged plate case 3 (D3)

FE(Displacement)	FE (κ_x)	FE (κ_y)	FE (κ_{xy})
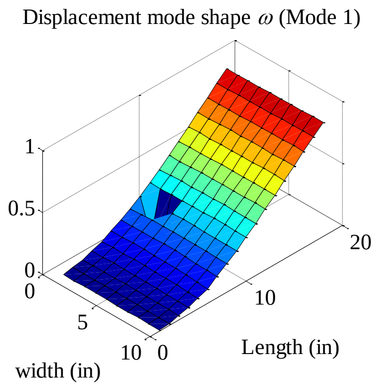	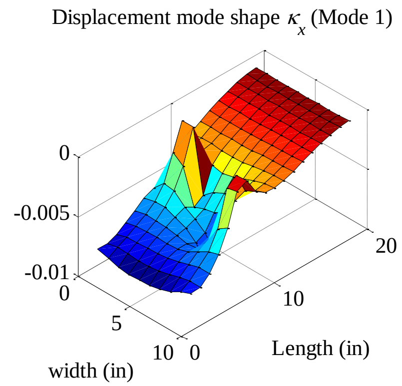	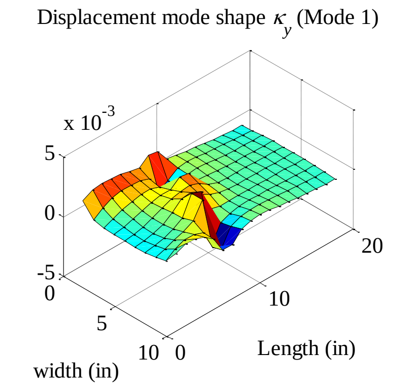	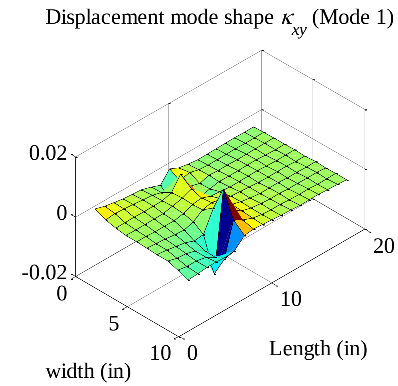
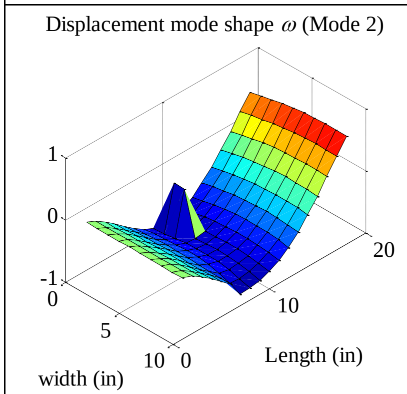	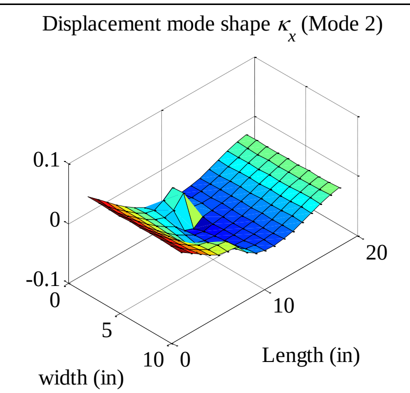	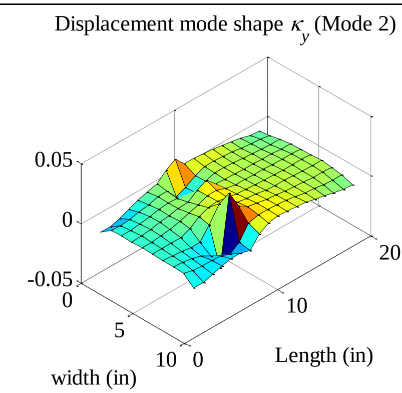	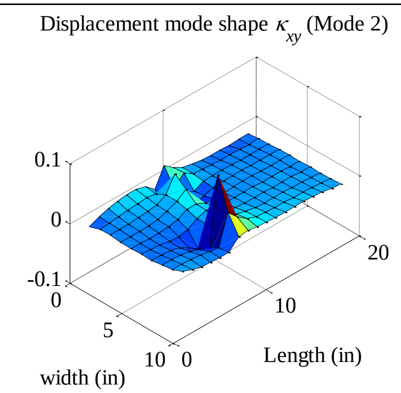

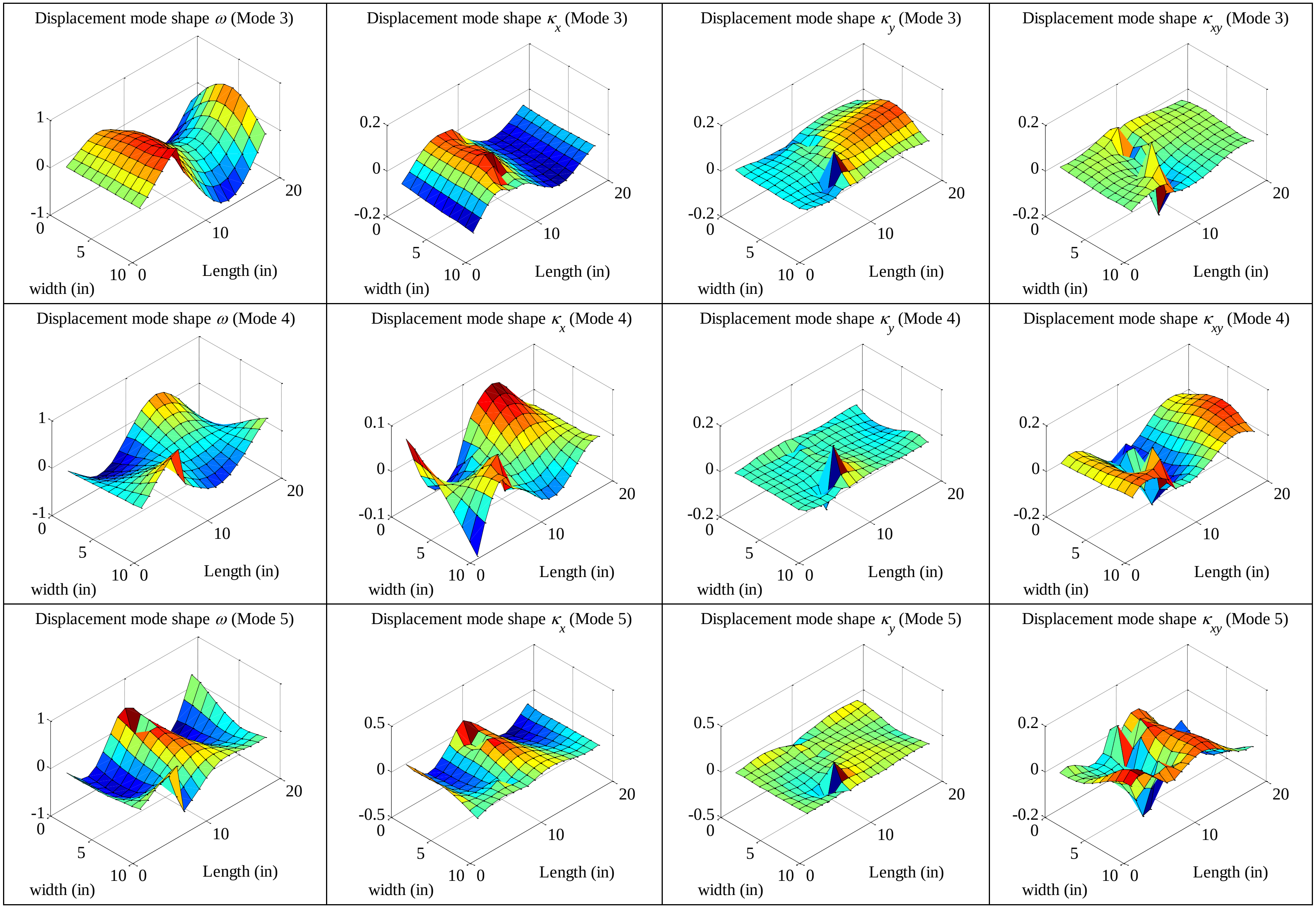
Displacement mode shape ω (Mode 3)
Displacement mode shape κx (Mode 3)
Displacement mode shape κy (Mode 3)
Displacement mode shape κxy (Mode 3)
Displacement mode shape ω (Mode 4)
Displacement mode shape κx (Mode 4)
Displacement mode shape κy (Mode 4)
Displacement mode shape κxy (Mode 4)
Displacement mode shape ω (Mode 5)
Displacement mode shape κx (Mode 5)
Displacement mode shape κy (Mode 5)
Displacement mode shape κxy (Mode 5)
width (in)
Length (in)

3.3 Comparison of Finite Element results Vs Experimental Analysis results

Referring to Tables 2.4 and 3.3 and taking consideration of only the modes 3, 4 and 5, a comparison between the FE and experimental results is made. It can be seen that all of the modes, either the displacement or curvatures (κ_x, κ_y, or κ_{xy}) acquired from the FE analysis, more or less match those obtained from the experimental modal analysis. But because experimental κ_{xy} includes noise from the strains in three directions ($\varepsilon_x, \varepsilon_y\ and\ \varepsilon_{45}$), the mode shapes are noisier and much harder to tell if they match their corresponding FE results. Another difference is that some of the FE mode shapes have a negative magnitude of the corresponding experimental mode shapes. But it is correct and anticipated since any vibration mode shape oscillates between the two extremes.

3.4 Damage detection based on Finite Element Analysis

3.4.1 Curvature-based damage detection

This section presents the application of several damage detection algorithms using the finite element-generated curvature mode shapes of the plate in all directions (κ_x, κ_y, *and* κ_{xy}). As already discussed, the outcome of PZT-PVDF system is the strain mode shapes in the *x*, *y* and *xy* directions which were confirmed to be proportional to the curvature. Since the normalized mode shapes are to be used, and then the strain mode shapes could be directly used in the place of the curvature mode shape. A different set of combinations including the use of single and multiple modes of vibration as well as using of the curvatures in the *x*, *y*, and *xy* directions was tested to get the best detectability of the damage.

3.4.1.1 Damage Case 1

The application of three different algorithms to damage case 1 (D1) is shown in Table 3.5. Modes 1 to 5 as well as the combinations of multiple modes are presented. All the considered damage detection methods were able to detect and localize the damage. It can be observed that each method has its advantages and setbacks. The GFD gives a high damage index which in return gives higher and easier detectability to smaller damages. GSM tends to give a reasonable damage index but at the same time showing the size and localization accuracy that cannot be found using GFD. SEM tends to give a false indication of the damage but giving relatively a lower damage index compared to GFD and GSM.

Table 3.5 Application of damage detection algorithms to damage case one (D1)

	GSM	GFD	SEM
Mode 1	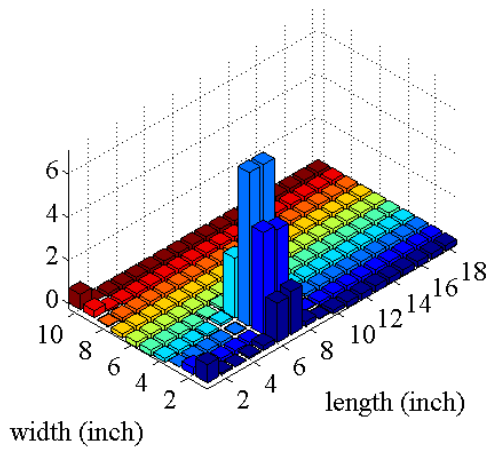	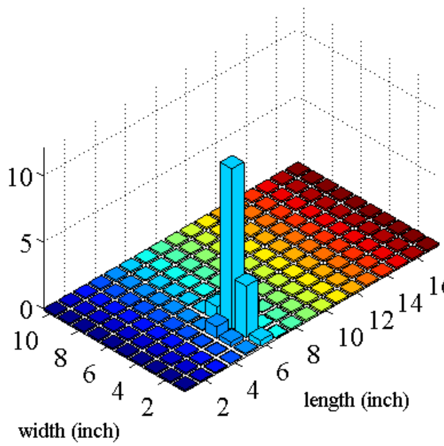	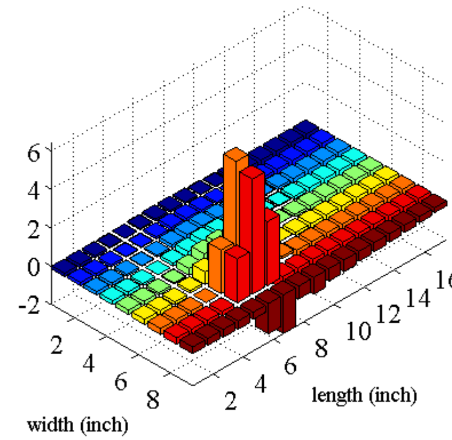
Mode 2	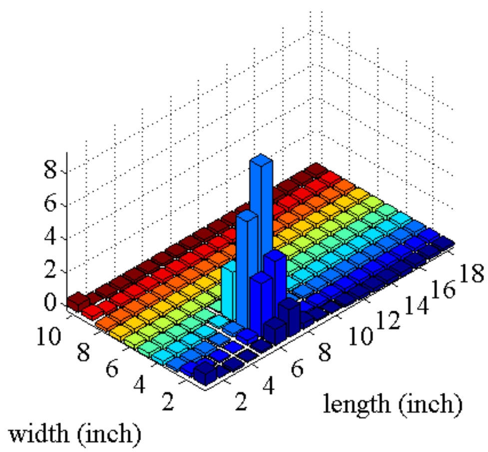	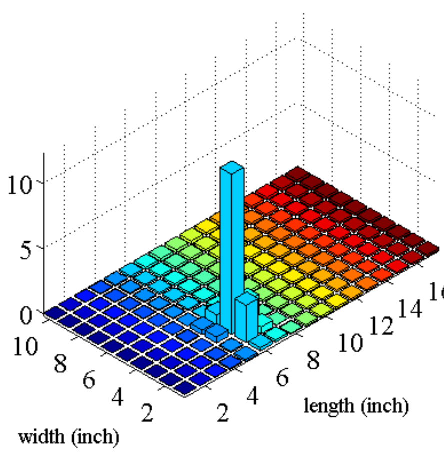	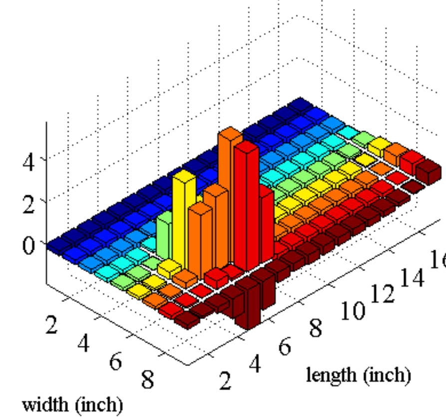

<table>
<tr>
<td>Mode 3</td>
<td>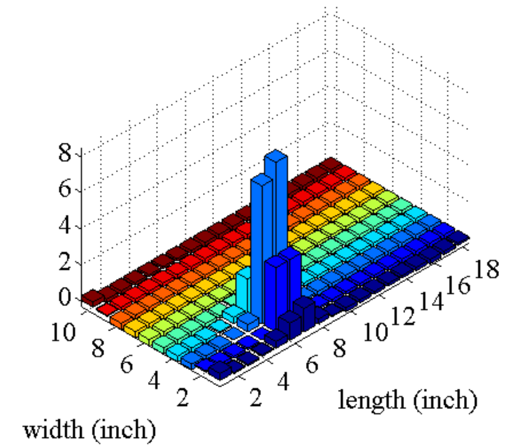</td>
<td>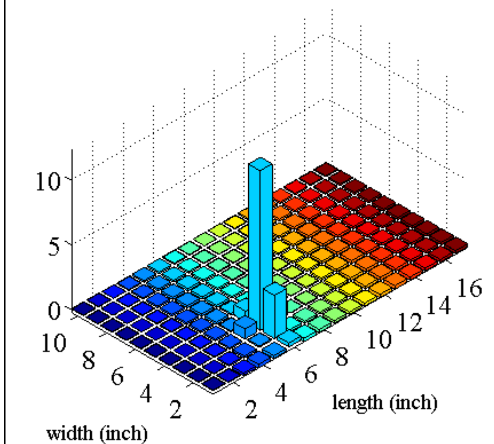</td>
<td>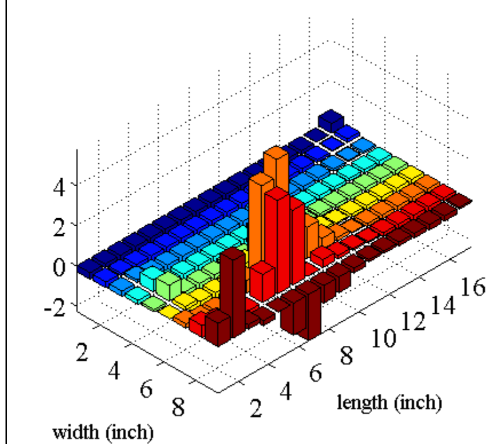</td>
</tr>
<tr>
<td>Mode 4</td>
<td>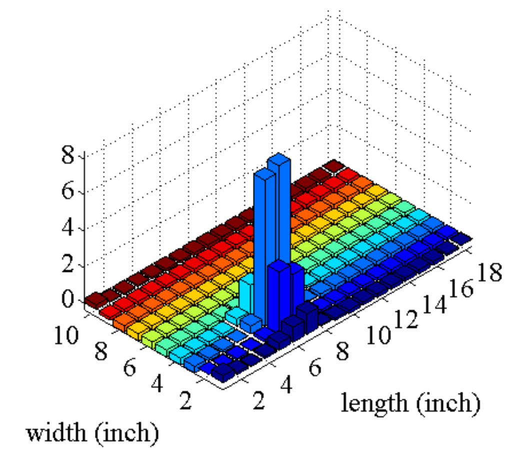</td>
<td>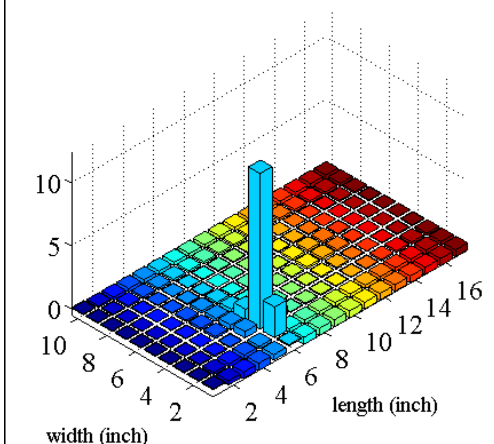</td>
<td>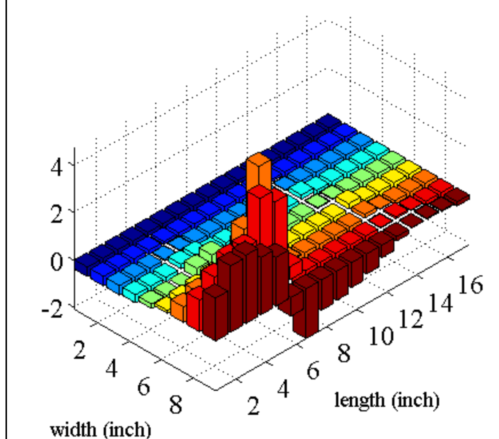</td>
</tr>
</table>

Mode 5	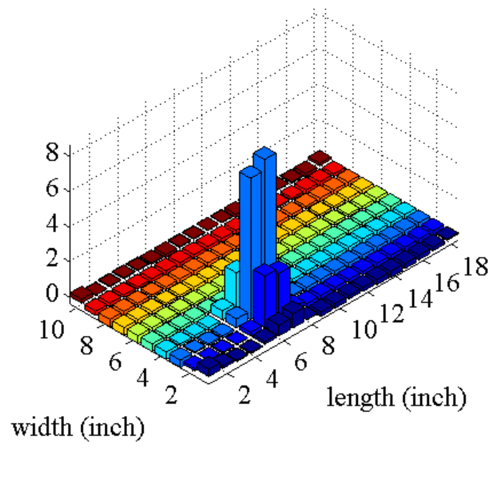	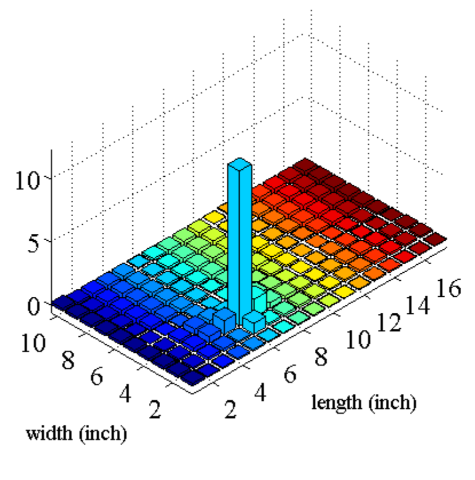	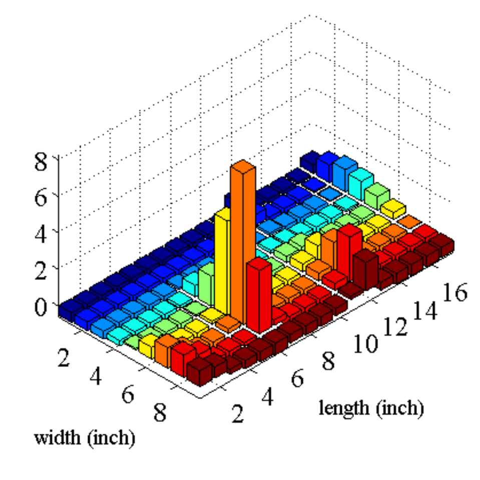
Modes 1-5	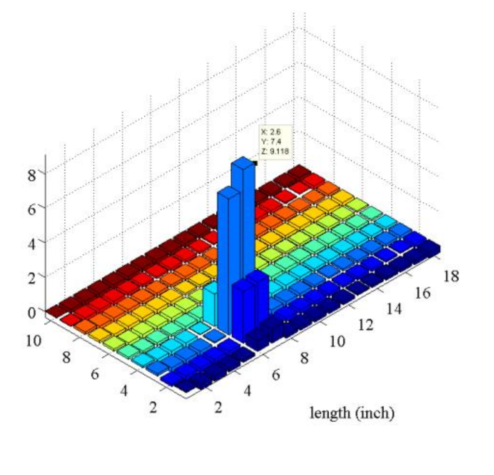	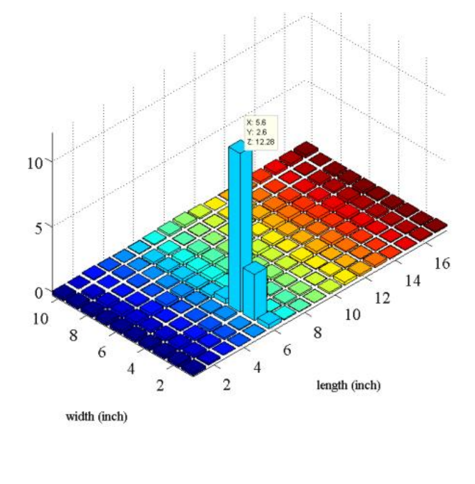	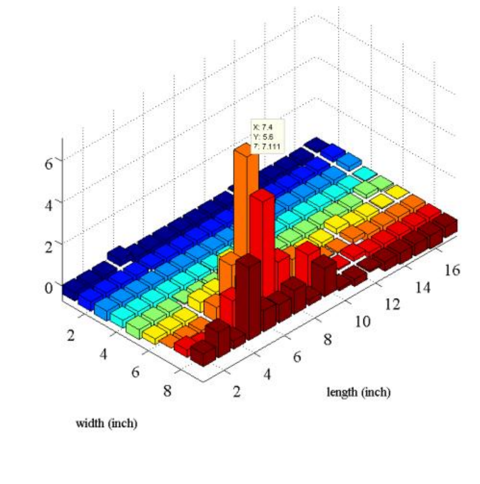

Damage detection algorithms were applied to the curvatures in each direction separately to investigate the effectiveness and usefulness of using the curvature in a single direction or all the directions as before. From Table 3.6, it can be seen that the damage is best detected and localized using the curvature in the *y*-direction κ_y as well as in the *xy*-direction κ_{xy}. The damage is falsely indicated using the curvature in the *x*-direction κ_x. The reason might be due to the fact that the damage (the saw-cut) is oriented in the *y*-direction (the transverse direction to the *x*-axis), consequently the change in the curvature around the damage was manifested in the *y* and *xy* directions rather than the *x*-direction. As for the detection algorithms, the advantages and disadvantages of the algorithms mentioned earlier seem applicable. The GSM has the best detectability and localization abilities, followed by the GFD. While the SEM gives the false indication of the damage size.

Table 3.6 Application of all the damage detection algorithms to κx, κy, and κxy for the damage case one (D1).

	GSM	GFD	SEM
κ_x	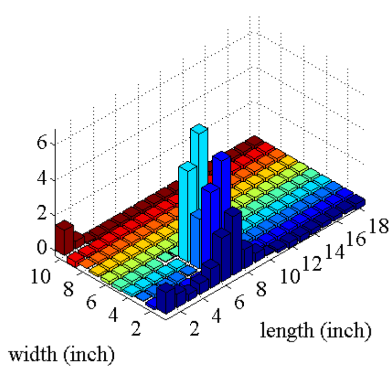	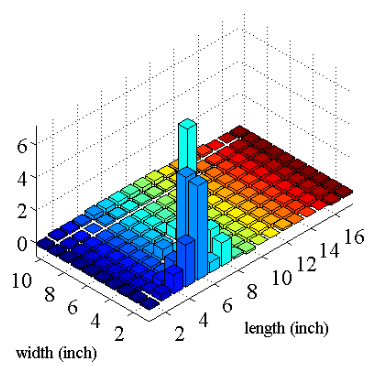	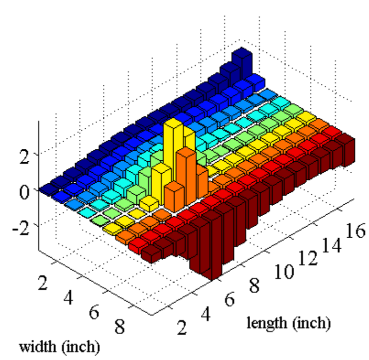

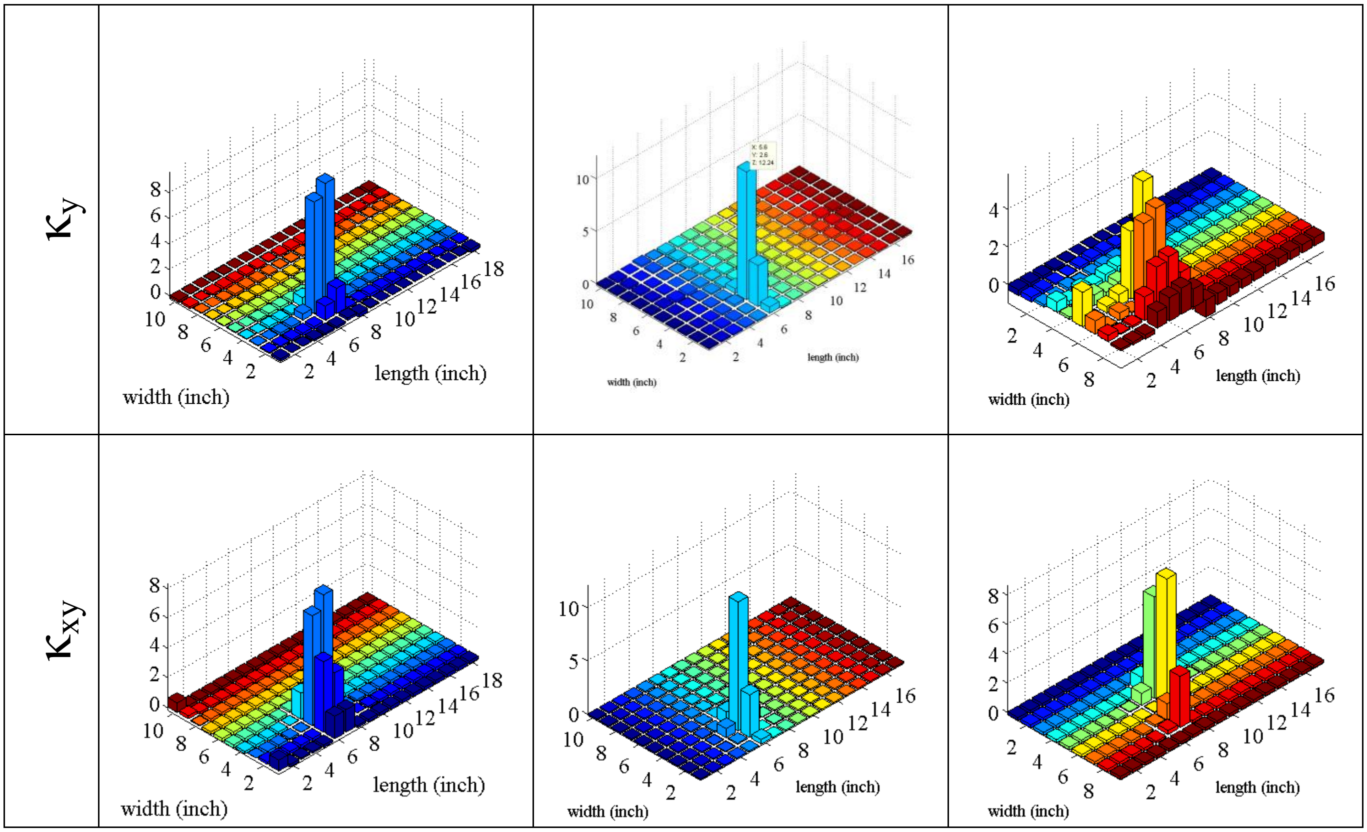

3.4.1.2 Damage case 2

As the damage severity increases the damage index for each of the algorithms should increase. From Table 3.7, it can be seen that the damage index indeed increases. Unfortunately, the setback for SEM can be found at a larger scale, and there is an excessive false indication of damage. On the other hand, the GSM damage index shows higher values on all the nodes surrounding the damage, indicating the severity change as well as the size change reflecting the enlarged saw-cut damage. GFD shows a higher damage index value, but the change is concentrated in a single area around the tip of the crack with almost no indication of damage on the other end of the crack (edge of the plate), which makes it hard to use it for localization or quantification.

Table 3.7 Application of damage detection algorithms to damage case two (D2)

<table>
<tr><td></td><td>GSM</td><td>GFD</td><td>SEM</td></tr>
<tr><td>Mode 1</td><td>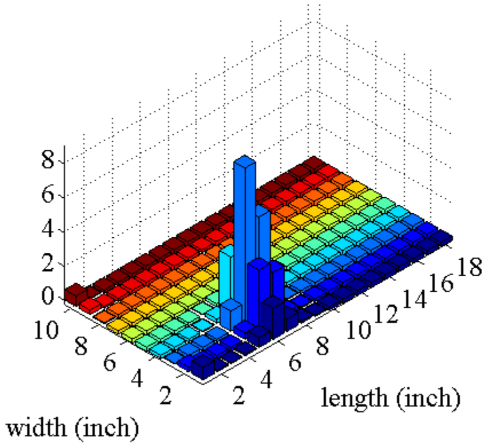
</td><td>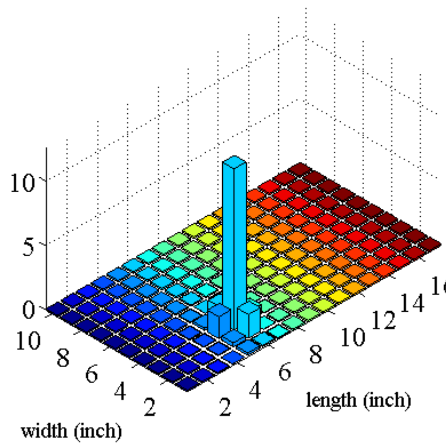
</td><td>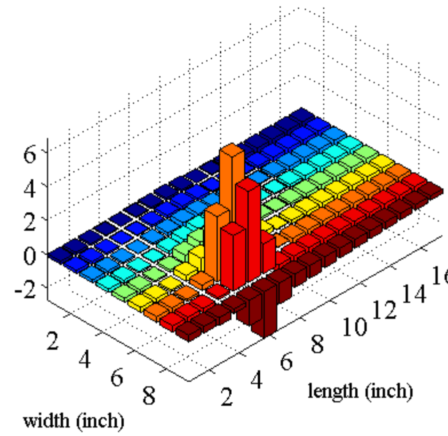
</td></tr>
<tr><td>Mode 2</td><td>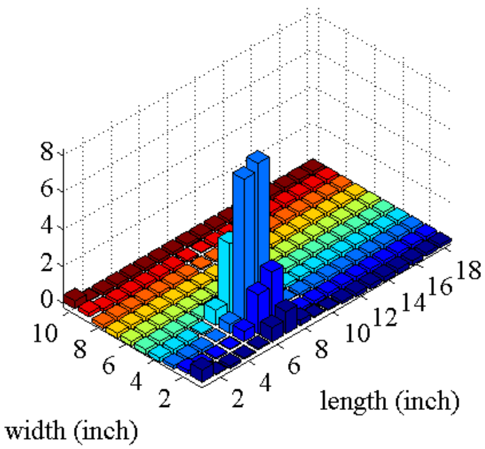
</td><td>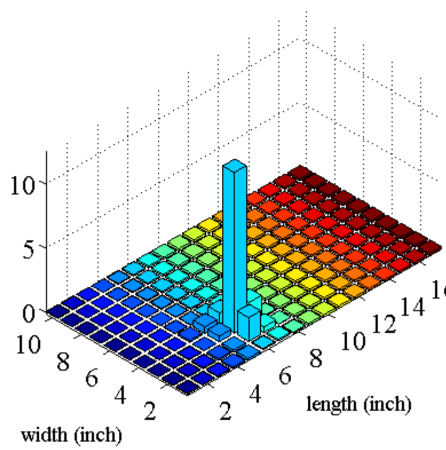
</td><td>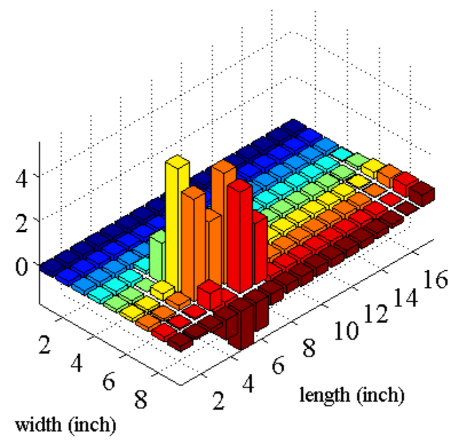
</td></tr>
</table>

Mode 3

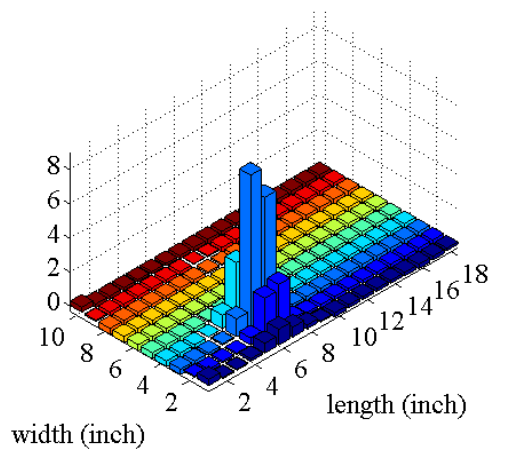

width (inch)
length (inch)

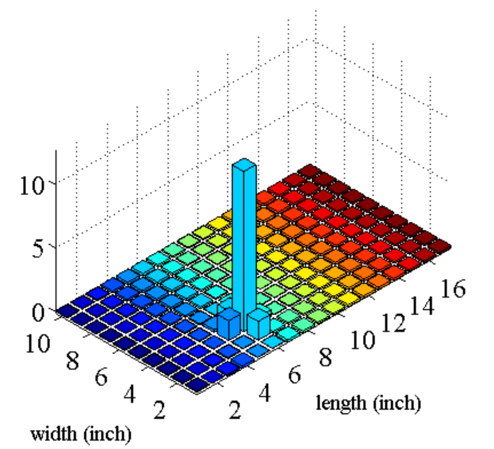

width (inch)
length (inch)

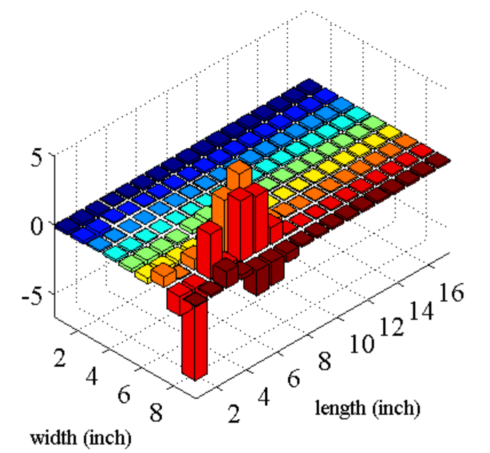

width (inch)
length (inch)

Mode 4

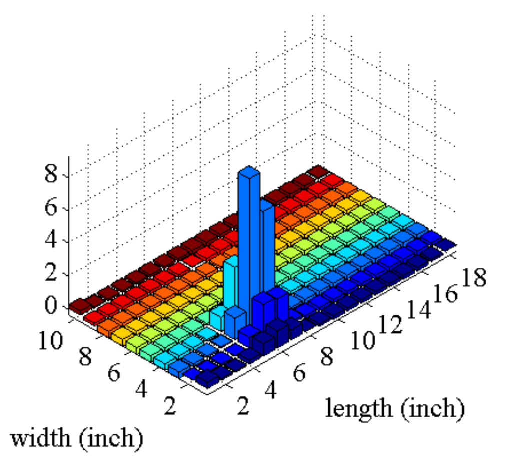

width (inch)
length (inch)

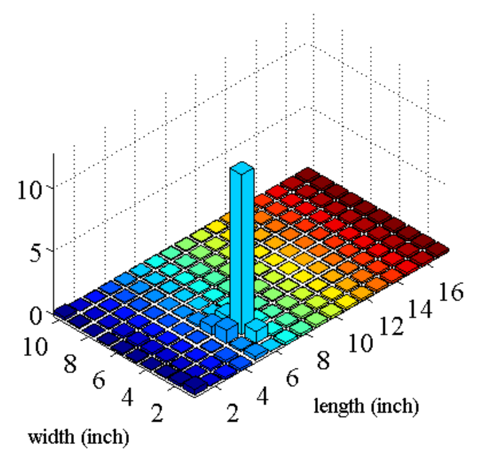

width (inch)
length (inch)

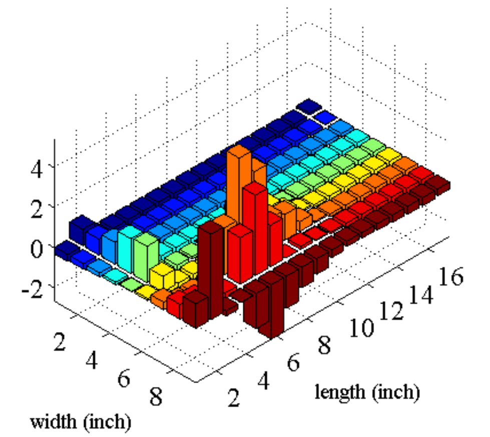

width (inch)
length (inch)

Mode 5	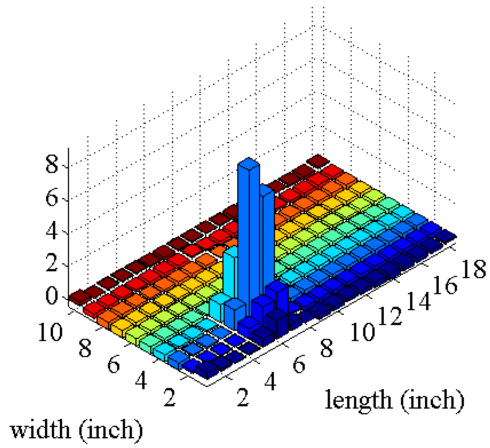	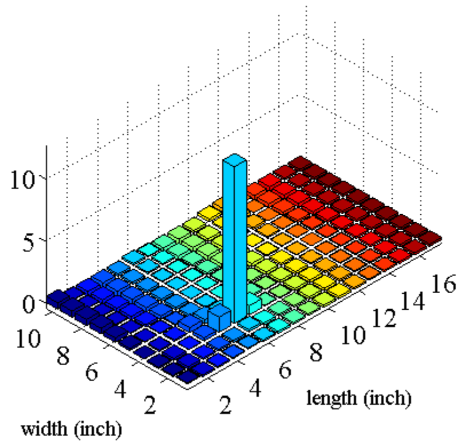	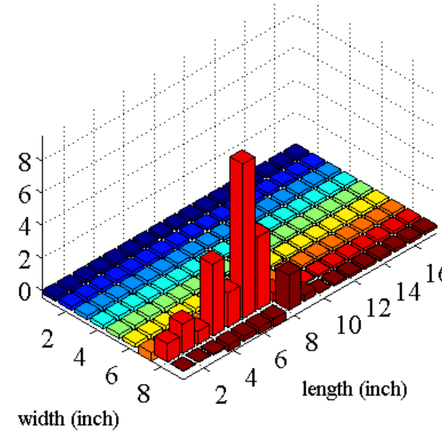
Combination Modes 1-5	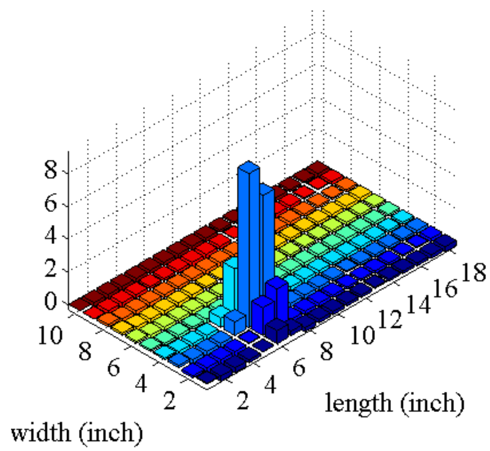	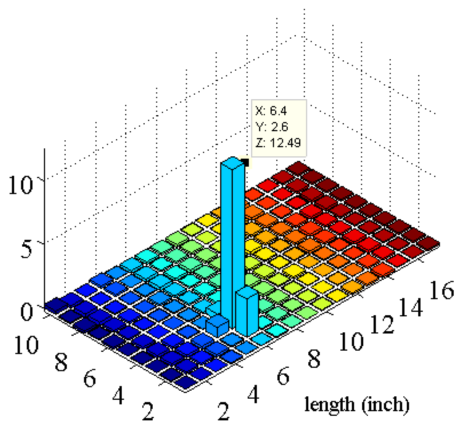	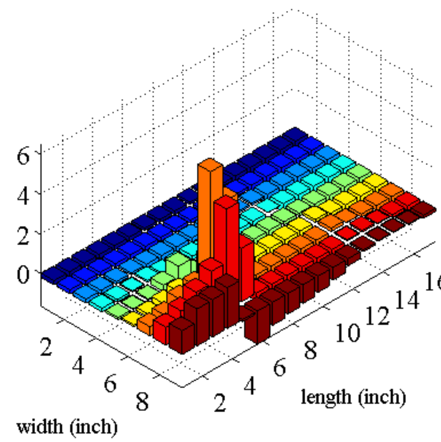

Similarly, Damage detection algorithms were applied to the curvatures in each direction separately to investigate the benefits of using the curvature in a single direction or all the directions as before. From Table 3.8, it can be seen that there is a trend for κ_x to overestimate or falsely indicate the damage by going further into the interior of the plate. κ_y and κ_{xy} on the other hand show the best performance in terms of detecting the damage as well as localizing it, following the same trend as shown for the damage case one. Moreover, GSM still provides a reasonably high damage index with regard to localization capabilities. GFD on the other hand performed the best regarding the value of the damage index. SEM performs the worst with the lowest damage index values and thus falsely indicates the damage.

Table 3.8 Application of all damage detection algorithms to κx, κy, and κxy for the damage case Two (D2)

	GSM	GFD	SEM
κ_x	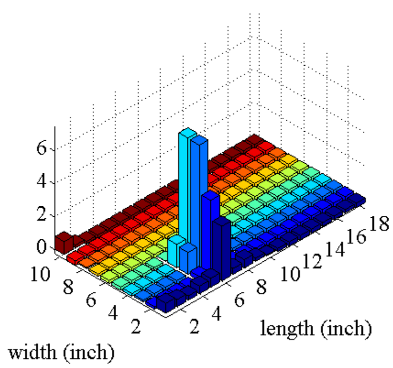	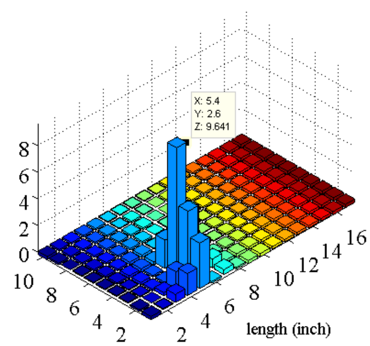	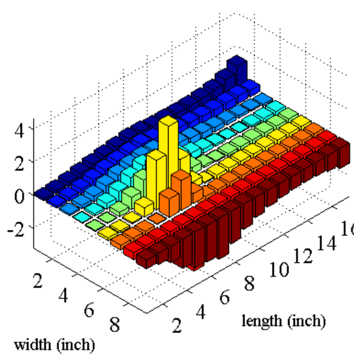
κ_y	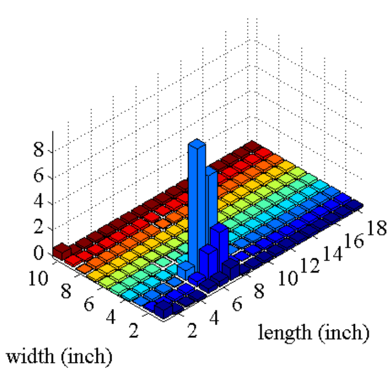	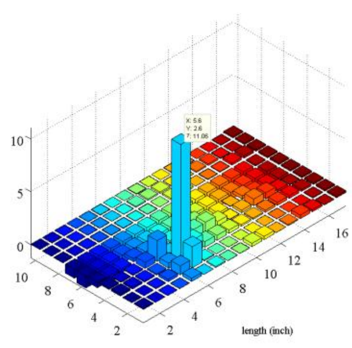	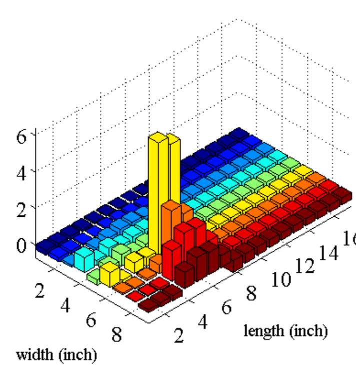

κ_{xy}	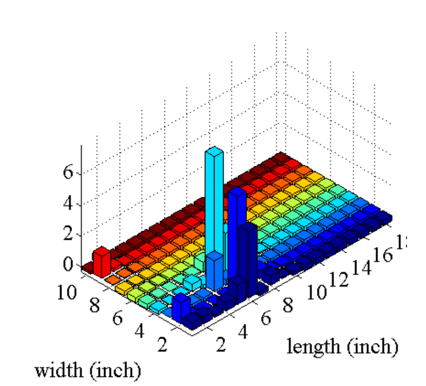	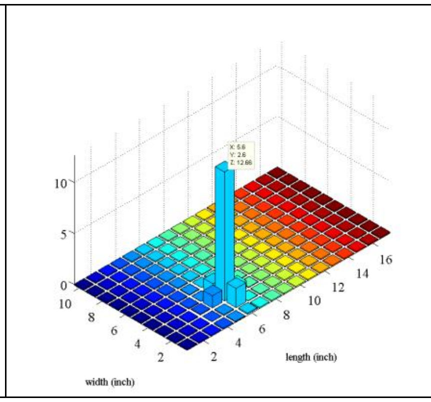	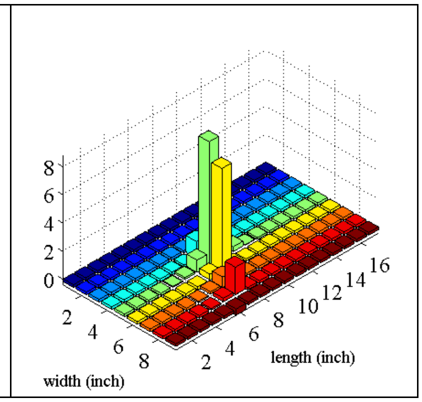

3.4.1.3 Damage case 3

As described before, the damage case 3 (D3) is an added 2 in. diamond hole on the other side of the plate to the second damage (D2). This case was selected to investigate the applicability of different algorithms to detect multiple damages in the plate. From Table 3.9, it can be seen that from the first mode, GSM and SEM were able to detect and localize both the damages. But as we go to the higher modes, SEM fails to detect any damage; whereas GSM continues to detect and localize both the damages accurately and successfully. GFD on the other hand was unable to detect the second damage using a single mode of vibration, but the combination of all the modes helped to refine the second damage and brought it into the picture.

Table 3.9 Application of damage detection algorithms to damage case three (D3)

<table>
<tr><th></th><th>GSM</th><th>GFD</th><th>SEM</th></tr>
<tr><td>Mode 1</td>
<td>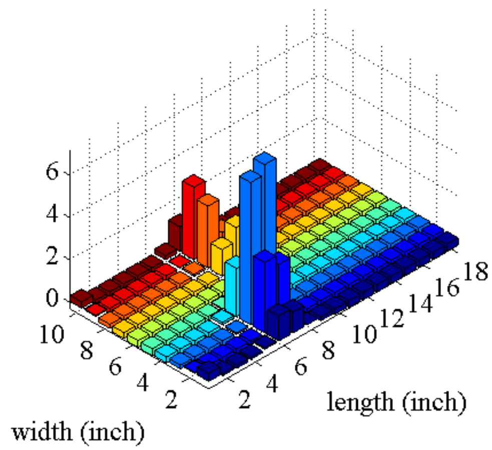
</td>
<td>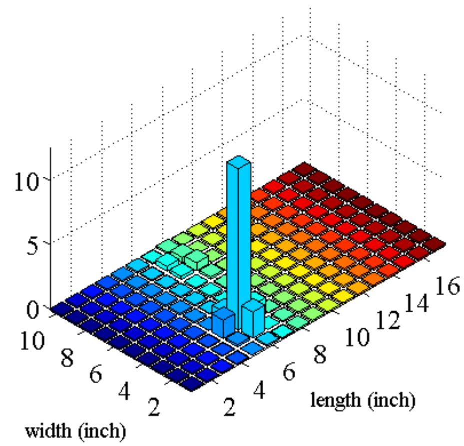
</td>
<td>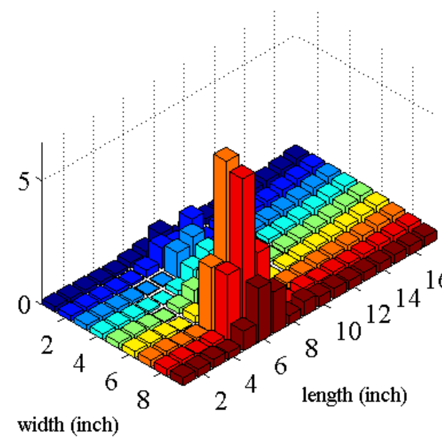
</td></tr>
<tr><td>Mode 2</td>
<td>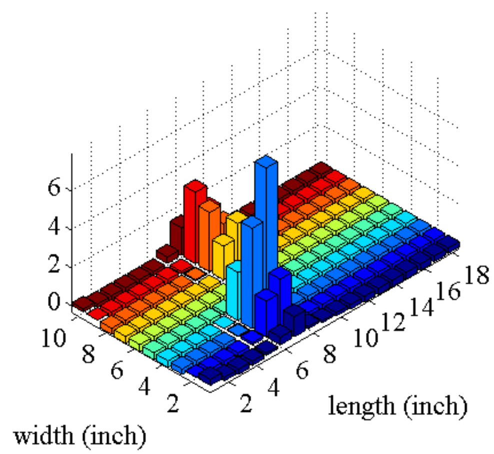
</td>
<td>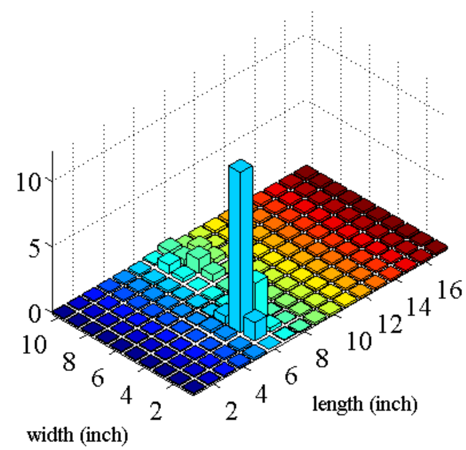
</td>
<td>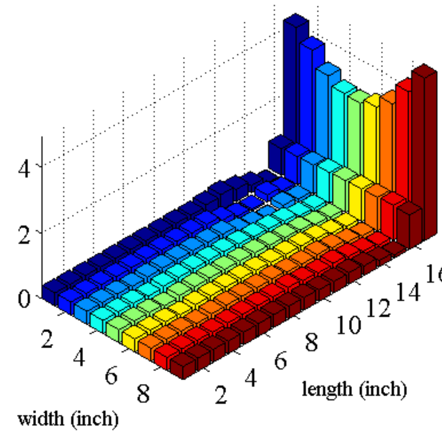
</td></tr>
</table>

Mode 3	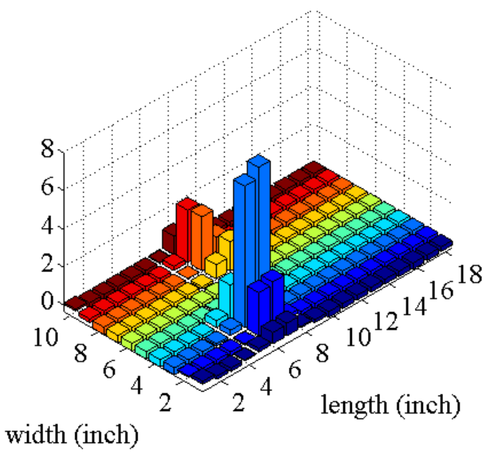 width (inch) length (inch)	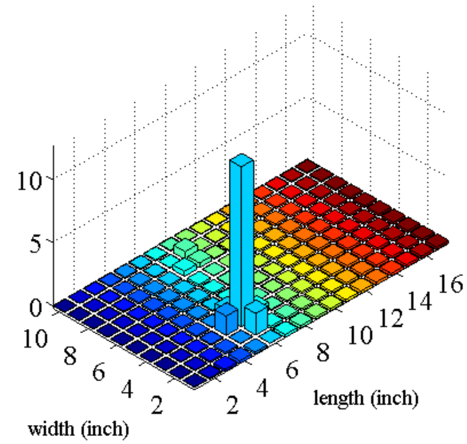 width (inch) length (inch)	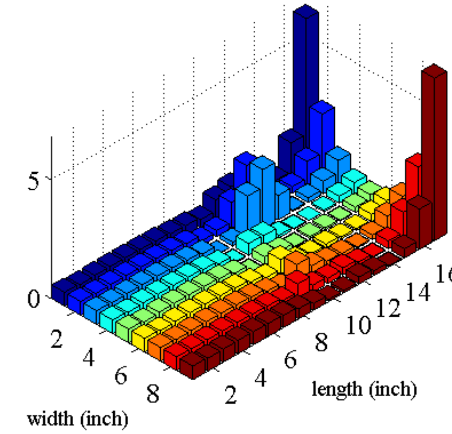 width (inch) length (inch)
Mode 4	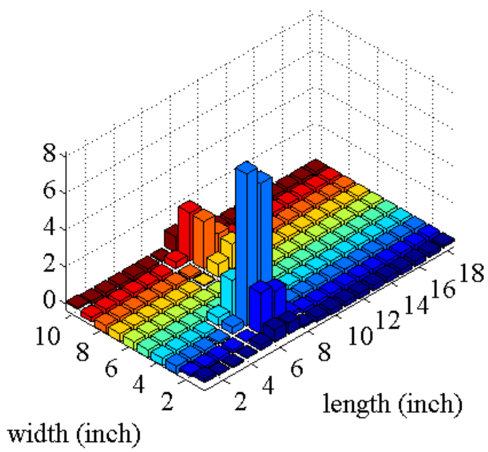 width (inch) length (inch)	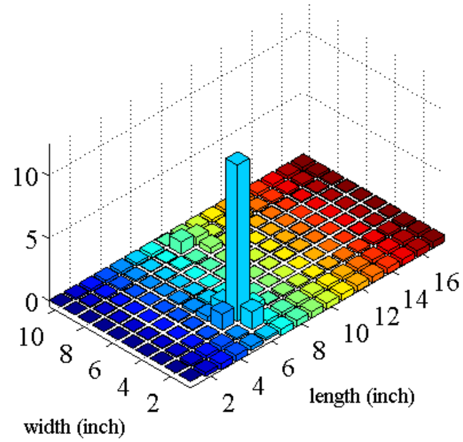 width (inch) length (inch)	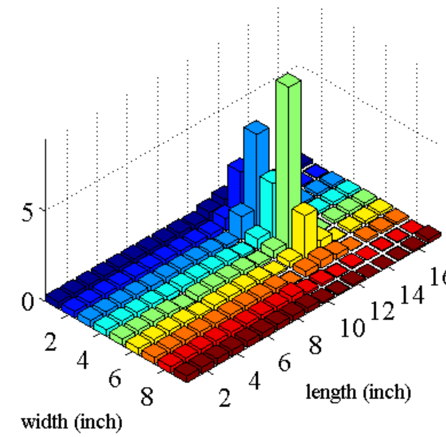 width (inch) length (inch)

Mode 5	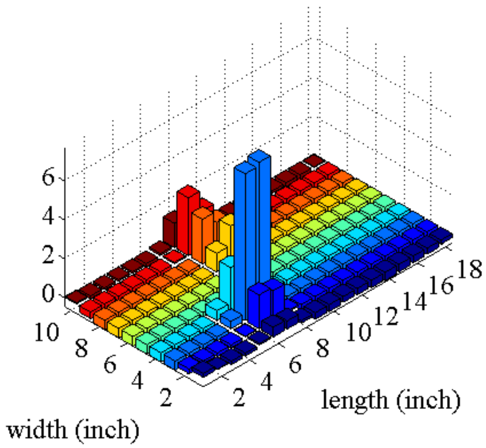	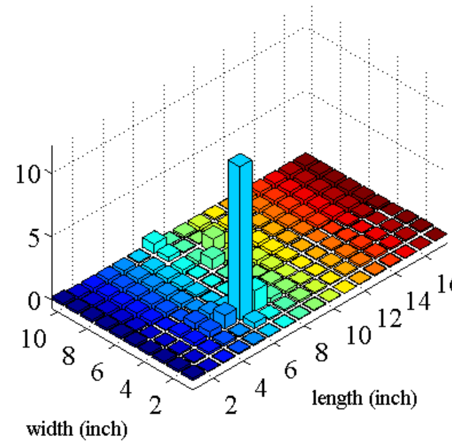	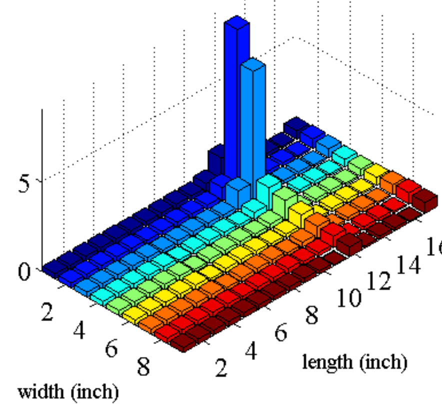
Combination Modes 1-5	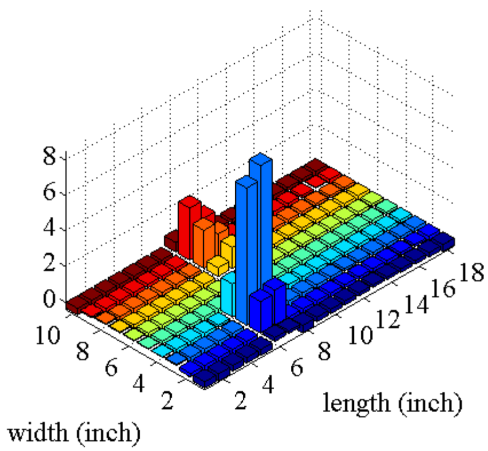	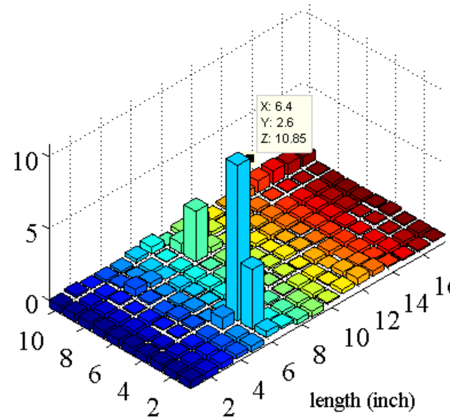	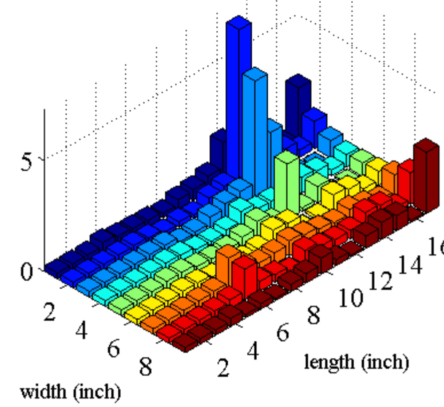

Using the same approach as before, all the algorithms were applied to the curvature in each direction separately to investigate whether they are able to detect and localize multiple damages or not. Table 3.10 shows the results for the application of GSM, GFD and SEM using $\kappa_{x,}$ κ_y and κ_{xy}. It shows that the general trend for all the algorithms is that the curvature in the x-direction as well as the xy-direction was better in detecting the damage, with the curvature in the x-direction giving false indication of the damage. SEM however failed to detect the damage using any direction. Again here the GSM had the superiority above all of the others in terms of being able both of the damages using the curvature in all three directions, whereas the GFD failed to do so using the curvature in the y-direction.

Table 3.10 Application of all damage detection algorithms to κx, κy, and κxy for the damage case three (D3).

	GSM	GFD	SEM
κ_x	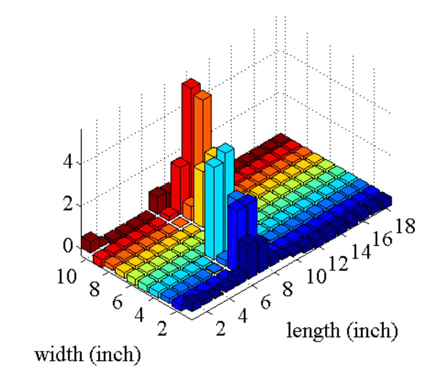	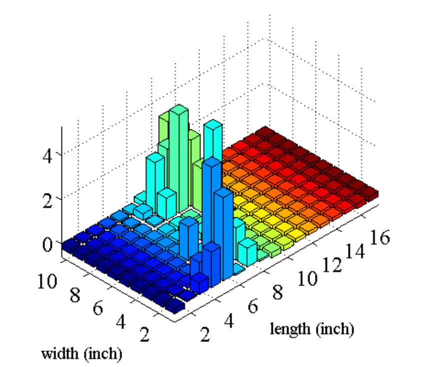	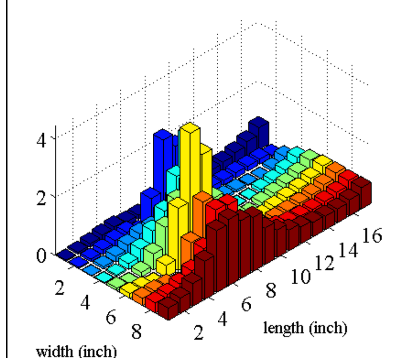
κ_y	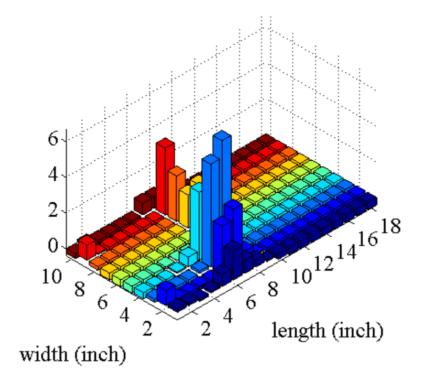	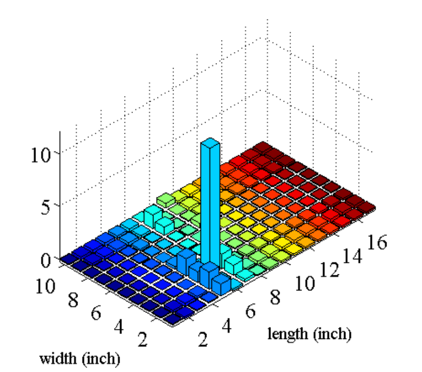	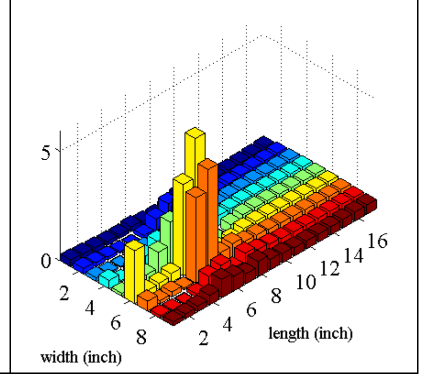

κ_{xy}

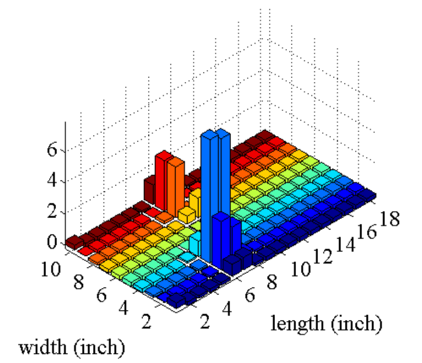

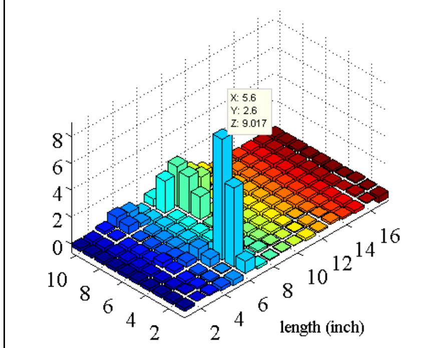

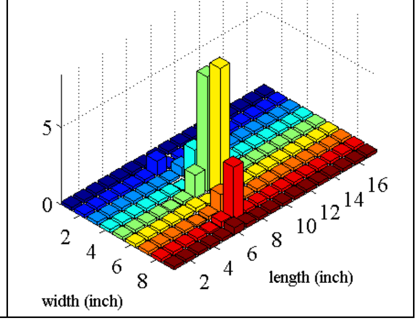

3.4.2 Displacement-based damage detection

This section presents the application of several damage detection algorithms using the numerical displacement mode shapes of the plate. A different set of combinations including the use of different modes of vibration were tested to get the best detectability of the damage. The damage case two (D2) as well as the damage case three (D3) were employed for the purpose of comparison between the curvature-based and displacement-based methods.

3.4.2.1 Damage case 2

The results of the application of all the damage detection algorithms using displacement mode shapes for damage case two (D2) are shown in Table 3.11. It can be seen that GFD and SEM had a good start in detecting damage, but beginning from the third mode, both of the algorithms lose their ability to detect the damage. However, the GSM algorithm started with a first mode unable to detect the damage; afterwards, it is still capable of locating the damage.

Table 3.11 Application of damage detection algorithms to damage case two (D2)

<table>
<tr><th></th><th>GSM</th><th>GFD</th><th>SEM</th></tr>
<tr><td>Mode 1</td><td>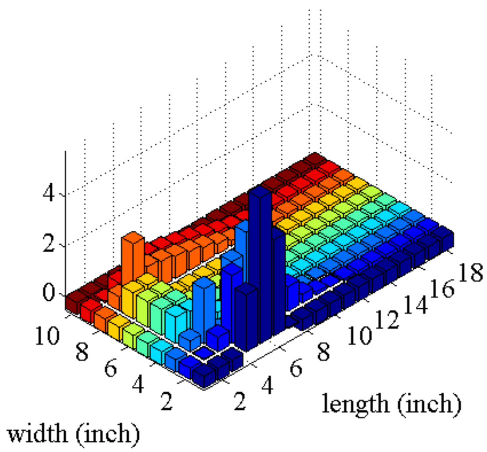
</td><td>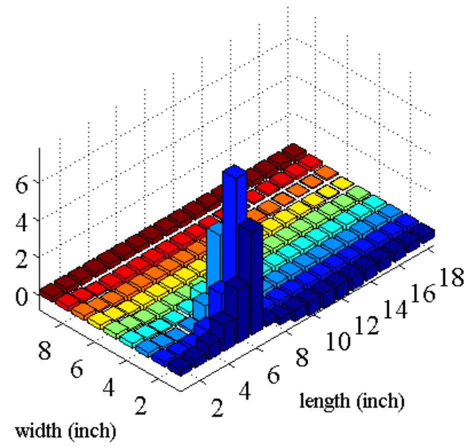
</td><td>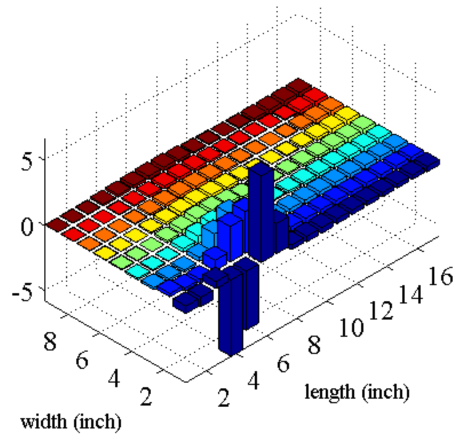
</td></tr>
<tr><td>Mode 2</td><td>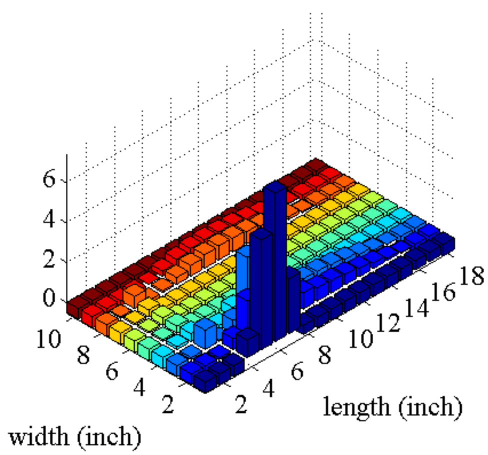
</td><td>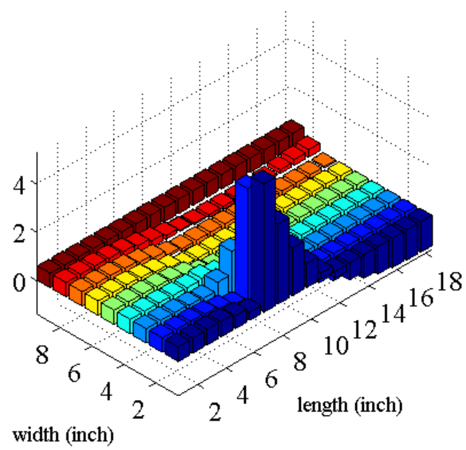
</td><td>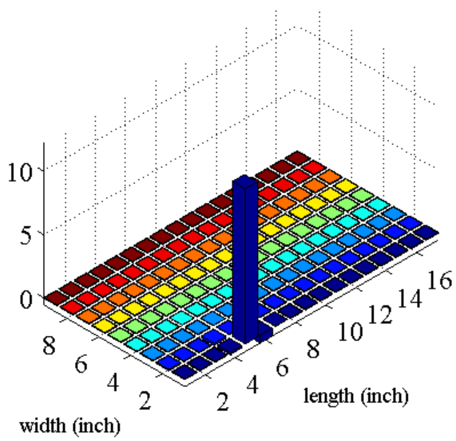
</td></tr>
</table>

Mode 3

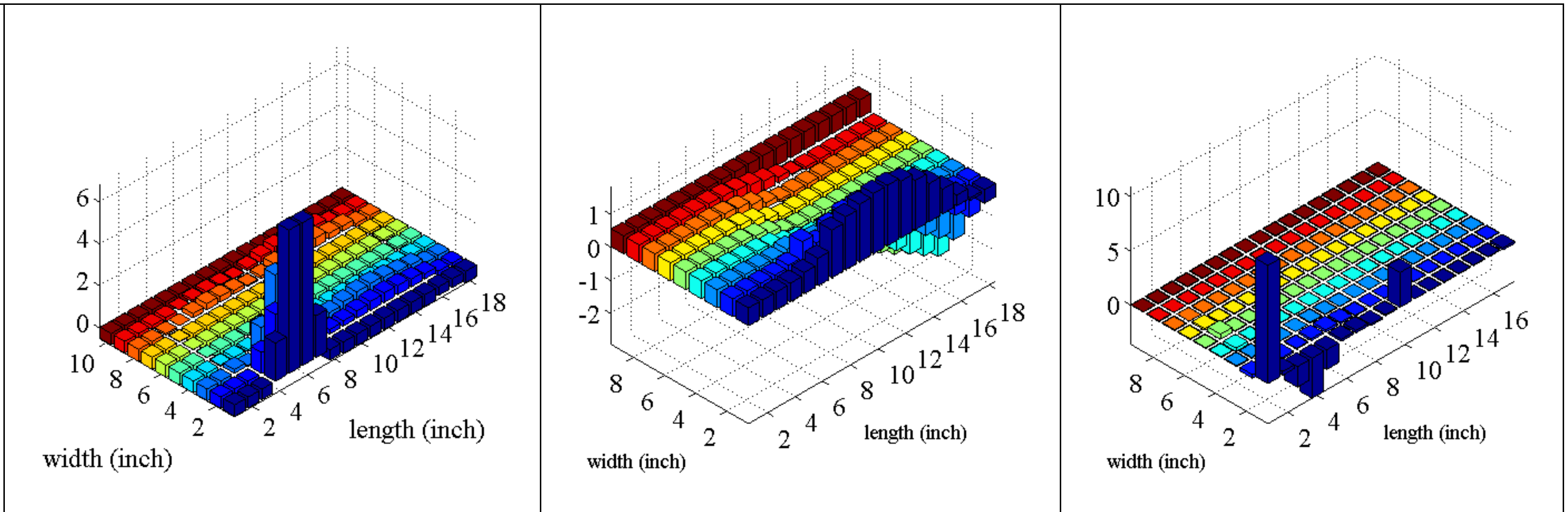

Mode 4

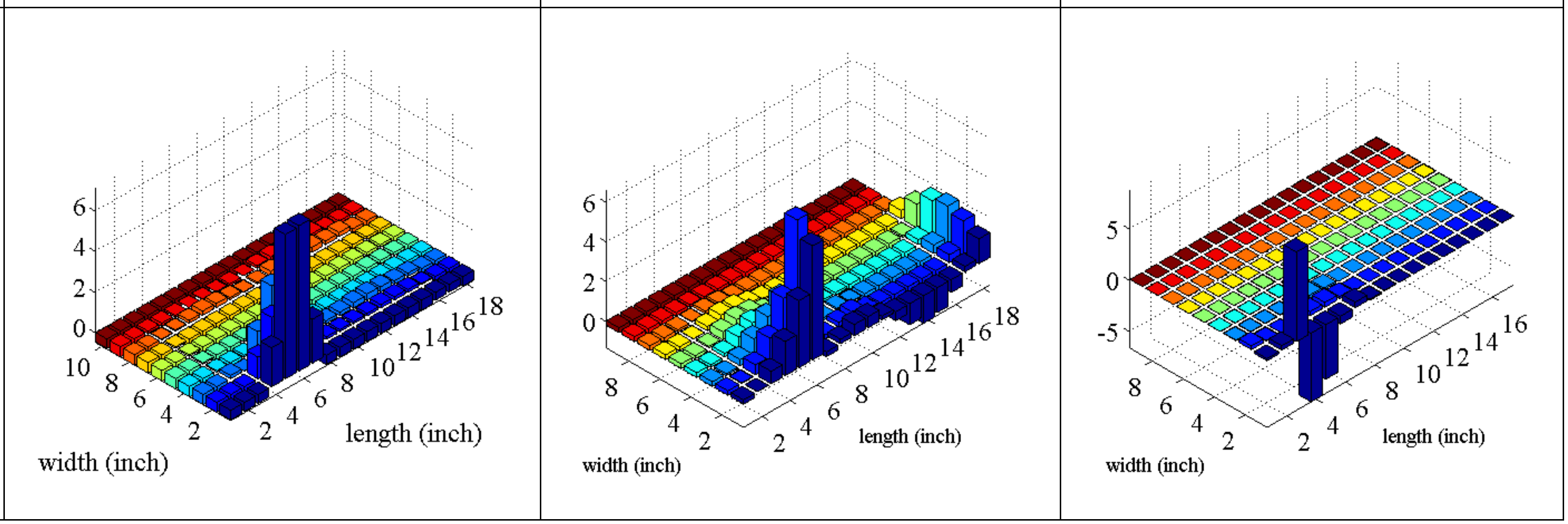

Mode 5	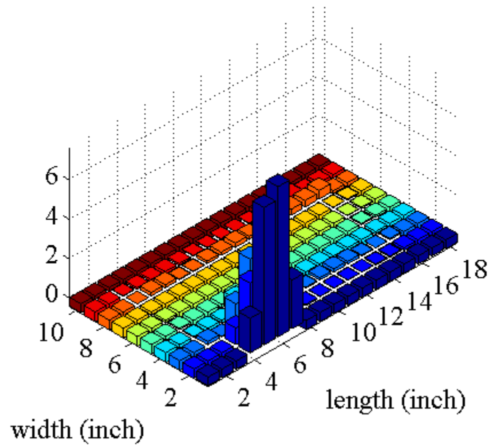	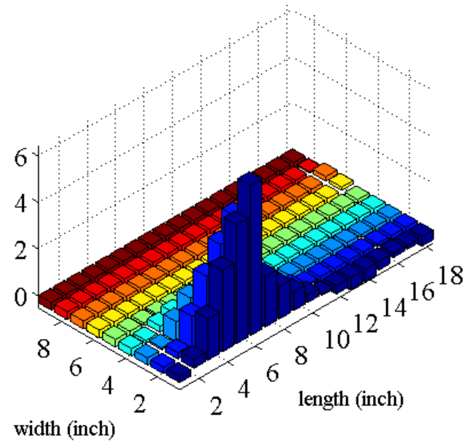	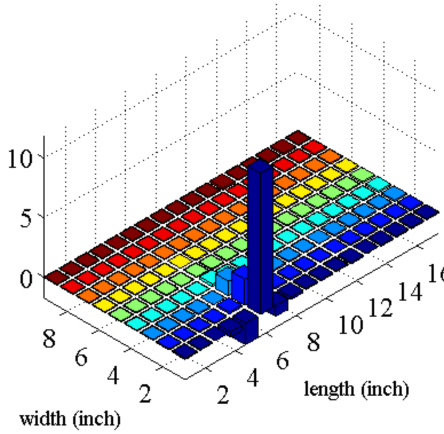
Combination Modes 1-5	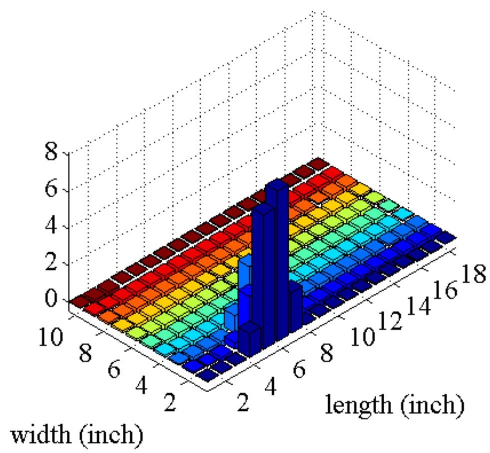	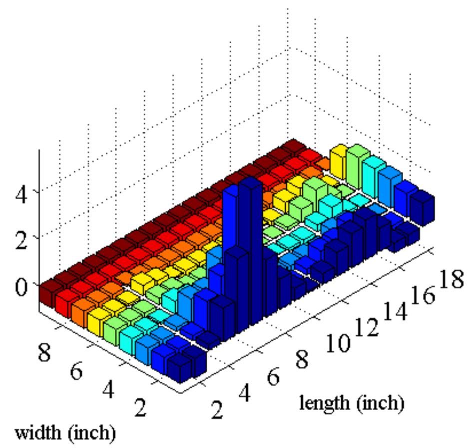	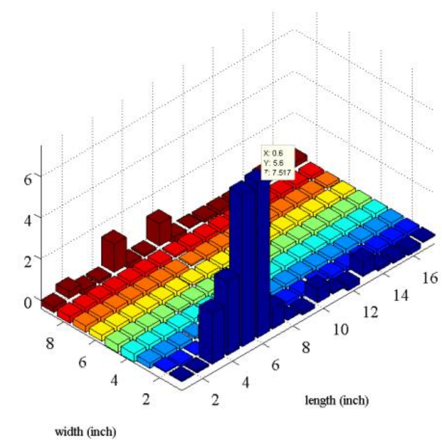

3.4.2.2 Damage case 3

The results for the application of all the algorithms on damage case three (D3) is shown in Table 3.12. It can be observed that some of the modes were able to detect the second damage and some others were able to detect the first damage separately. And the combinations of all the modes were able to detect both the damages. In to the numerical modal analysis, it is able to obtain all the modes as desired; but in the experimental modal testing, sometime it may not be able to obtain all the modes, especially the first few low modes, due to the ambient noise and other factors.

Table 3.12 Application of damage detection algorithms to damage case three (D3)

<table>
<tr><th></th><th>GSM</th><th>GFD</th><th>SEM</th></tr>
<tr><td>Mode 1</td><td>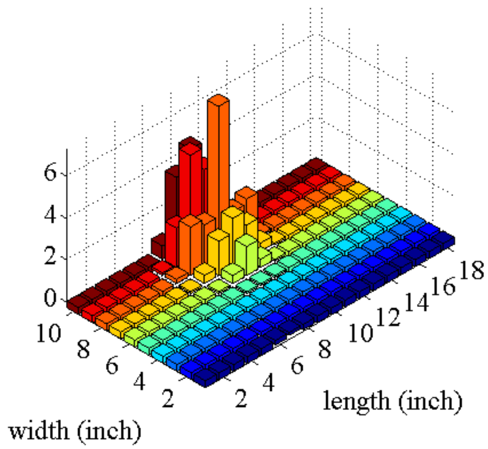
</td><td>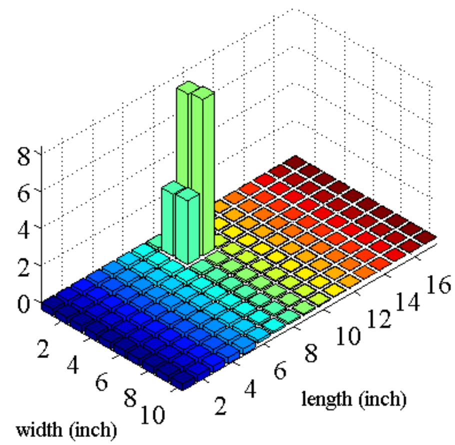
</td><td>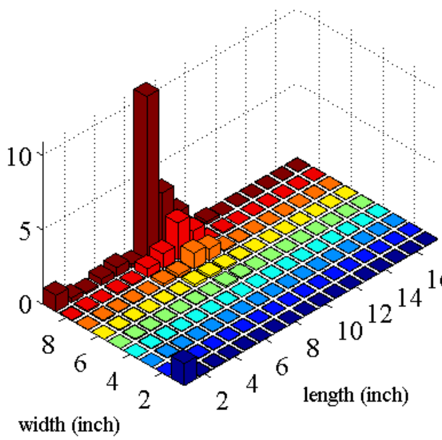
</td></tr>
<tr><td>Mode 2</td><td>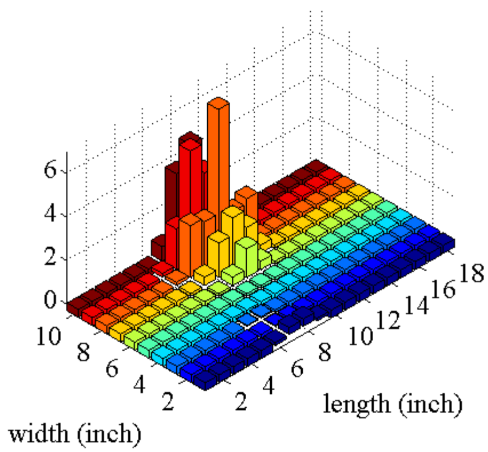
</td><td>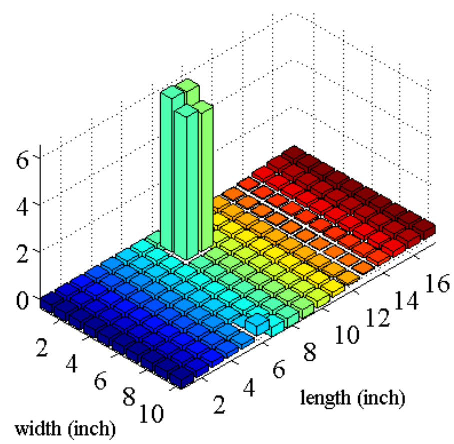
</td><td>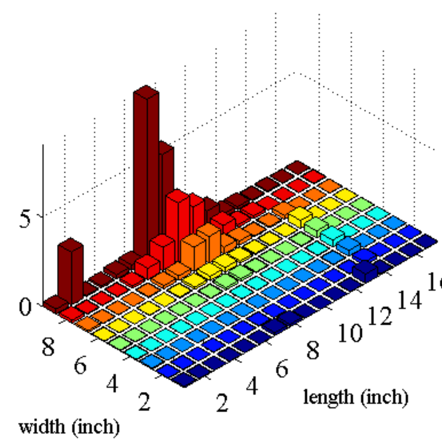
</td></tr>
</table>

Mode 3

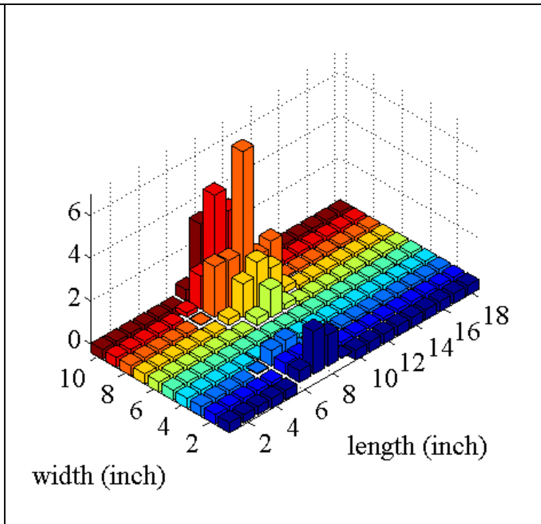

width (inch)
length (inch)

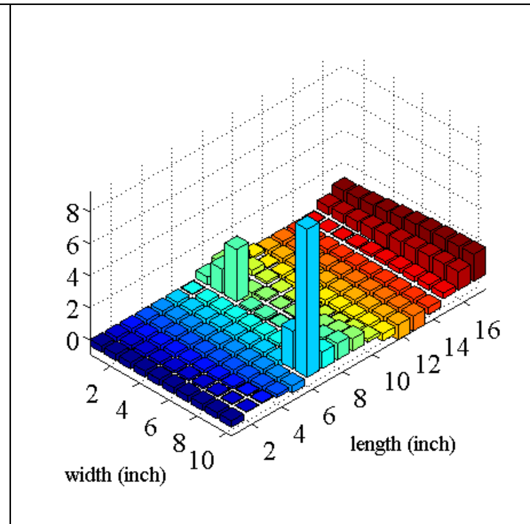

width (inch)
length (inch)

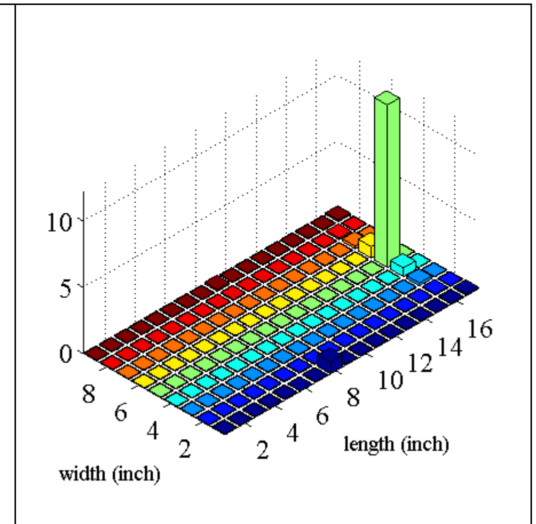

width (inch)
length (inch)

Mode 4

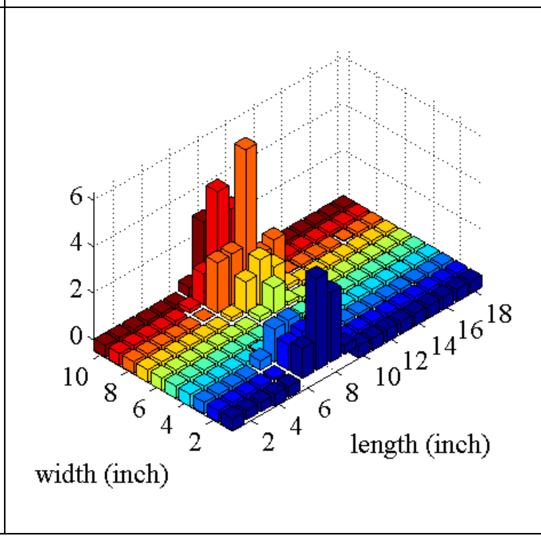

width (inch)
length (inch)

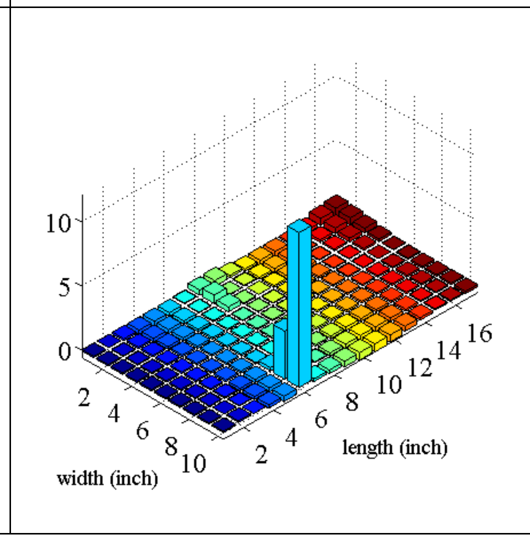

width (inch)
length (inch)

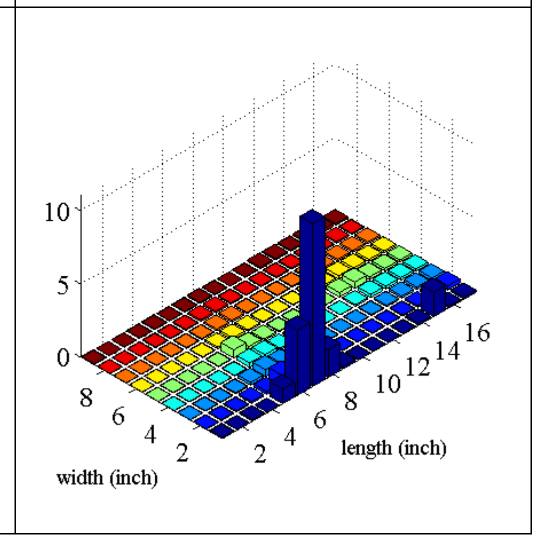

width (inch)
length (inch)

Mode 5	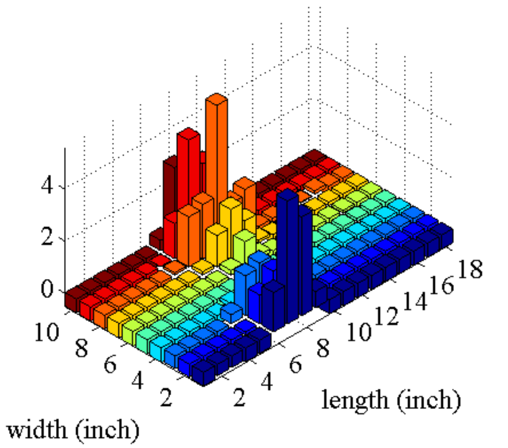	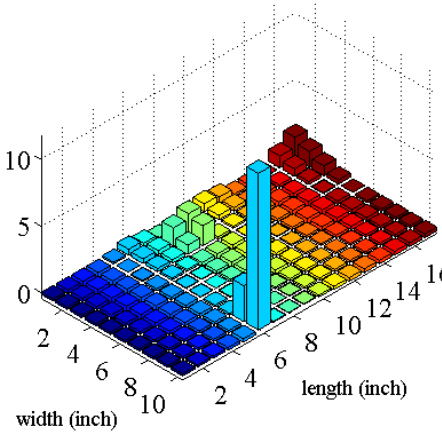	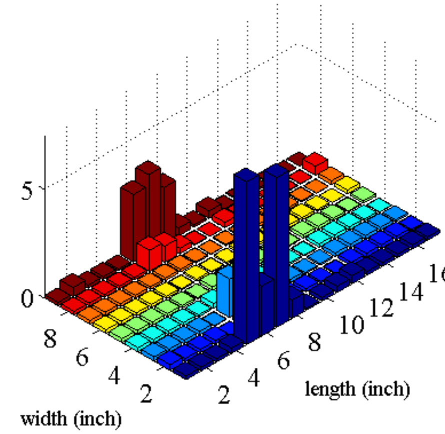
Combination Modes 1-5	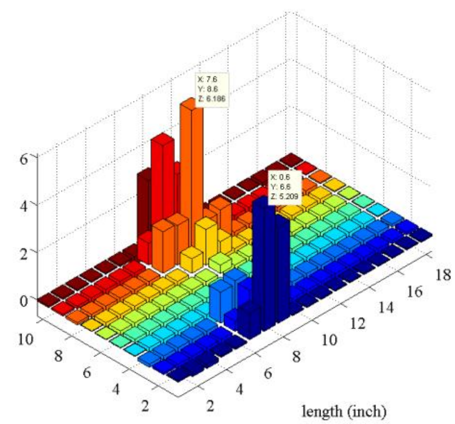	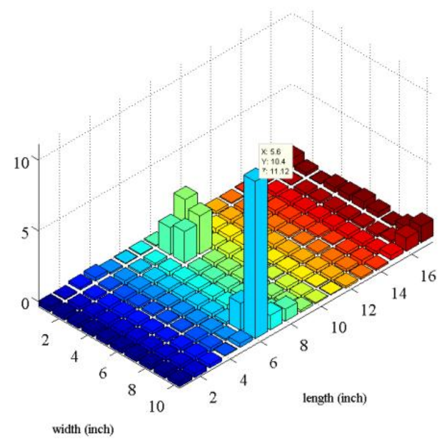	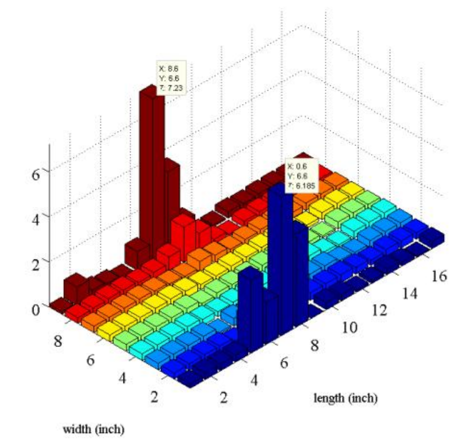

3.5 Displacement vs. Curvature

From Section 3.4.1 for curvature-based damage detection and Section 3.4.2 for displacement-based damage detection, we can observe the superiority of the curvature method because the normalized damage index for all the cases is always higher when the curvature more shape is used.

To study the localization capabilities of these approaches, the false indications from these methods are investigated, i.e., false positive and false negative. The former represents the elements that were mistakenly assumed to be damaged; while the latter represents the elements that were damaged but not detected. The damage is assumed to occur if the value of the normalized damage index is larger than 2. Table 3.13 shows a comparison between the curvature-based and displacement-based damage detection methods in terms of their abilities to localize the damage. It can be noticed that the value of the false positive for displacement is higher than its corresponding curvature value, and this is an indication of the tendency of the displacement method to overestimate the size of the damage or give a false indication of the existence of the damage. On the other hand, looking at the false negative results, it can be noted that the performance of both the methods is close, though the curvature-based methods performed better.

Table 3.13 Comparison between curvature-based and displacement-based damage detection

	D2				D3			
	False pos. elements		False neg. elements		False pos. elements		False neg. elements	
	Curv.	Disp.	Curv.	Disp.	Curv.	Disp.	Curv.	Disp.
GSM	2	3	1	0	2	2	4	4
GFD	0	4	1	0	0	0	4	5
SEM	2	3	1	2	0	3	5	6

3.6 Noise effect

In this section, the noise effect was investigated. Several noise levels expressed as the signal to noise ratios (SNR) were applied to the noise free finite element curvature mode shape for the damage case two, and Gaussian white noise was employed for this purpose which is basically is a random signal normally distributed with a zero mean and a standard deviation σ (in this study, the standard deviation of the mode shape was used). The function awgn (Add white Gaussian noise to signal) from MATLAB library was used to induce the noise. Considering the damage case two as a case study, five noise levels were induced, starting from the noise free case of a 100 dB and ending in a highly noisy case of 10 dB. The results of the application of all the algorithms to the noise induced mode shapes with different noise levels are shown in Tables 3.14 to 3.18. Starting from the noise free, all the algorithms were able to detect the damage successfully. But as the noise increased to 20 dB, damage delectability degraded dramatically using SEM; while GFD and GSM detected the damage clearly and successfully. Decreasing the signal to noise ratio to 30 dBs made the damage hard to recognize when SEM was used, and it affected the clarity of the damage with GSM. At SNR of 20 dB, SEM and GSM failed to detect or localize the damage; whereas GFD can still detect and localize the damage with a reasonable clarity. At SNR of 10 dB, all algorithms failed to detect the damage.

From the above observations, it can be noticed that GFD has the best noise immunity, followed by GSM and then SEM.

Table 3.14 Application of damage detection algorithms with SNR value of 100 dB (noise free)

SEM	GFD	GSM
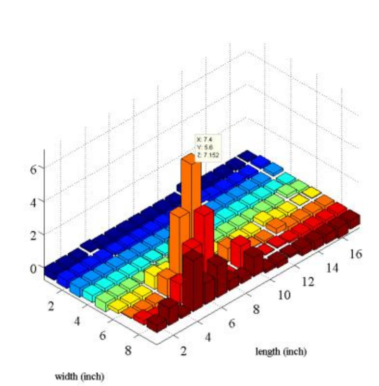	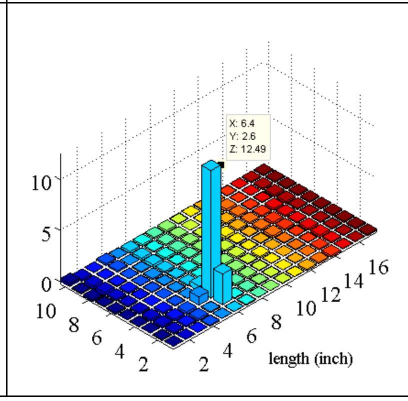	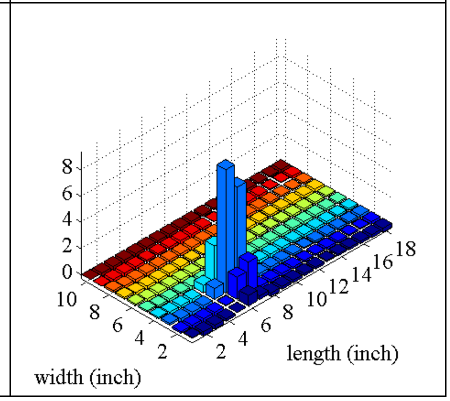

Table 3.15 Application of damage detection algorithms with SNR value of 40dB

SEM	GFD	GSM
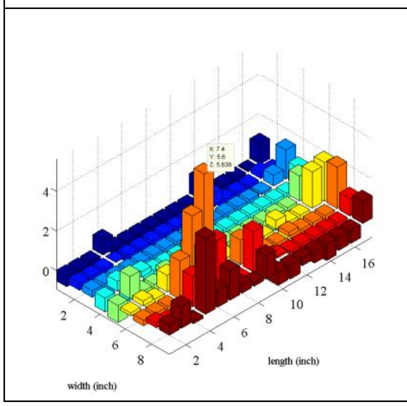	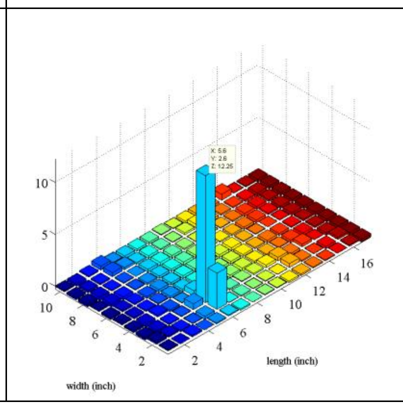	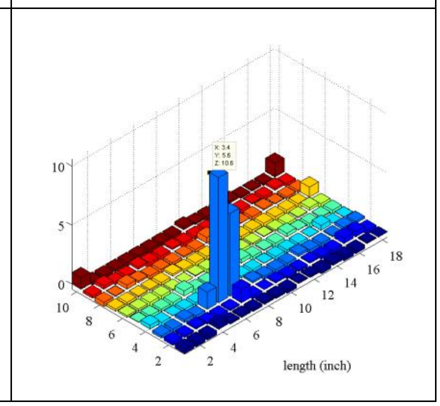

Table 3.16 Application of damage detection algorithms with SNR value of 30dB

SEM	GFD	GSM
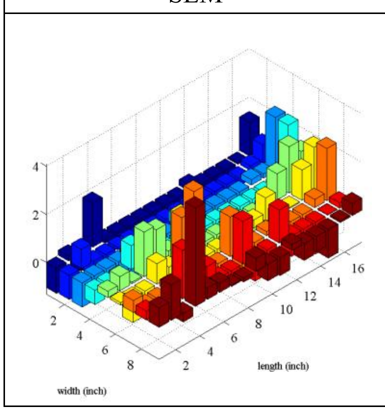	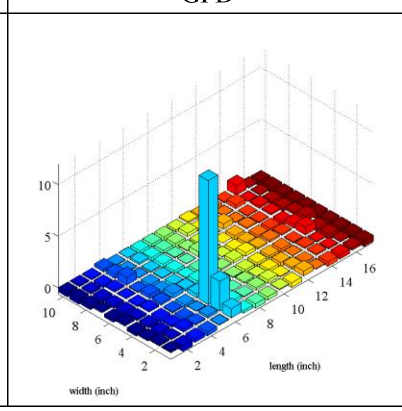	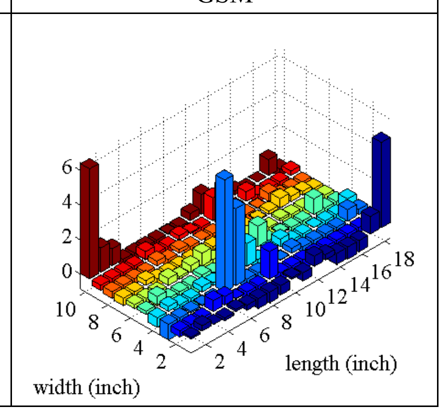

Table 3.17 Application of damage detection algorithms with SNR value of 20dB

SEM	GFD	GSM
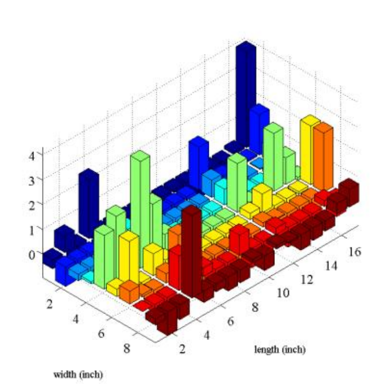	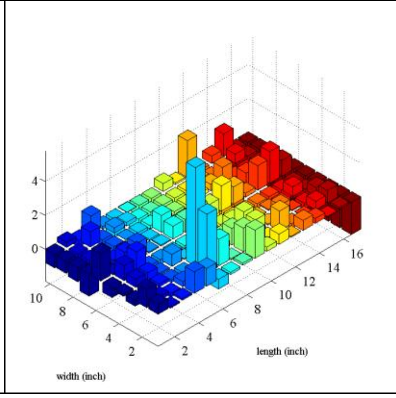	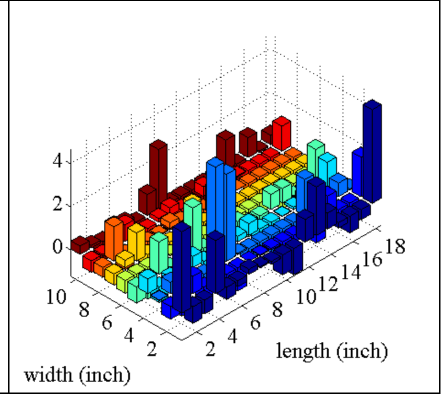

Table 3.18 Application of damage detection algorithms with SNR value of 10dB

SEM	GFD	GSM
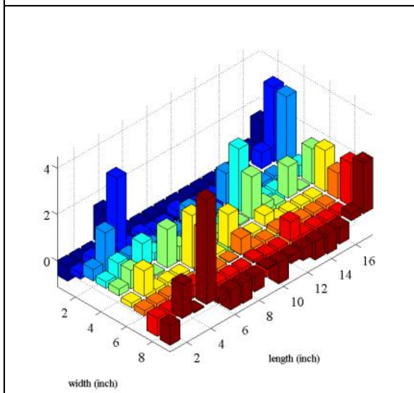	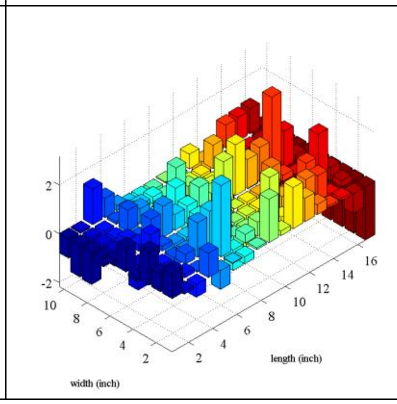	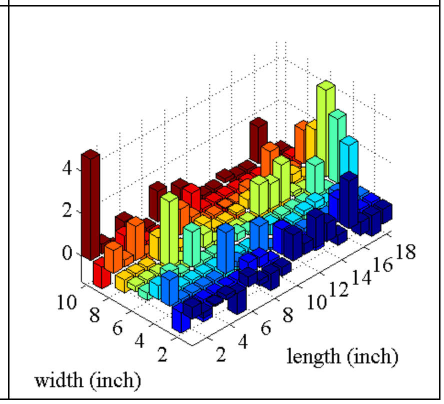

3.7 Sensor spacing effect

The original spacing considered in both the experimental program as well as the finite element analysis was 1.0 in., while one of the objectives of this study is to minimize the number of sensors required for damage detection. Therefore, in this section, three sensor spacing cases are investigated: 1.0, 2.0 and 3.0 in. Again, the damage case 2 will be the case study.

Starting with the 1.0 in. original spacing, 180 points were present (18 × 10), and all algorithms were able to identify the damage. Increasing the spacing into 2.0 in. decreased the number of points to 45 (9 × 5). The increased spacing of sensors affected the damage index value for all the algorithms almost by a factor of one half. Also, the SEM ability to refine the singularity of the damage was affected intensely while both GFD and GSM were sufficient. Finally, increasing the spacing to 3.0 in. decreased the number of points to 24 points (6 × 4), and as a result, SEM and GFD failed to identify the damage while GSM was still able to identify the damage with a reasonable clarity.

From the above observations, it can be seen that the GSM algorithm is the best in detecting and localizing the damage with the minimum amount of noise, followed by GFD and then SEM.

Table 3.19 Application of damage detection algorithms with one inch sensor spacing (original arrangement)

SEM	GFD	GSM
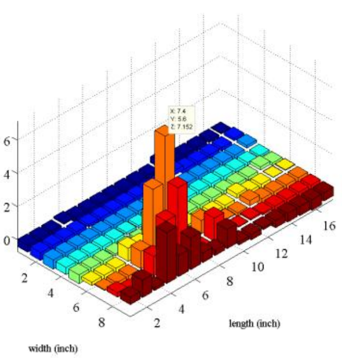	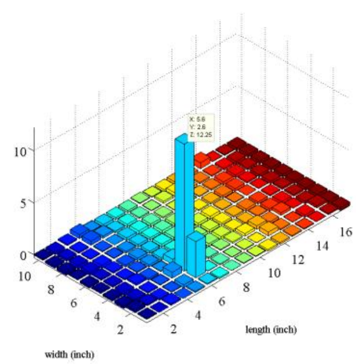	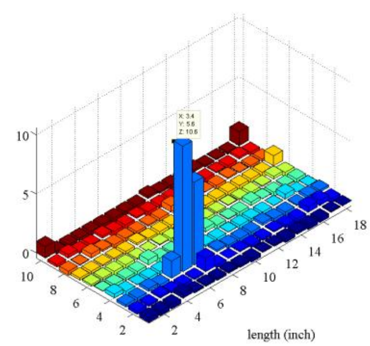

Table 3.20 Application of damage detection algorithms with two inches sensor spacing

SEM	GFD	GSM
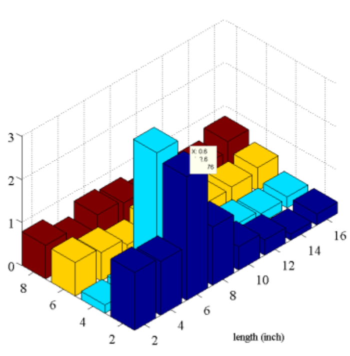	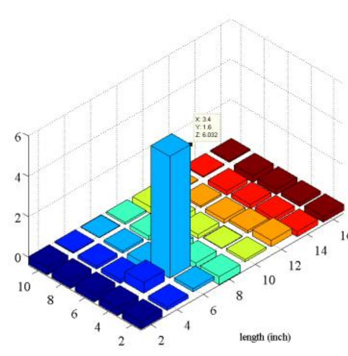	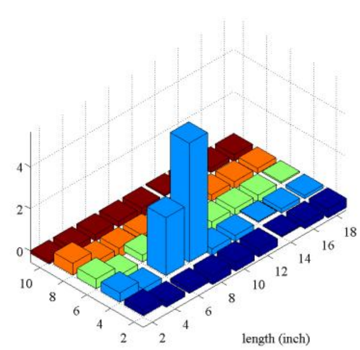

Table 3.21 Application of damage detection algorithms with three inches sensor spacing

SEM	GFD	GSM
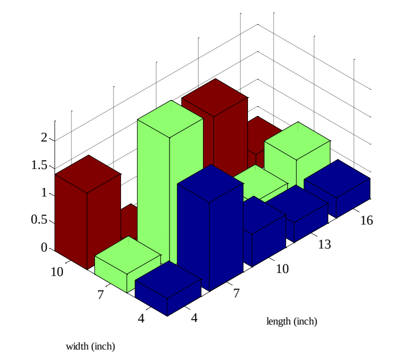	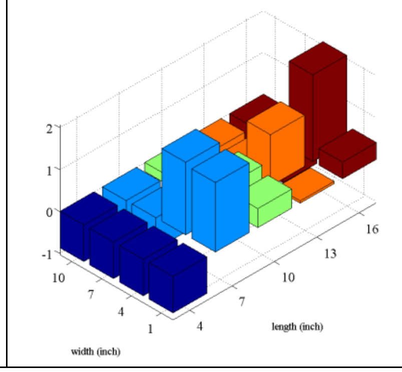	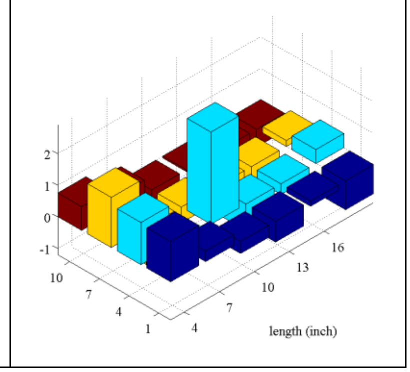

3.8 Summary

In this chapter, the finite element (FE) model was presented, and three damage cases were modeled using ABAQUS CAE 6.10. The curvature mode shapes as well as displacement mode shapes were extracted from the specific node points. Three damage detection algorithms were applied to the FE results. GSM was the best in terms of both damage detection and localization. For the first and the second damage cases, κ_y was the dominant curvature to use for detecting the saw cut damage in the y-direction. While in the third damage case, κ_{xy} has the best ability to detect and localize two damages present in the plate. Then, the same damage detection algorithms were applied to the displacement mode shape for the damage cases two and three, and the results showed that using the displacement lead to some false damage indication in both the damage cases. In addition, the noise effect was studied, and it showed that GFD has the best noise immunity. Finally, the sensor spacing effect was evaluated, and GSM showed the best performance with the increased sensor spacing.

Chapter 4

DAMAGE DETECTION OF FRP COMPOSITE PLATES FROM EXPERIMENTAL TESTING DATA

4.1 Introduction

In this chapter, different damage detection algorithms will be utilized for the purpose of detecting several scenarios of damage induced to the FRP plate, and the three damage cases already mentioned in previous chapters will be tested with three different algorithms. The curvature mode shapes (using the PZT-PVDF system) as well as displacement mode shapes (using the Hammer-Accelerometer system) presented in Chapter 2 will be used to detect the damage.

4.2 Curvature-based damage detection

The application of several damage detection algorithms using the experimentally-measured curvature mode shapes of the plate in all directions (κ_x, κ_y, and κ_{xy}) are presented. As already discussed, the outcome of PZT-PVDF system is the strain mode shapes in the *x*, *y* and *xy* directions which are proportional to the curvature via a constant. Since the normalized mode shapes are used, the strain mode shapes could be used in the place of the curvature mode shape. The use of single mode as well as a combination of all the modes (3^{rd}-5^{th}) was investigated as well. In addition, the use of the curvatures in *x*, *y* and *xy* directions was tested and compared to the use of all the curvatures to get the best detectability of the damage.

4.2.1 Damage Case 1

The application of three different algorithms to the damage case 1 is shown in Table 4.1. Modes 3 to 7 as well as a combination of multiple modes are presented. As a difference from the analysis of finite element data, the noise factor comes to picture in the experimental data. Therefore, the variability in the results between different modes is expected as each type of noise has a specific frequency or a range of frequencies. From Table 4.1, it can be observed that GSM had managed to detect the damage using all the modes, whereas GFD and SEM fluctuated. For instance, using the third mode, all the methods (including GSM, GFD and SEM) were able to detect the damage with minimal amount of false indication. Using the fourth and fifth modes, only GSM were able to detect the damage; while GFD and SEM failed to do so. However, Using the combination of all these modes reduced the false indication levels intensively and refined the localization of damage.

Table 4.1 Application of damage detection algorithms to damage case one

<table>
<tr><th></th><th>GSM</th><th>GFD</th><th>SEM</th></tr>
<tr><td>Mode 3</td>
<td>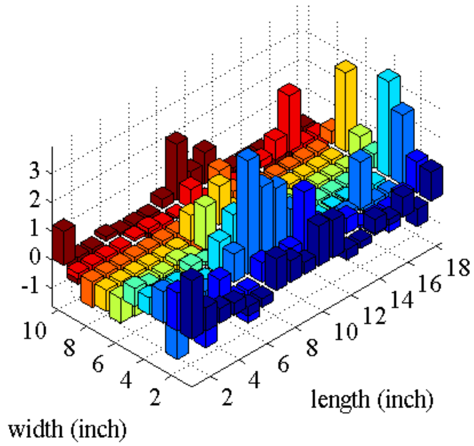
</td>
<td>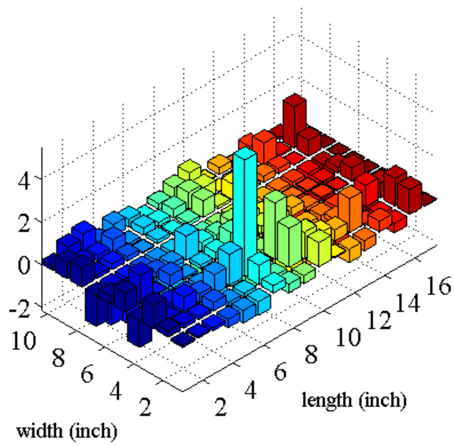
</td>
<td>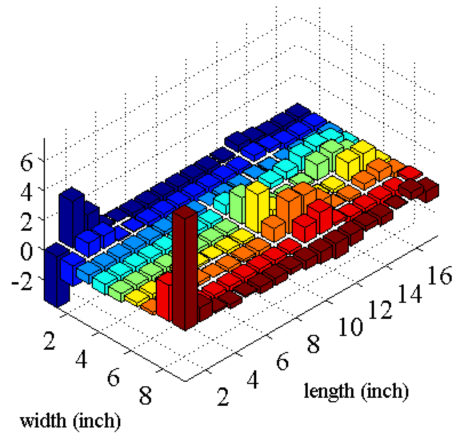
</td></tr>
<tr><td>Mode 4</td>
<td>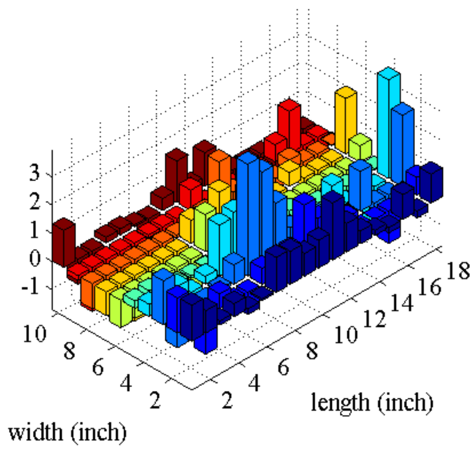
</td>
<td>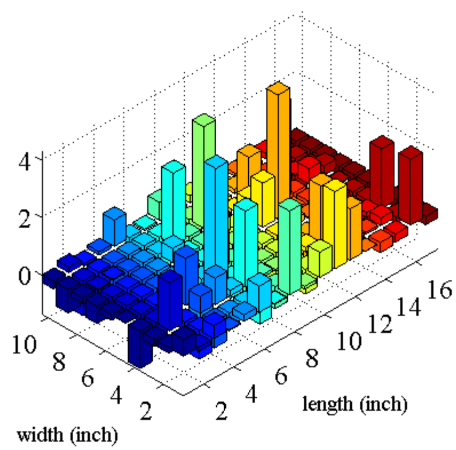
</td>
<td>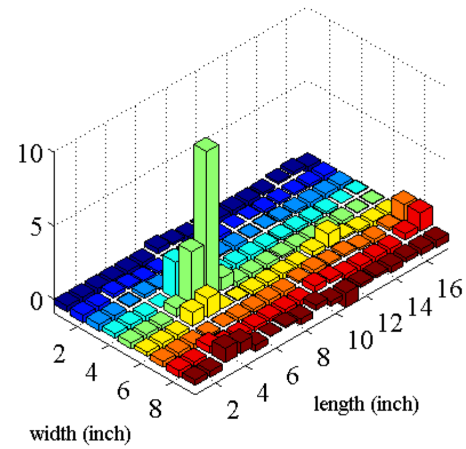
</td></tr>
</table>

<table>
<tr>
<td>Mode 5</td>
<td>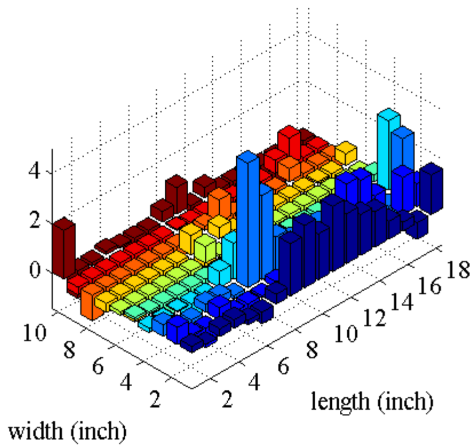
</td>
<td>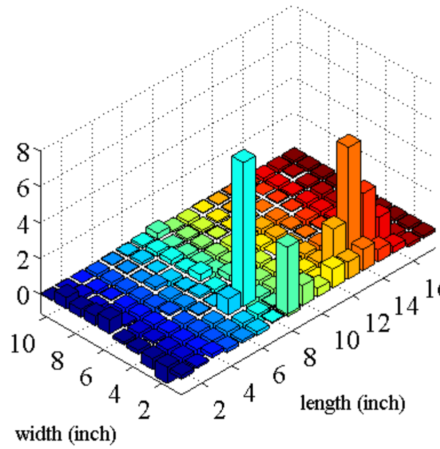
</td>
<td>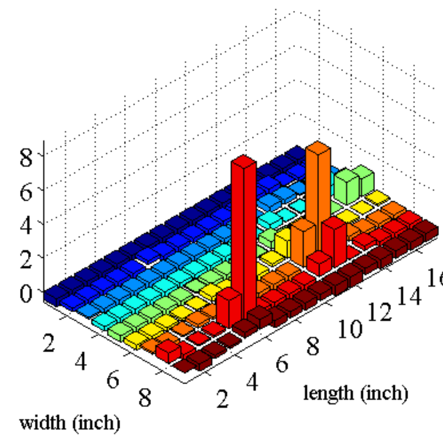
</td>
</tr>
<tr>
<td>Mode 6</td>
<td>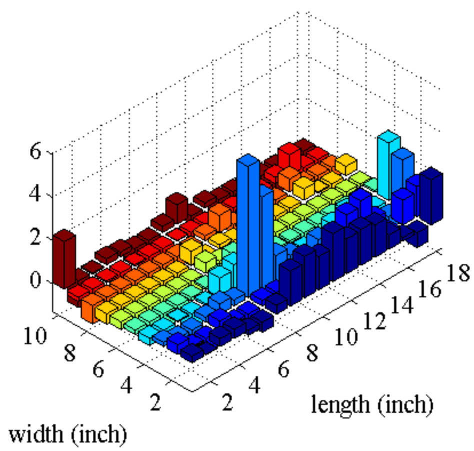
</td>
<td>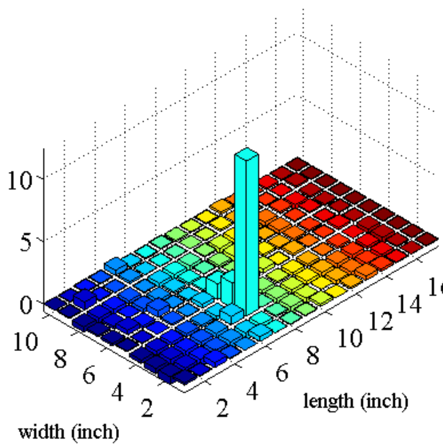
</td>
<td>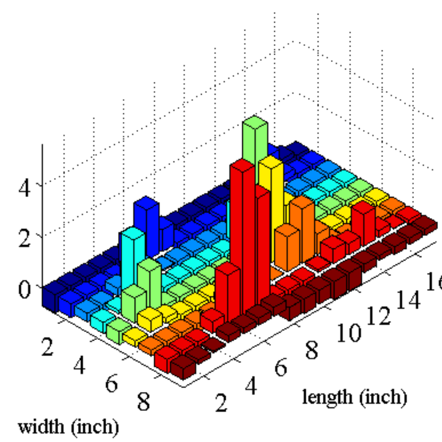
</td>
</tr>
</table>

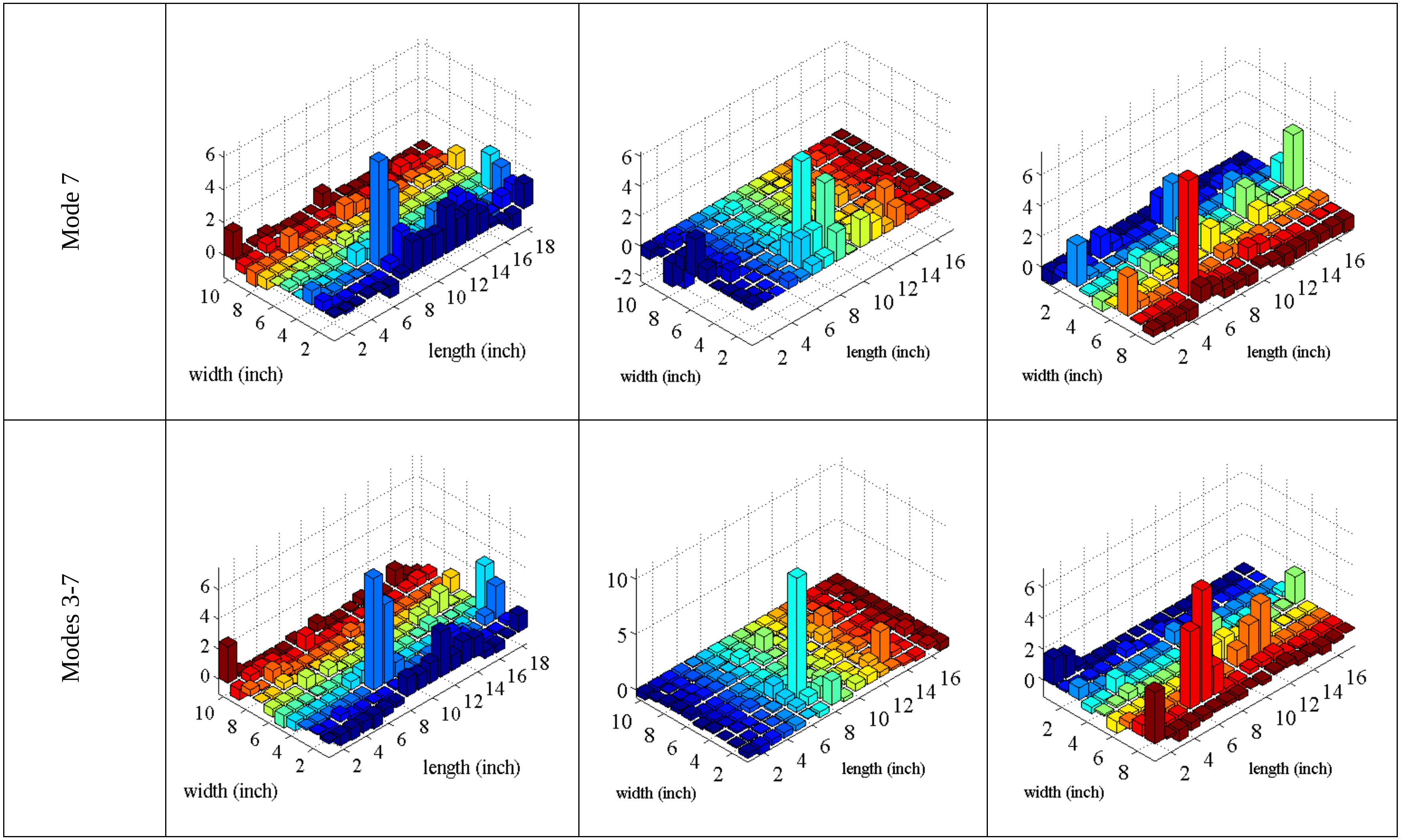
Mode 7
Modes 3-7
width (inch)
length (inch)

Damage detection algorithms were applied to the curvatures in each direction separately to investigate the effectiveness and usefulness of using the curvature in a single direction or all the directions as before. From Table 4.2, it can be seen that the damage is best detected and localized using the curvature in the y-direction (κ_y). Using κ_{xy} succeeded to detect the damage with GSM and GFD but with a large amount of false indication with SEM. Using κ_x failed to detect the damage with all three algorithms. As aforementioned, this can be explained that since the damage is oriented in the y-direction, consequently the change in the curvature will be more in the direction transverse to the damage. From a damage index point of view, GFD had the highest value of damage index using κ_y, followed by GSM and then SEM. In this damage localization wise, it can be seen that GSM had the best localization ability, followed by GFD, and then SEM.

Table 4.2 Application of damage detection algorithms to (κx, κy, and κxy) for damage case one

	GSM	GFD	SEM
κ_x	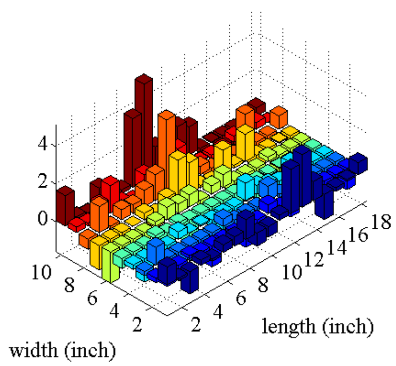	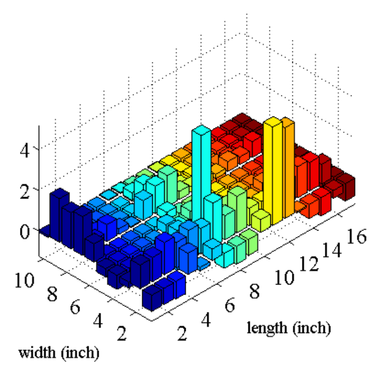	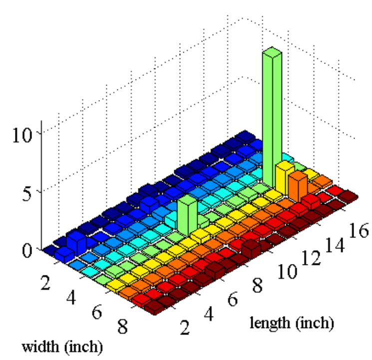

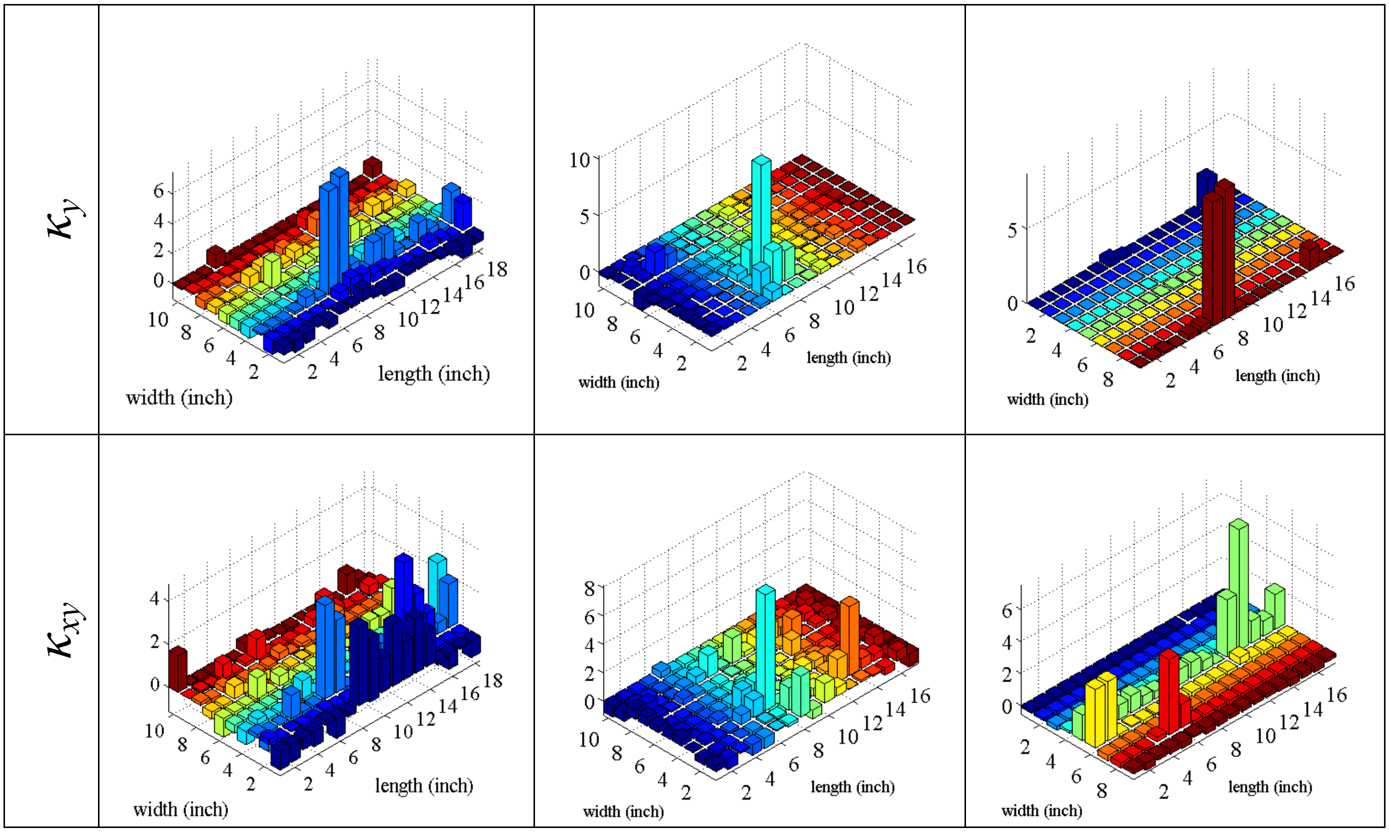

4.2.2 Damage case 2

As aforementioned, the damage case two is similar to the damage case one but with an increased damage severity. As the damage severity increases, the damage index should increase. From Table 4.3, it can be seen that the third mode failed in detecting the damage due to the noise. For the fourth mode, the damage can be clearly identified with the GSM and GFD algorithms, but not with the SEM algorithm. Using the modes five, six and seven, all the algorithms were able to detect and localize the damage. As expected, the application of the algorithms using a combination of modes decreased the false indication levels and refined the damage. It can also be noted that the damage index value increased; for instance, the damage index for the damage case two using a combination of modes and the SEM algorithm was 10.5, while the damage index for the damage case three was 17.3, which proved the difference in severities.

Table 4.3 Application of damage detection algorithms to damage case two

	GSM	GFD	SEM
Mode 3	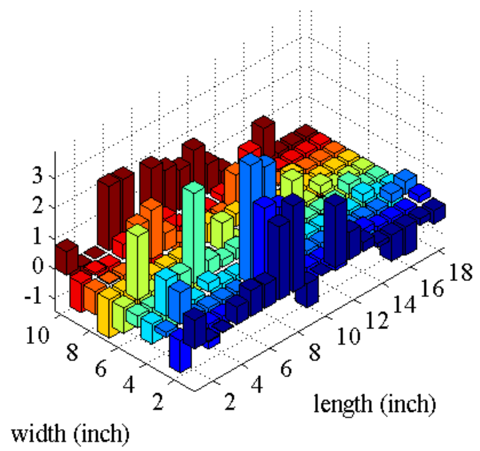	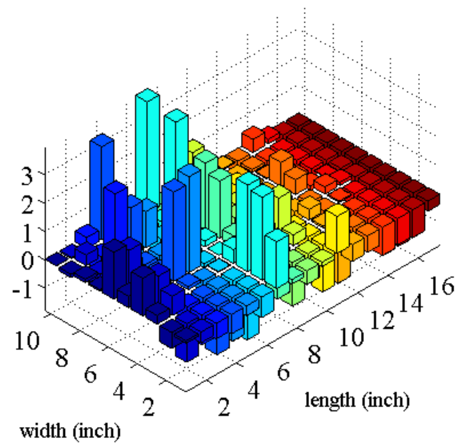	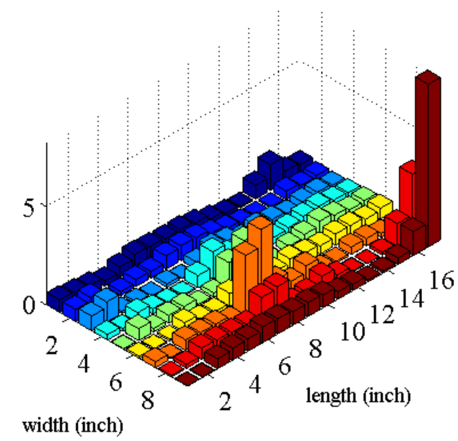
Mode 4	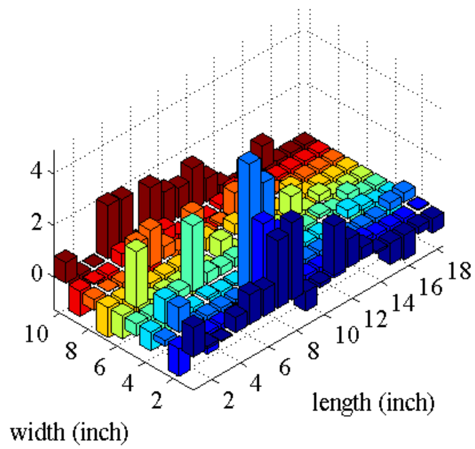	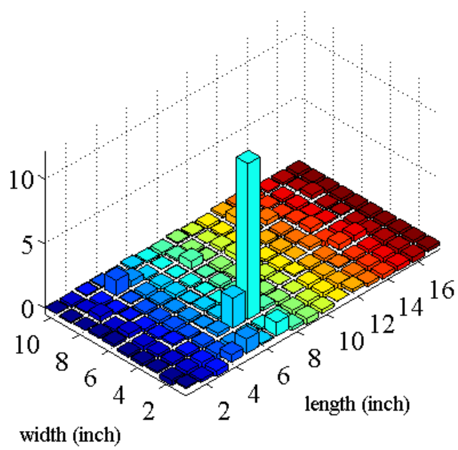	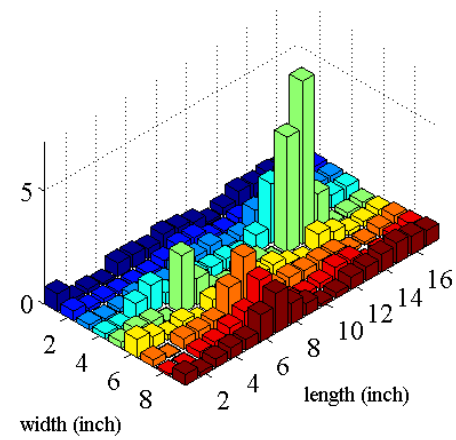

Mode 5	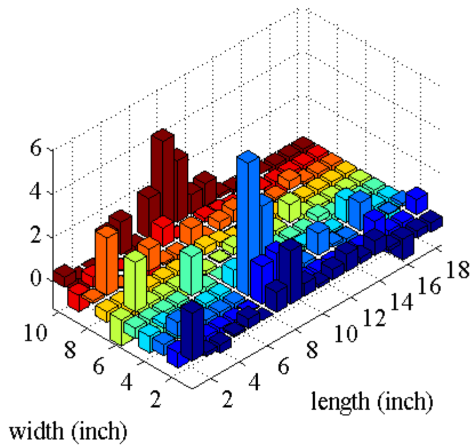width (inch) length (inch)	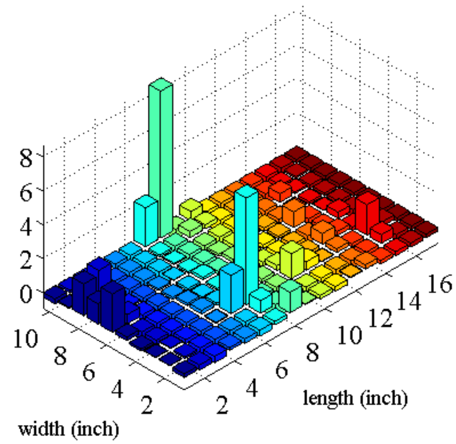width (inch) length (inch)	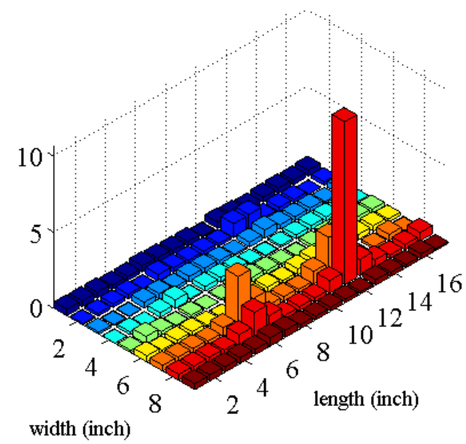width (inch) length (inch)
Mode 6	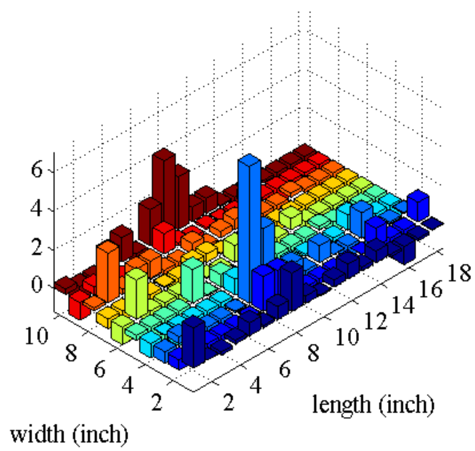width (inch) length (inch)	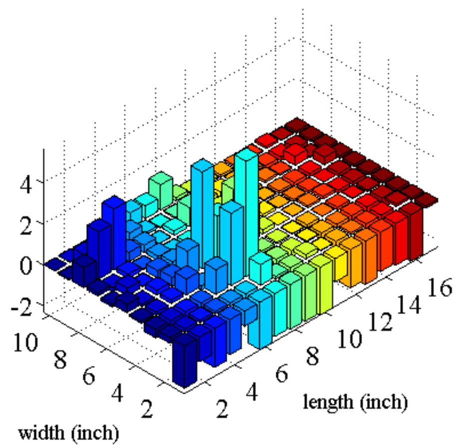width (inch) length (inch)	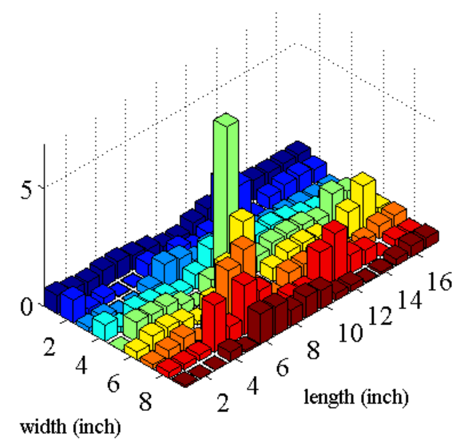width (inch) length (inch)

Mode 7

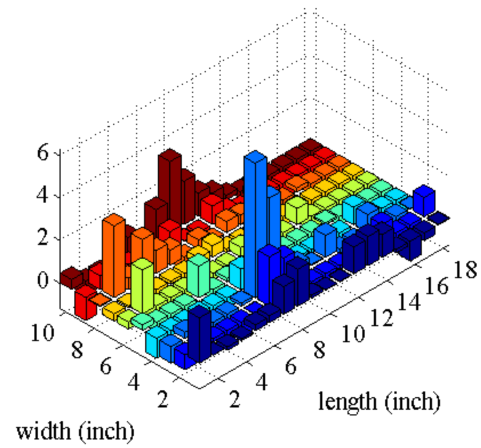

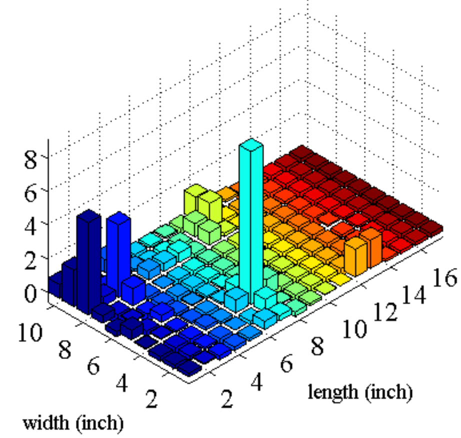

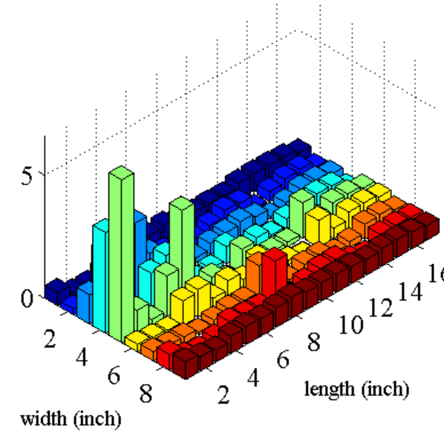

Combination Modes 3-7

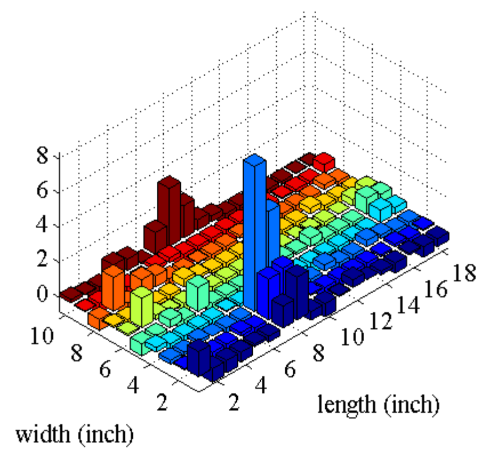

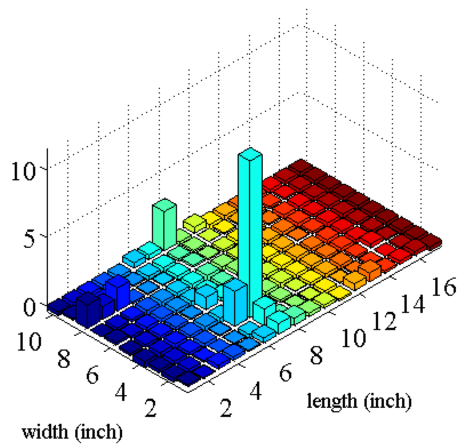

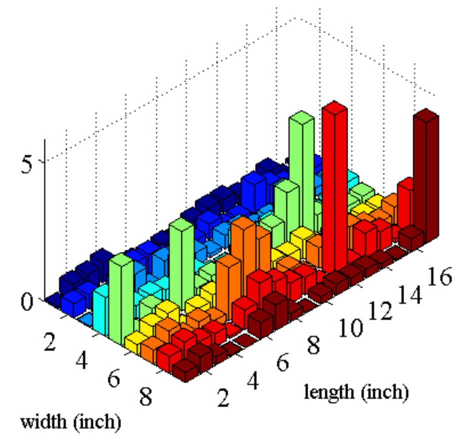

As discussed in the damage case one, the most influential curvature was the curvature in the y-direction. Because the severity was the only thing changed between the damage case 1 and damage case 2, the same conditions should apply here. From Table 4.4, it can be seen that the curvature in the y-direction still have the most effect on the value of the damage index, and it is thus sufficient to measure the curvature in the y-direction only and ignore the effect of the other two directions.

Table 4.4 Application of all damage detection algorithms to κx, κy, and κxy for the damage case two.

	GSM	GFD	SEM
κ_x	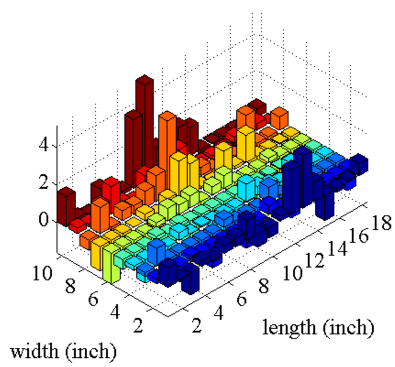	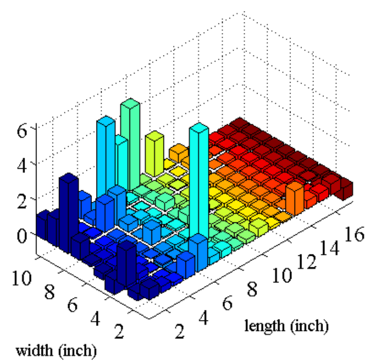	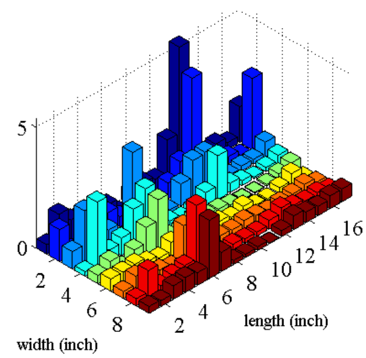
κ_y	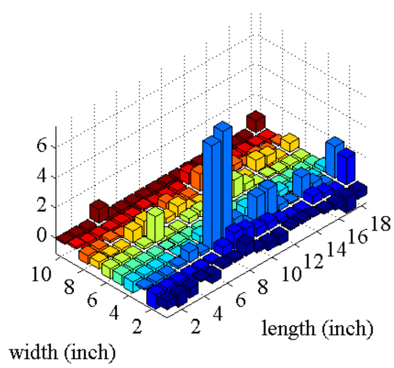	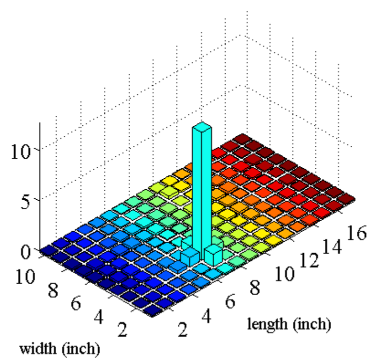	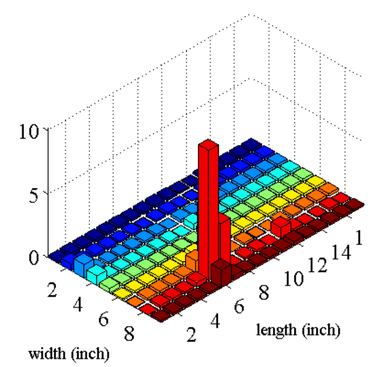

κ_{xy}	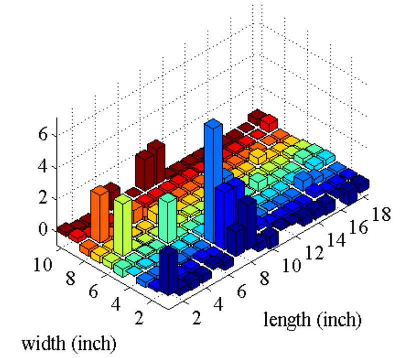	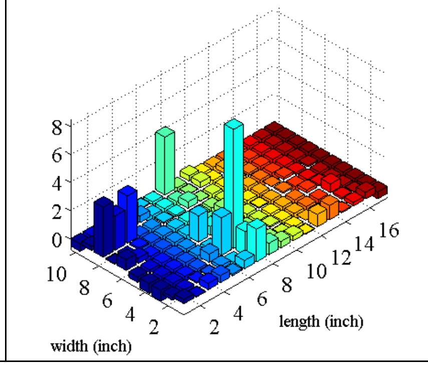	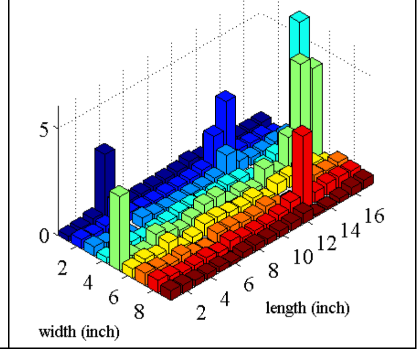

4.2.3 Damage case 3

The damage case 3 (D3) was created to investigate the applicability of different algorithms to multiple damage detection. From Table 4.5, it can be noted that different modes were able to detect a single damage; for instance, it can be seen that from the third mode GFD and SEM were able to detect and localize the first damage without any sign of the second damage existence. But as the mode number increases the second damage starts to appear until the mode seven where the second damage is the only thing that can be seen with SEM and GFD. In conclusion, using a combination of modes was successful in detecting the damage, with a minimum amount of false indication using GSM and GFD, and a relatively high false indication levels using SEM.

Table 4.5 Application of damage detection algorithms to damage case three

<table>
<tr><th></th><th>GSM</th><th>GFD</th><th>SEM</th></tr>
<tr><td>Mode 3</td><td>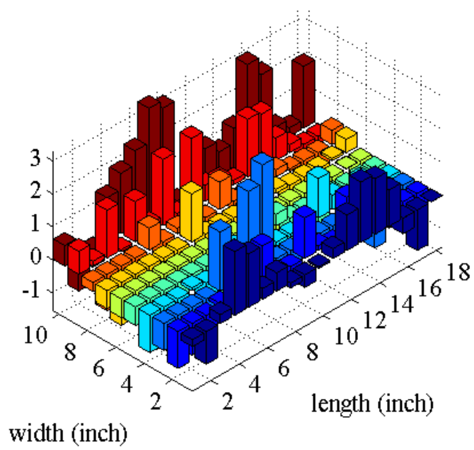
</td><td>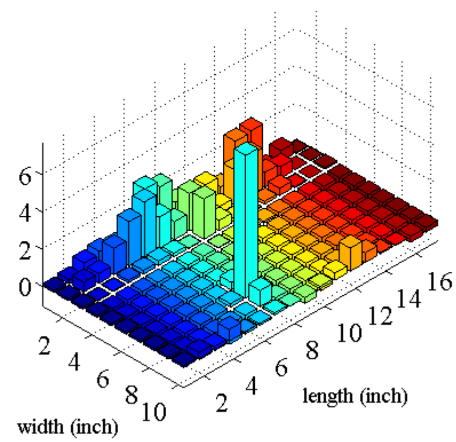
</td><td>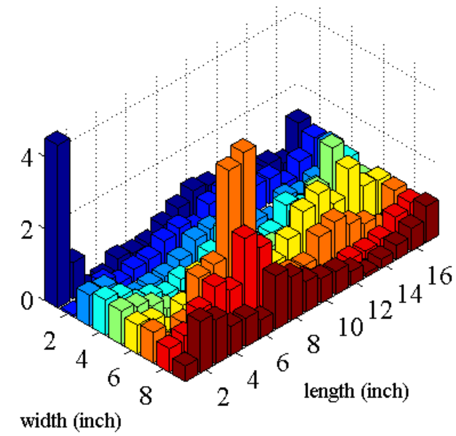
</td></tr>
<tr><td>Mode 4</td><td>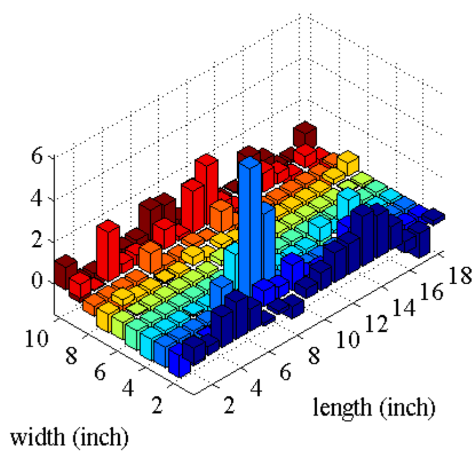
</td><td>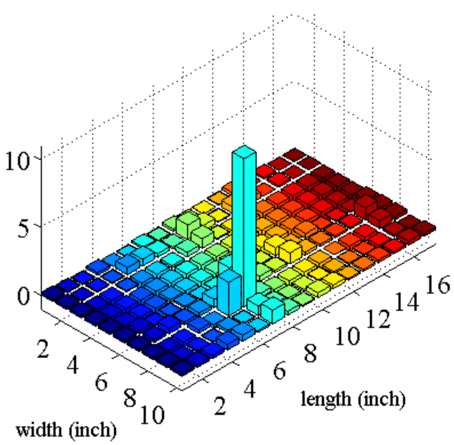
</td><td>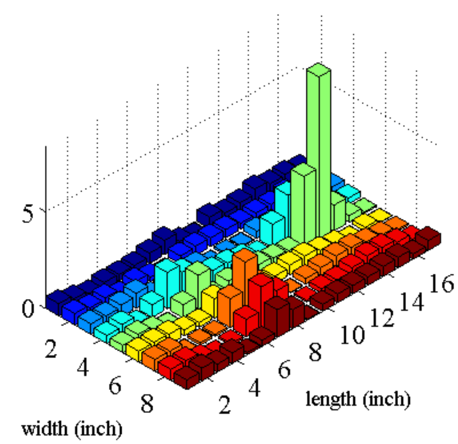
</td></tr>
</table>

Mode 5	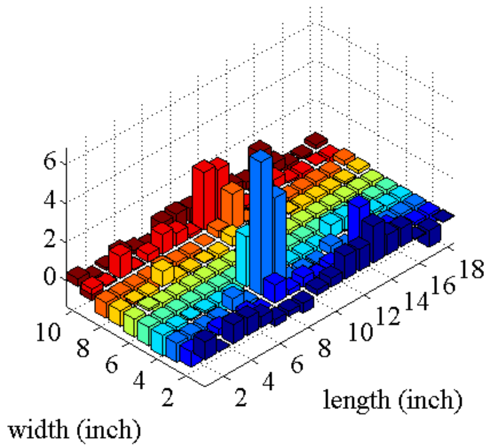	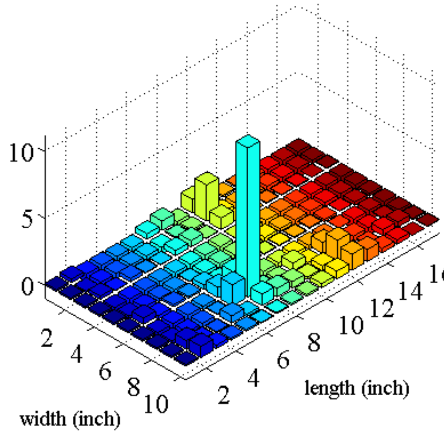	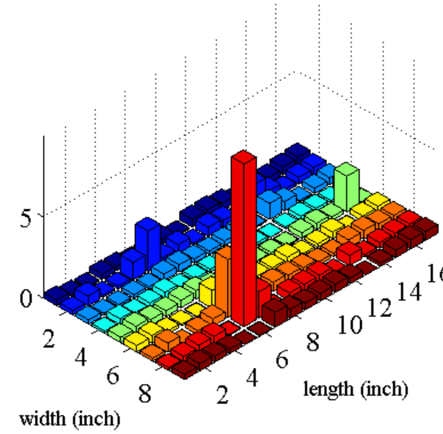
Mode 6	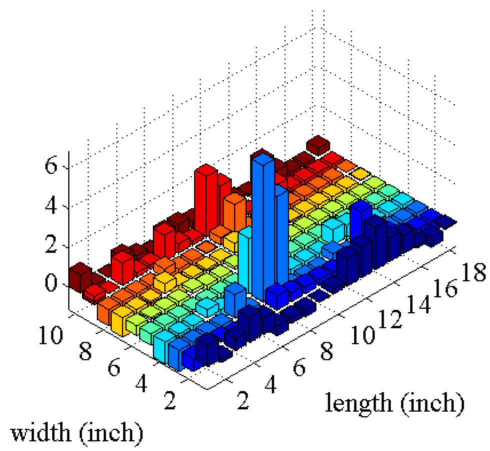	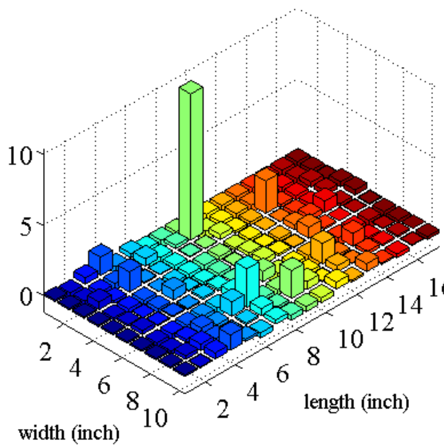	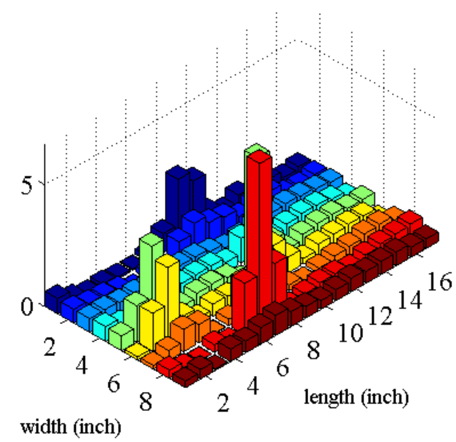

Mode 7

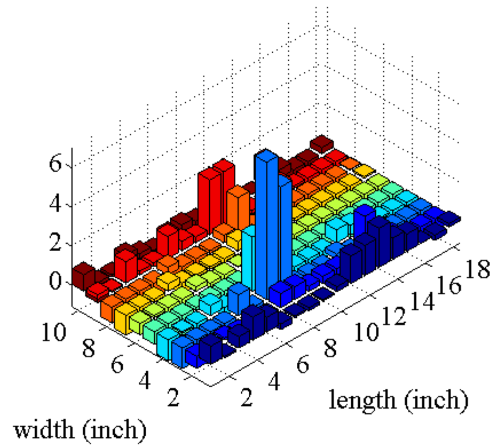

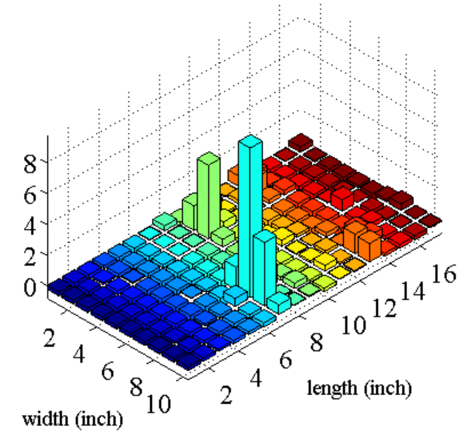

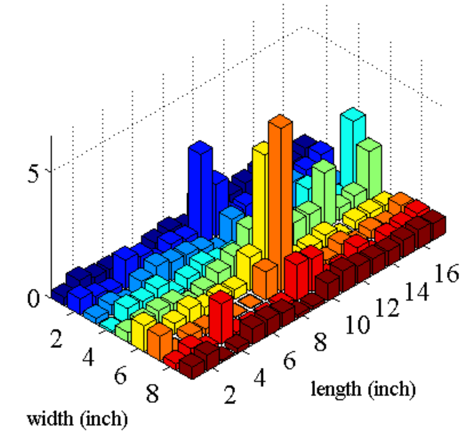

Combination Modes 3-7

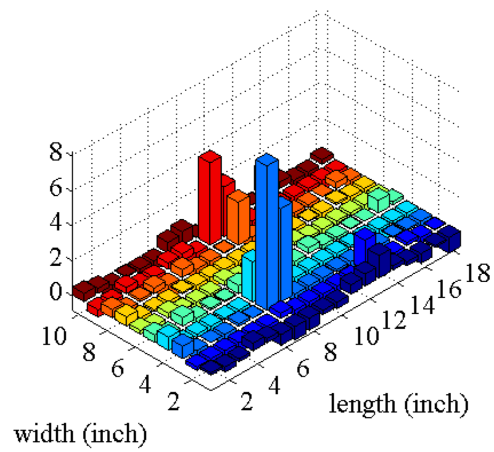

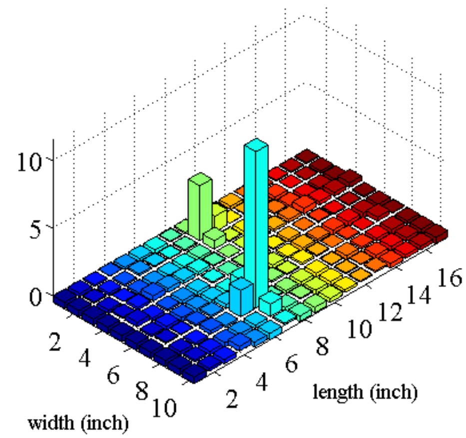

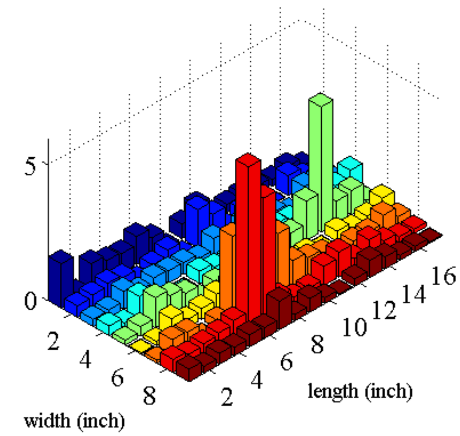

It is now important to investigate the effect of applying the algorithms curvature in each direction separately. From Table 4.6, GFD and GSM failed to detect any damage using the curvature in the x-direction; while SEM succeeded to detect the second damage. Using the y-direction curvature, all the algorithms were able to detect the first damage but failed to detect the second damage. Using the xy-curvature alone, GSM as well as GFD successfully detected both the damages with minimum amount of false indication, while the SEM failed to detect the damage.

Table 4.6 Application of damage detection algorithms using κx, κy, and κxy for the damage case three

<table>
<tr><th></th><th>GSM</th><th>GFD</th><th>SEM</th></tr>
<tr><td>κ_x</td>
<td>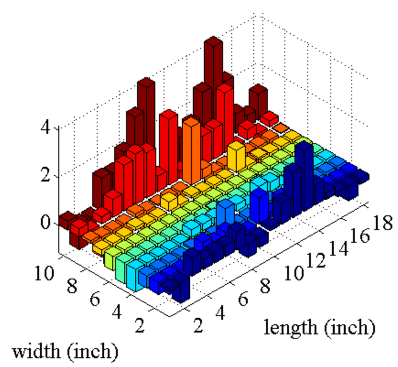
</td>
<td>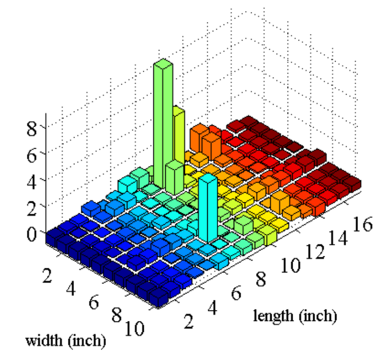
</td>
<td>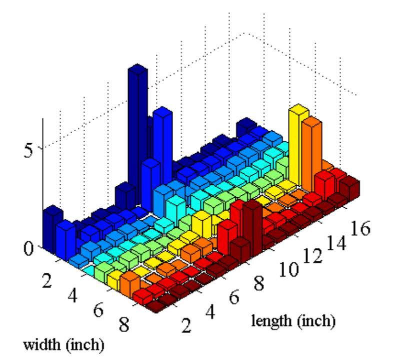
</td></tr>
<tr><td>κ_y</td>
<td>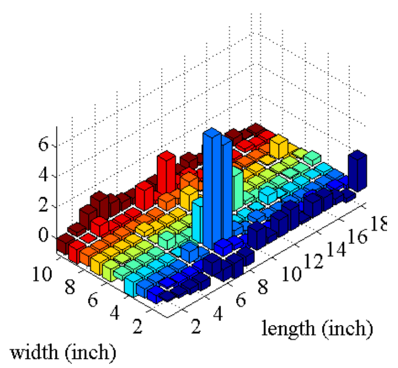
</td>
<td>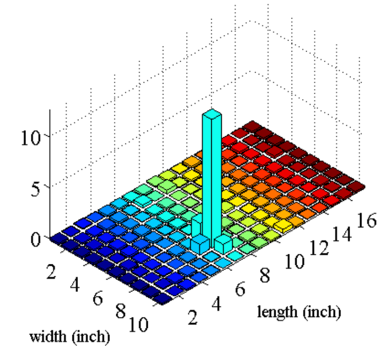
</td>
<td>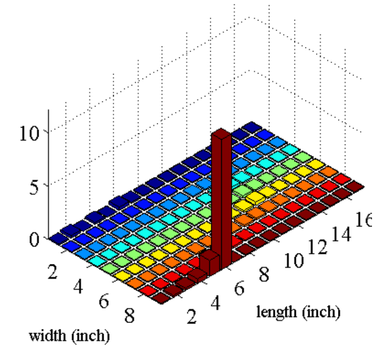
</td></tr>
</table>

κ_{xy}	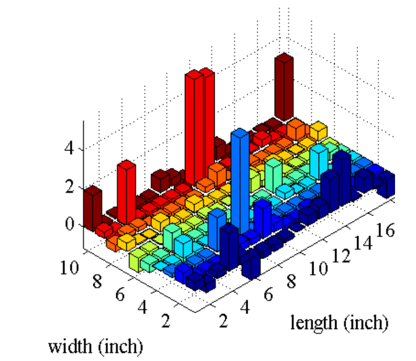	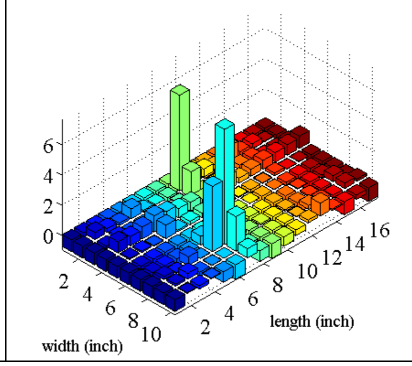	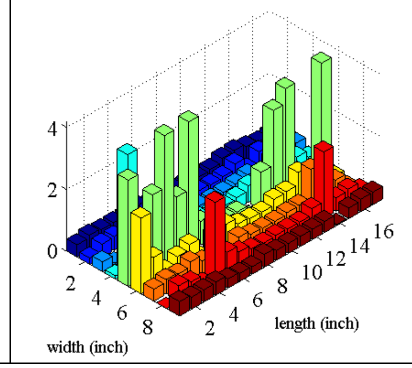

4.3 Displacement-based damage detection

This section presents the application of three damage detection algorithms with the experimentally-measured displacement mode shapes of the plate using the Hammer-Accelerometer system. A similar set of combinations including the use of different modes of vibration were tested to obtain the best detectability of the damage. The damage case two was employed for the purpose of comparison between the curvature-based and the displacement-based methods.

The results of the application of the damage detection algorithms using the displacement mode shapes for damage case two are shown in Table 4.7. As seen from the damage index for modes four, five, six and seven, GFD performed poorly when used with displacement; but using a combination of the modes was successful to detect the damage. GSM had the best performance in terms of noise, but as seen in the results with the finite element data in Chapter 3, the damage was falsely oversized. SEM also successfully detected the damage and had the highest damage index among the three algorithms. In comparison with curvature-based damage detection, the curvature resulted in the higher damage indices, with lower false indication; therefore, the curvature-based method performed better.

Table 4.7 Application of damage detection algorithms to damage case two

<table>
<tr><th></th><th>GSM</th><th>GFD</th><th>SEM</th></tr>
<tr><td>Mode 3</td><td>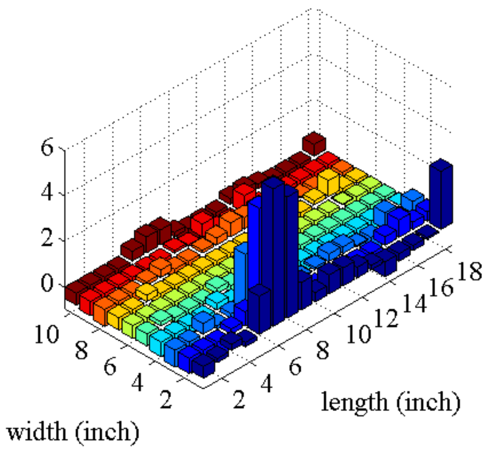
</td><td>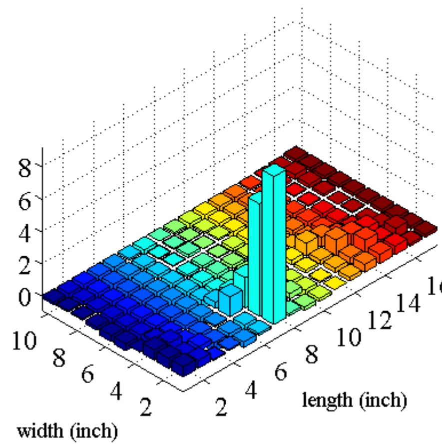
</td><td>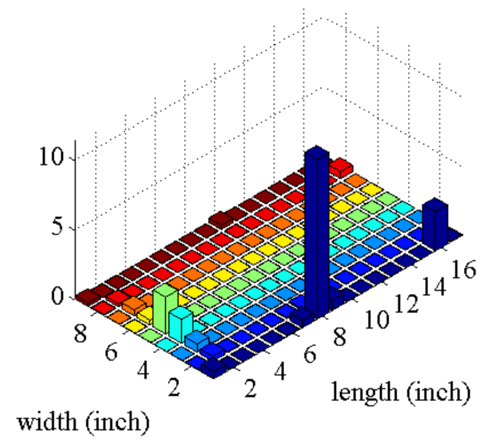
</td></tr>
<tr><td>Mode 4</td><td>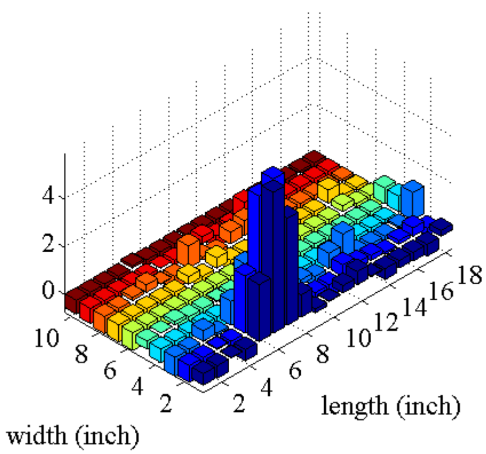
</td><td>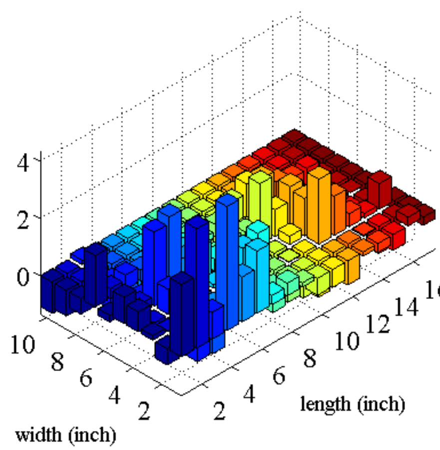
</td><td>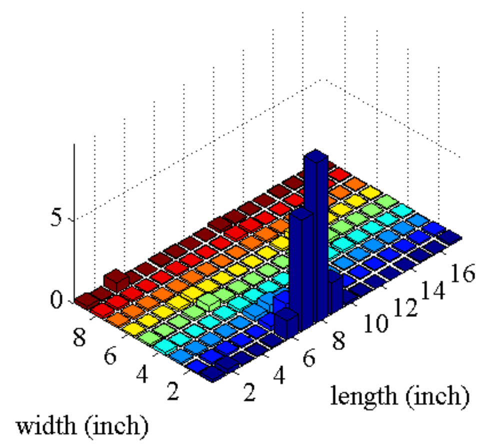
</td></tr>
</table>

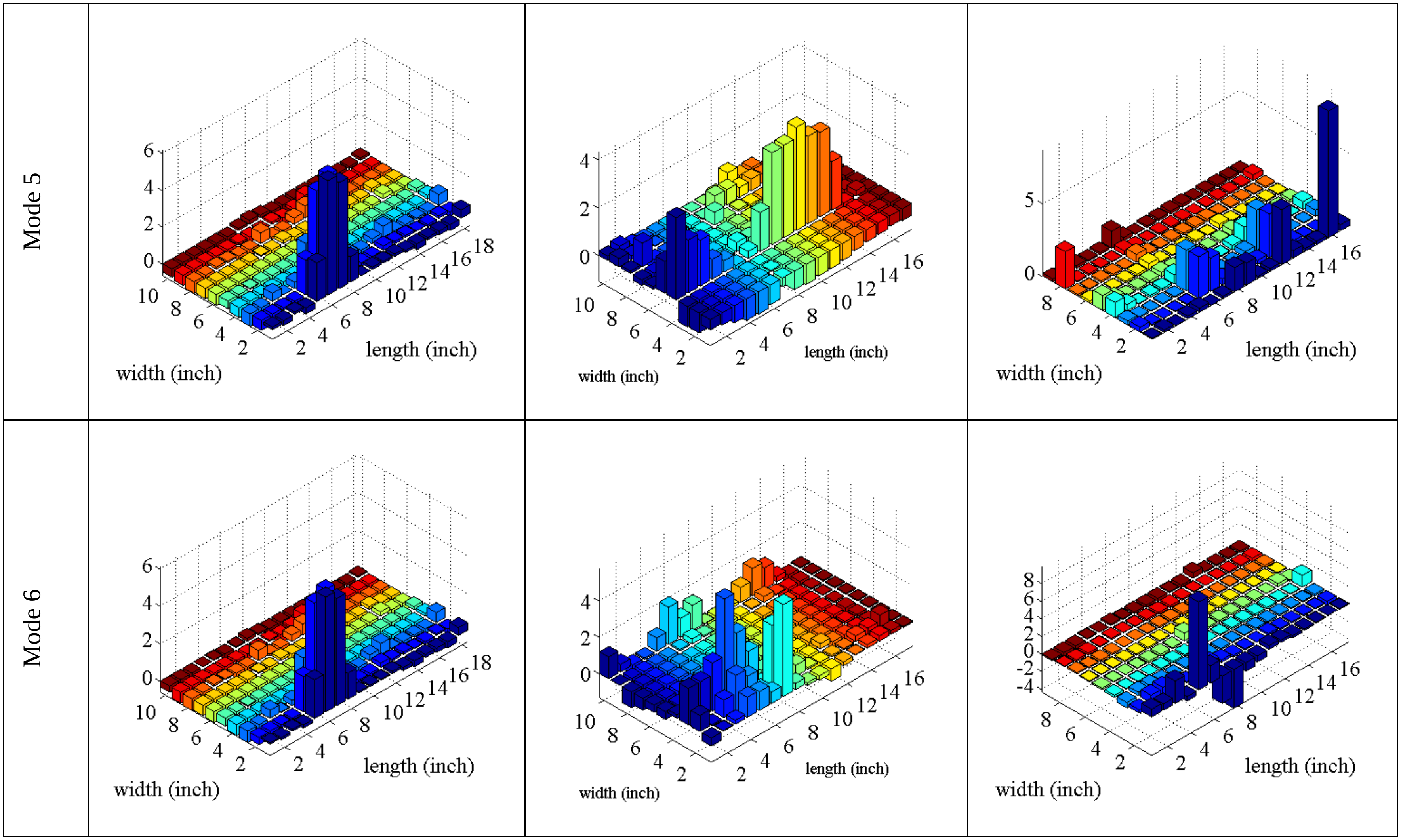
Mode 5
Mode 6
width (inch)
length (inch)

Mode 7	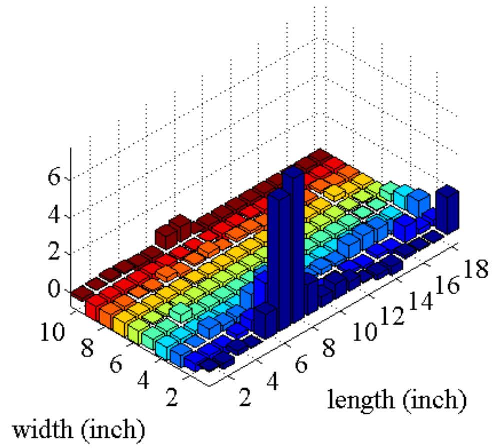	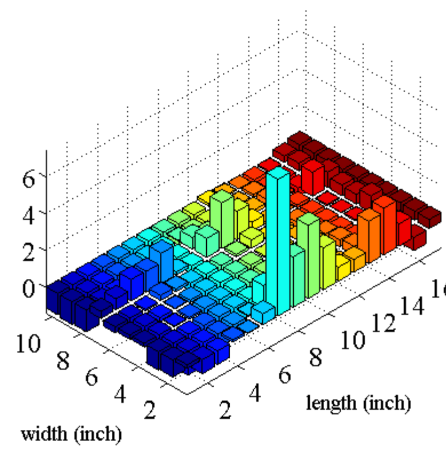	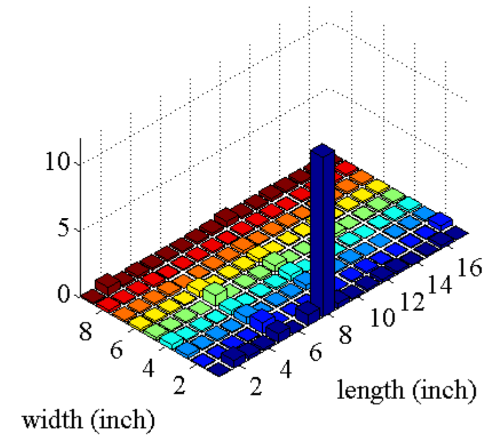
Combination Modes 3-7	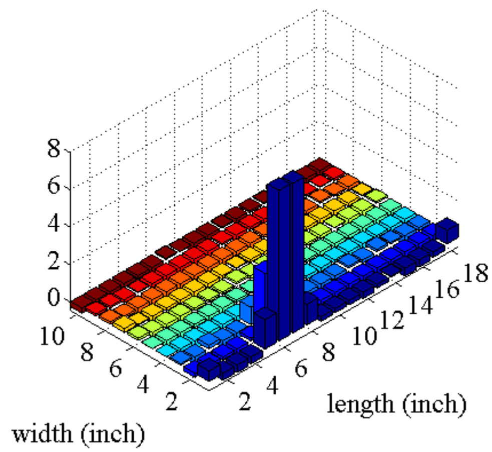	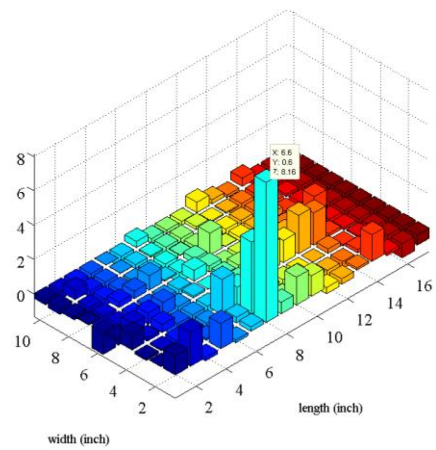	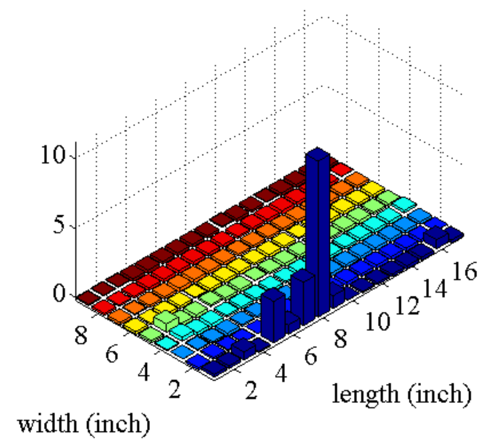

4.4 Sensor spacing effect

The original spacing considered in the experimental program was one inch. While by selecting the data points at the increasing sensor spacing, two inches and three inches sensor spacing were studied. Again, the damage case two was selected as the case study.

Starting with the one inch original spacing, 180 points were present (18 x 10), and all three algorithms were able to identify the damage. Increasing the sensor spacing up to two inches decreased the number of points to 45 (9×5), and it affected the damage index value for all the algorithms almost by a factor of one half. But it is still able to detect the damage and localize it. Finally, increasing the spacing to three inches apart decreased the number of points to 24 points (6 x 4), and as a result, SEM and GFD failed to identify the damage while GSM was still able to identify the damage with a reasonable clarity.

From the above observations, it can be seen that the GSM algorithm is the best in detecting and localizing the damage with the minimum amount of false indication, followed by GFD and then SEM.

Table 4.8 Application of damage detection algorithms with one inch sensor spacing (original arrangement)

SEM	GFD	GSM
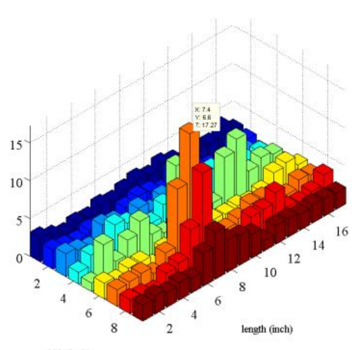	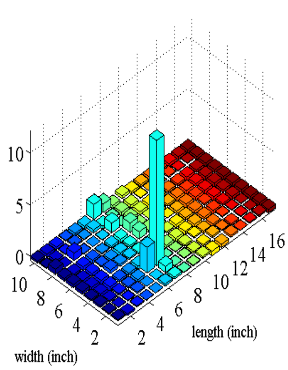	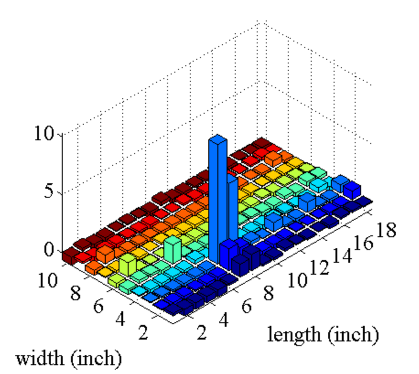

Table 4.9 Application of damage detection algorithms with two inches sensor spacing

SEM	GFD	GSM
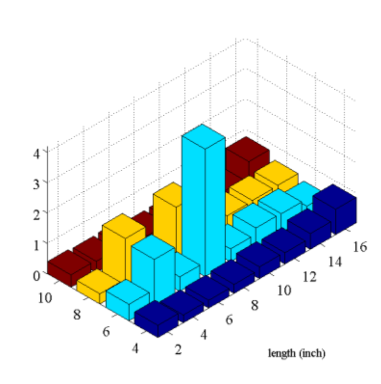	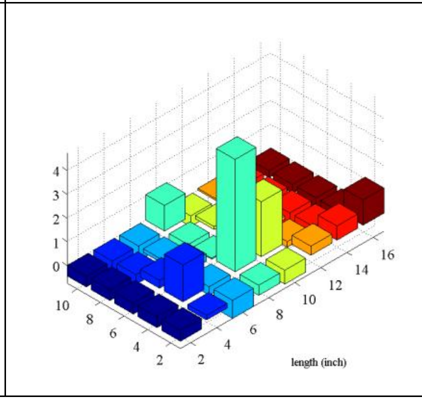	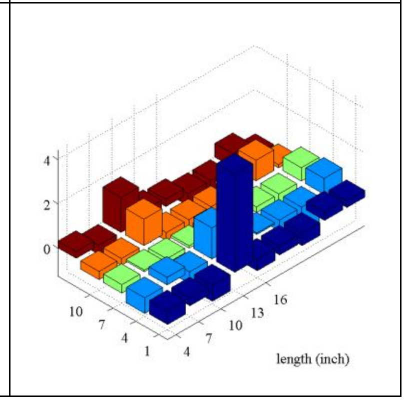

Table 4.10 Application of damage detection algorithms with three inches sensor spacing

SEM	GFD	GSM
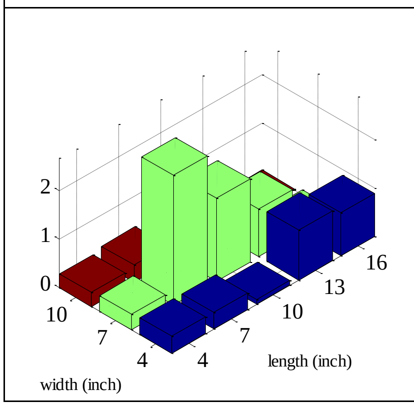	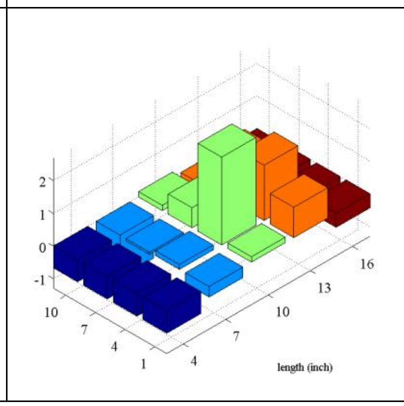	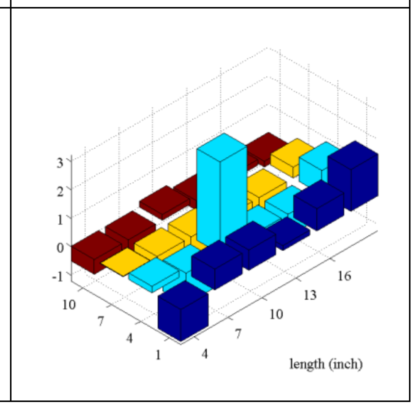

4.5 Summary

In this chapter, the experimental results obtained in Chapter two were used for damage detection. The three damage detection algorithms (i.e., GSM, GFD and SEM) were utilized. The same three damage cases considered in FE are considered for the experimental data analysis as well. Similar to FE, GSM had the best ability to detect and localize the damage. Applying the algorithms to the curvatures in the separate directions lead to the conclusion that κ_y is the most useful curvature for damage detection in case the damage is oriented in that direction and κ_{xy} .in case of the diamond hole damage case. This conclusion agrees with the FE results. Using the displacement mode shapes also agrees with the FE results, with GSM being superior to all others; while GFD performed poorly compared with curvature mode shapes. Finally, a sensor spacing study was conducted, and similar to the FE results, the GSM performed best.

Chapter 5

CONCLUSIONS

The study was focused on vibration-based damage identification for an FRP composite plate, and it included both the experimental testing and numerical finite element modeling. The experimental program included evaluating the frequencies and mode shapes for each mode of vibration through the modal testing. Two sensor-actuator systems were used for the modal testing: the PZT-PVDF system and the Hammer-Accelerometer system. The first used a PZT patch for actuation and a PVDF on each point as sensors, and this system output is the strain mode shapes (i.e., the strain difference between the PVDF film ends) which was treated as curvatures. The second system used an impact hammer as an actuator on each point and an accelerometer as a sensor at a fixed point, and the output of this system is the displacement mode shape. The numerical finite element model using ABAQUS was created to verify the experimental analyses and results. Three damage detection algorithms were selected for application: strain energy method (SEM), gapped smoothing method (GSM) and generalized fractal dimension (GFD). Both the experimental data and finite element data were used as an input for these algorithms. The sensor spacing effect was investigated based on both of the experimental and finite element data. Three damage cases were considered, an edge crack on the plate, an enlarged edge crack at the same location as the first, and finally a diamond hole in the plate.

The following concluding remarks were made from the presented experimental and numerical studies:

1. Curvature vs. displacement mode shapes:

The curvature mode shapes were extracted using the PZT-PVDF system and finite element model, while the displacement mode shapes were extracted using the Hammer-Accelerometer system and finite element model. The displacement system was able to identify more modes of vibration, i.e., more natural frequencies and corresponding mode shapes. The displacement system is less sensitive to noise. Nevertheless, the curvature mode shapes are more effective in locating the damage even with noise infected data. Both the experimental and numerical results lead to the same conclusion regarding the best algorithm as well as the best curvature to use.

2. Using all curvatures vs. using single direction curvature

   Both the ways were tested for damage detection, and the results varied from one case to another according to the orientation or the damage. The damage cases one (D1) and two (D2) were along the y-direction, and using y-direction curvature is more effective than using a combination of all the directions. And for damage case three (D3), the xy-direction curvature was the most effective in detecting the damage. This observation of effectively using the curvature along one direction can reduce the testing work significantly.

3. Using single mode or multiple modes for damage detection

   In single damage cases (i.e., D1 and D2), there might be a mode or modes that performs better than the combination. But in order to reduce the risk of getting a false damage indication, it is best to observe the trend that devleops with all the modes and make a decision accordingly. Using a combination of modes can produce consistent damage detection results. For the multiple damage case (D3), some modes were able to detect one damage while others were able to detect the other damage. As a conclusion, it is preferable to use the combination of modes for damage detection as they are always more representative of the damage.

4. Damage detection algorithms

   Three damage detection algorithms were used: GSM, GFD and SEM, and each has its own pros and cons. Based on the false damage indication, GSM and SEM tend to have high positive false indications, while GFD has a tendency to have negative false indications. As a result, GFD was the best in locating the damage, followed by GSM and SEM. Regarding the noise immunity, GFD had the best noise immunity as it was able to detect the damage at 20 dB of SNR; while the other two failed to do so. GSM was the second in the noise immunity followed by SEM. GSM performed the best when increasing the sensor spacing, followed by GFD and then SEM. Moreover, GSM performed best in the multiple damage detection, followed by GFD and SEM. GSM and GFD have an advantage of not requiring the healthy mode shapes to process the algorithm. Another drawback of SEM is that the algorithm requires relatively high computing recourses compared with GSM and GFD. This will result in higher cost in computing as well as time wise. A drawback of GFD is its poor performance when applied to the displacement mode shapes. In conclusion, if the displacement mode shapes are available, the best damage detection algorithm to use is GSM. If the curvature mode shapes are available, the best to use is GFD.

Based on the above conclusions, the following are recommendations for future research:

a) Investigate the pattern of the sensors on the efficiency of the damage detection.
b) Investigate more boundary conditions, damage types, and different materials.

c) Discover new ways to reduce the noise during an experiment.

d) Develop a “real” two dimensional fractal dimension algorithm.

Reference

1. Farrar, C.R. and K. Worden, *An introduction to structural health monitoring.* Philosophical Transactions of the Royal Society a-Mathematical Physical and Engineering Sciences, 2007. **365**(1851): p. 303-315.
2. Rytter, *Vibration based inspection of civil engineering structures.* University of Aalborg, Denmark, 1993.
3. Fan, W. and P. Qiao, *Vibration-based damage Identification Methods: A Review and Comparative Study.* Structural Health Monitoring, 2010.
4. Zou, Y., L. Tong, and G.P. Steven, *Vibration-Based Model-Dependent Damage (Delamination) Identification and Health Monitoring For Composite Structures -- A Review.* Journal of Sound and Vibration, 2000. **230**(2): p. 357-378.
5. L.B. Crema, A.C., G. Coppotelli, *Damage localization in composite material structures by using eigenvalue measurements.* Materials and Design Technology ASME PD-71, 1995: p. 201–205.
6. A. Paolozzi, I.P., *Detection of debonding damage in a composite plate through natural frequency variations.* Journal of Reinforced Plastics and Composites, 1990. **9**: p. 369–389.
7. J.J. Tracy, G.C.P., *Effect of delamination on the natural frequencies of composite laminates, Journal of Composite Materials.* 1989(23): p. 1200–1215.
8. Gibson, R.F., *Modal vibration response measurements for characterization of composite materials and structures.* Composite Science and Technology, 2000. **15**(60): p. 2769–2780.
9. Salawu, O.S., *Detection of structural damage through changes in frequency: A review.* Engineering Structures, 1997. **19**(9): p. 718-723.
10. Farrar, C.R. and G.H. James, *System identification from ambient vibration measurements on a bridge.* Journal of Sound and Vibration, 1997. **205**(1): p. 1-18.
11. Khan, A.Z., A.B. Stanbridge, and D.J. Ewins, *Detecting damage in vibrating structures with a scanning LDV.* Optics and Lasers in Engineering, 1999. **32**(6): p. 583-592.
12. Salawu, O.S. and C. Williams, *Damage location using vibration mode shapes.* International Modal Analysis Conference, 1994: p. 933-9.
13. Huth, O., et al., *Damage identification using modal data: Experiences on a prestressed concrete bridge.* Journal of Structural Engineering-Asce, 2005. **131**(12): p. 1898-1910.
14. Pandey, A.K., M. Biswas, and M.M. Samman, *Damage detection from changes in curvature mode shapes.* Journal of Sound and Vibration, 1991. **145**(2): p. 321-332.
15. Lu, Q., G. Ren, and Y. Zhao, *MULTIPLE DAMAGE LOCATION WITH FLEXIBILITY CURVATURE AND RELATIVE FREQUENCY CHANGE FOR BEAM STRUCTURES.* Journal of Sound and Vibration, 2002. **253**(5): p. 1101-1114.
16. Kim, J.T., et al., *Damage identification in beam-type structures: frequency-based method vs mode-shape-based method.* Engineering Structures, 2003. **25**(1): p. 57-67.
17. Shi, Z.Y. and S.S. Law, *Structural damage localization from modal strain energy change.* Journal of Sound and Vibration, 1998. **218**(5): p. 825-844.
18. Shi, Z.Y., S.S. Law, and L.M. Zhang, *Damage localization by directly using incomplete mode shapes.* Journal of Engineering Mechanics-Asce, 2000. **126**(6): p. 656-660.
19. Stubbs, N. and J.T. Kim, *Damage localization in structures without baseline modal parameters.* Aiaa Journal, 1996. **34**(8): p. 1644-1649.

20. Kim, J.T. and N. Stubbs, *Model-Uncertainty Impact and Damage-Detection Accuracy in Plate Girder.* Journal of Structural Engineering-Asce, 1995. **121**(10): p. 1409-1417.
21. Stubbs, N., J.T. Kim, and C.R. Farrar, *Field verification of a nondestructive damage localization and severity estimation algorithm.* Proceedings of 13th International Modal Analysis Conference, 1995. **1**: p. 210-8.
22. Pandey, A.K. and M. Biswas, *Damage Detection in Structures Using Changes in Flexibility.* Journal of Sound and Vibration, 1994. **169**(1): p. 3-17.
23. Zhang, Z. and A.E. Aktan, *Application of modal flexibility and its derivatives in structural identification.* Research in Nondestructive Evaluation, 1998. **10**(1): p. 43-61.
24. Wu, D. and S.S. Law, *Damage localization in plate structures from uniform load surface curvature.* Journal of Sound and Vibration, 2004. **276**(1-2): p. 227-244.
25. Wu, D. and S.S. Law, *Sensitivity of uniform load surface curvature for damage identification in plate structures.* Journal of Vibration and Acoustics-Transactions of the Asme, 2005. **127**(1): p. 84-92.
26. Wang, J. and P.Z. Qiao, *Improved damage detection for beam-type structures using a uniform load surface.* Structural Health Monitoring-an International Journal, 2007. **6**(2): p. 99-110.
27. Ratcliffe, C.P., *DAMAGE DETECTION USING A MODIFIED LAPLACIAN OPERATOR ON MODE SHAPE DATA.* Journal of Sound and Vibration, 1997. **204**(3): p. 505-517.
28. Ratcliffe, C.P., *A frequency and curvature based experimental method for locating damage in structures.* Transactions of the American Society of Mechanical Engineers Journal of Vibration and Acoustics, 2000(122): p. 324-329.
29. M.K. Yoon, D.H., J.W. Gillespie Jr., C.P. Ratcliffe, R.M. Crane, *Local damage detection using a global fitting method on mode shape data.* IMAC XIX: A Conference on Structural Dynamics,Kissimmee, FL, 2001. **1**: p. 231–237.
30. M.K. Yoon, D.H., J.W. Gillespie Jr., C.P. Ratcliffe, R.M. Crane, *Local damage detection using the two-dimensional gapped smoothing method.* Journal of Sound and Vibration, 2005(279): p. 119-139.
31. N. STUBBS, J.-T.K.a.K.T., *An e • fficient and robust algorithm for damage localization in o€ shore platforms.* Proceedings of the ASCE Tenth Structures Congress, 1992: p. 543-546.
32. Cornwell, P., S.W. Doebling, and C.R. Farrar, *APPLICATION OF THE STRAIN ENERGY DAMAGE DETECTION METHOD TO PLATE-LIKE STRUCTURES.* Journal of Sound and Vibration, 1999. **224**(2): p. 359-374.
33. YOUNG, D., *Vibration of rectangular plates by the Ritz method.* Journal of Applied Mechanics, 1965: p. 448-453.
34. Mandelbrot, B.B. and J.W. Van Ness, *Fractional Brownian Motions, Fractional Noises and Applications.* SIAM Review, 1968. **10**(4): p. 422-437.
35. Wang, J. and P. Qiao, *Improved Damage Detection for Beam-type Structures using a Uniform Load Surface.* Structural Health Monitoring, 2007. **6**(2): p. 99-110.
36. Hadjileontiadis, L.J.a.D., E., *Crack detection in plates using fractal dimension.* Engineering Structures, 2007(29): p. 1612–1625.
37. Wang, J.a.Q., P.Z., *Improved damage detection for beam-type structures using a uniform load surface.* Structural Health Monitoring-an International Journal of Applied Mathematics and Physics, 2007(6): p. 99-110.

38. Zhao, J., *Sensitivity Study for Vibrational Parameters Used in Damage Detection.* J. Struct. Eng., 1999. **125**(4): p. 410.
39. Alex Berman And William G. Flannelly, *Theory of Incomplete Models of Dynamic Structures* American Institute of Aeronautics and Astronautics Journal Journal 1971. **0001-1452 vol.9** (no.8): p. 1481-1487.
40. Ovanesova, A.V. and L.E. Suárez, *Applications of wavelet transforms to damage detection in frame structures.* Engineering Structures, 2004. **26**(1): p. 39-49.
41. Liew, K.M. and Q. Wang, *Application of Wavelet Theory for Crack Identification in Structures*. Vol. 124. 1998: ASCE. 152-157.
42. Quek, S.-T., et al., *Sensitivity analysis of crack detection in beams by wavelet technique.* International Journal of Mechanical Sciences, 2001. **43**(12): p. 2899-2910.
43. Gentile, A. and A. Messina, *On the continuous wavelet transforms applied to discrete vibrational data for detecting open cracks in damaged beams.* International Journal of Solids and Structures, 2003. **40**(2): p. 295-315.
44. Douka, E., S. Loutridis, and A. Trochidis, *Crack identification in beams using wavelet analysis.* International Journal of Solids and Structures, 2003. **40**(13-14): p. 3557-3569.
45. Chang, C.-C. and L.-W. Chen, *Damage detection of a rectangular plate by spatial wavelet based approach.* Applied Acoustics, 2004. **65**(8): p. 819-832.
46. Douka, E., S. Loutridis, and A. Trochidis, *Crack identification in plates using wavelet analysis.* Journal of Sound and Vibration, 2004. **270**(1-2): p. 279-295.
47. Loutridis, S., et al., *A two-dimensional wavelet transform for detection of cracks in plates.* Engineering Structures, 2005. **27**(9): p. 1327-1338.
48. Kim, B.H., H. Kim, and T. Park, *Nondestructive damage evaluation of plates using the multi-resolution analysis of two-dimensional Haar wavelet.* Journal of Sound and Vibration, 2006. **292**(1-2): p. 82-104.
49. Rucka, M. and K. Wilde, *Application of continuous wavelet transform in vibration based damage detection method for beams and plates.* Journal of Sound and Vibration, 2006. **297**(3-5): p. 536-550.
50. Jean-Pierre Antoine, R.M., Pierre Vandergheynst and S.T. Ali, *Frontmatter Two-Dimensional Wavelets and their Relatives*. 2004: Cambridge University Press.
51. Qiao, P., et al., *Curvature mode shape-based damage detection in composite laminated plates.* Composite Structures, 2007. **80**(3): p. 409-428.
52. Qiao, P., et al., *Dynamics-based Damage Detection of Composite Laminated Beams using Contact and Noncontact Measurement Systems.* Journal of Composite Materials, 2007. **41**(10): p. 1217-1252.
53. Fan, W. and P. Qiao, *A 2-D continuous wavelet transform of mode shape data for damage detection of plate structures.* International Journal of Solids and Structures, 2009. **46**(25-26): p. 4379-4395.
54. Khan, A.Z., A.B. Stanbridge, and D.J. Ewins, *Detecting damage in vibrating structures with a scanning LDV.* Optics and Lasers in Engineering, 2000. **32**(6): p. 583-592.
55. Kawai, H., *The Piezoelectricity of Poly (vinylidene Fluoride).* Japanese Journal of Applied Physics. **8**(Copyright (C) 1969 Publication Board, Japanese Journal of Applied Physics): p. 975.
56. Vepa, R., *Dynamics of Smart Structures*. 2010: John Wiley & Sons.
57. *The New and Improved Pultex ® Pultrusion Design Manual of Standard and Custom Fiber Reinforced Polymer Structural Profiles.* 2004. **Volume 4**(Revision 6).

58. He, J. and Z.F. Fu, *Modal analysis*. 2001: Butterworth-Heinemann.
59. Avitabile, P., *Experimental Modal Analysis - A Simple Non-Mathematical Presentation.* Sound &Vibration Magazine, 2001.